

2016

Analysis of blood flow and drug concentration distribution in tumor-affected cerebral artery tissue region

Sindhuja Moda

Follow this and additional works at: <https://huskiecommons.lib.niu.edu/allgraduate-thesesdissertations>

Recommended Citation

Moda, Sindhuja, "Analysis of blood flow and drug concentration distribution in tumor-affected cerebral artery tissue region" (2016). *Graduate Research Theses & Dissertations*. 1445.
<https://huskiecommons.lib.niu.edu/allgraduate-thesesdissertations/1445>

This Dissertation/Thesis is brought to you for free and open access by the Graduate Research & Artistry at Huskie Commons. It has been accepted for inclusion in Graduate Research Theses & Dissertations by an authorized administrator of Huskie Commons. For more information, please contact jschumacher@niu.edu.

ABSTRACT

CFD ANALYSIS OF BLOOD FLOW AND DRUG CONCENTRATION DISTRIBUTION IN TUMOR-AFFECTED CEREBRAL ARTERY TISSUE REGION

Sindhuja Moda, MS
Department of Mechanical Engineering
Northern Illinois University, 2016
Pradip Majumdar, Director

Brain tumors occur in the brain with the growth of abnormal cells. Despite the advancements in medical technologies and treatments, the complex geometry of the brain impedes the treatment of tumors in the brain. A promising and efficient drug targeting to the diseased regions with limited dosage input reduces the risk of potential damage of healthy tissue cells in the vicinity of tumor. Insertion of drug particles into the bloodstream through intravenous administration is one of the efficient treatment methods which is gaining importance. Currently, extensive research is being conducted in the areas of treating brain tumors effectively with direct administration of drug through blood. In this study a three-dimensional computational simulation model of the artery-capillary network with cerebral part is developed and reconstructed using multiple CT and MRI scan images of a tumor-affected patient. The simulation model includes solution of governing equations of blood flow dynamics based on Navier-Stokes equations and mass species transport based on Lagrangian particle flow dynamics in the artery network and capillaries of the adjacent tissue-tumor regions subjected to typical cardiac cycle. Computational analysis is performed to evaluate and analyze the blood flow and drug particle distributions around the targeted region with varying concentrations. The main objective of this study is to evaluate and optimize the effectiveness of the drug delivery to the internal targeted tumor region for different input drug parameters such as drug type, density and dose concentrations.

**NORTHERN ILLINOIS UNIVERSITY
DEKALB, ILLINOIS**

MAY 2016

**ANALYSIS OF BLOOD FLOW AND DRUG CONCENTRATION
DISTRIBUTION IN TUMOR-AFFECTED CEREBRAL ARTERY TISSUE
REGION**

BY

**SINDHUJA MODA
©2016 Sindhuja Moda**

**A THESIS SUBMITTED TO THE GRADUATE SCHOOL
IN PARTIAL FULFILLMENT OF THE REQUIREMENTS
FOR THE DEGREE
MASTER OF SCIENCE
DEPARTMENT OF MECHANICAL ENGINEERING**

Thesis Director:

Dr. Pradip Majumdar

ACKNOWLEDGEMENTS

I would like to express deep gratitude to my advisor, Dr. Pradip Majumdar, for his constant encouragement and support throughout this work. It is his expertise in the field and continuous support while guiding that made this work possible. This master's degree, the dream of my life, would not have been possible for me without his financial support throughout my course work. It is an honor to work with him.

I would like to thank my committee members, Dr. John Shelton and Dr. Amartya Chakrabarti, for their valuable suggestions which were helpful in making improvements to the model. This made me to work more on concepts and helped me to become conceptually stronger. I would also like to express my deepest gratitude to my parents, Jayasimha and Venkata Rani, for their love and continuous encouragement.

I am also thankful to my brother, especially for his constant help, and my friends for helping me in achieving my goal.

DEDICATION

To my brother with love and affection

TABLE OF CONTENTS

LIST OF TABLES.....	viii
LIST OF FIGURES.....	ix
1.INTRODUCTION.....	1
1.1 Motivation.....	1
1.2 Literature Review.....	2
1.3 Objective.....	4
2. BLOOD FLOW IN BRAIN AND BRAIN TUMORS.....	6
2.1 Circulatory System.....	6
2.2 Cardiac Cycle.....	7
2.3 Blood.....	7
2.4 Blood Vessels.....	8
2.5 Tissues.....	10
2.6 Brain and Blood Flow.....	10
2.7 Brain Tumors.....	12
2.8 Treatment Methods.....	14
2.9 Anti-Cancer Drugs for Treating Tumors.....	16
2.10 Blood -Brain Barrier.....	16

Chapter	Page
2.11 Human Equivalent Dosage.....	16
2.12 Flows in Cerebral Arteries	17
3. MODELING OF FLUID FLOW AND DRUG DISTRIBUTION	18
3.1 Design of Physical Model for Flow Analysis.....	18
3.2 Design Procedure and Model Description	19
3.3 Selected Physics for Flow Model.....	25
3.4 Designed Simulation Model.....	31
3.5 Mesh Generation for Approximated Healthy Tissue with Artery-Capillary Network.....	33
3.6 Governing Equations	36
3.7 Boundary Conditions for Model.....	36
3.8 Unsteady Computational Parameters.....	39
4. RESULTS AND DISCUSSIONS.....	40
4.1 Results for Blood Flow in the Artery with Approximated Tissue-Tumor Connection.....	40
4.2 Results for Blood Flow in Reconstructed cerebral Artery-Brain-Tumor Connection.....	50
4.3 Results with Dosage.....	66
4.4 Comparison of Velocities with respect to Concentration in Increasing Order	83
4.5 Velocity Changes with respect to Cardiac Cycle in Tumor at the Central Area	87
4.6 Results for Drug Distribution in Reconstructed Brain.....	92

Chapter	Page
4.7 Results for Drug Concentration Distribution in Realistic Brain at the Site of Tumor.....	102
5. CONCLUSION.....	108
REFERENCES	109

LIST OF TABLES

Table	Page
1. Brain and Their Functions.....	10
2. Properties of Anti-Cancer Drugs.....	15
3. Physical Dimensions of the Computational Models.....	25
4. Physics Assigned to the Model.....	26
5. Mesh Values of Two Models.....	35
6. Velocity Range with respect to Varying Velocities Wave Form.....	37
7. Porosity Assigned for Different Regions of Brain.....	38
8. Drug Particle Parameters.....	38

LIST OF FIGURES

Figure	Page
2.1 Circulatory System.....	6
2.2 Capillary and Artery-Arteriole Network.....	9
2.3 Path of Blood Flow to Brain.....	11
2.4 Cerebral Flow origin and Flow Chart of Blood Flow in Cerebral Arteries.....	12
2.5 MRI Scan of Diseased Patient.....	13
2.6 MRI Scan of Diseased Patient.....	14
3.1 Flow Chart of Design.....	19
3.2 Steps of Design.....	20
3.3 Design of CT scan.....	21
3.4 3D Design from CT scan.....	22
3.5 3D Design of Reconstructed Brain from the MRI Scans.....	24
3.6 3D Design Model of Reconstructed Brain from the MRI Scans.....	24
3.7 Transparent and Opaque 3 D Design View.....	25
3.8 Geometry of the Healthy Artery-Capillary Network with Healthy Network.....	31

Figure	Page
3.9 Geometry of the Model with Approximated Tissue-Tumor Connection.....	32
3.10 3D Model with Tumor View.....	32
3.11 Artery Mesh with Node Values.....	33
3.12 Unhealthy Spherical-Shaped Approximated Tissue with Tumor.....	33
3.13 Mesh of Reconstructed Brain Issue.....	34
3.14 (a) Mesh of Node values of Artery and Tumor with Reconstructed Brain Tissue.....	34
3.14 (b) Mesh of Node values of Artery and Tumor with Reconstructed Brain Tissue.....	35
3.15 Inlet Velocity Waveform.....	37
4.1 (a) Pressure at 0.01 sec in Healthy Artery Tissue Region.....	40
4.1 (b) Pressure at 0.01 sec in Tumored Artery Tissue Region	40
4.2 (a) Pressure at 0.1 sec in Healthy Artery Tissue Region	41
4.2 (b) Pressure at 0.1 sec in Tumored Artery Tissue Region	42
4.3 (a) Pressure at 0.25 sec in Healthy Artery Tissue Region	42
4.3 (b) Pressure at 0.25 sec in Tumored Artery Tissue Region	43
4.4 (a) Pressure at 0.5 sec in Healthy Artery Tissue Region	43
4.4 (b) Pressure at 0.5 sec in Tumored Artery Tissue Region.....	44
4.5 (a) Velocity at 0.1 sec in Healthy Artery Tissue Region	44

Figure	Page
4.5 (b) Velocity at 0.1 sec in Tumored Artery Tissue Region.....	45
4.6 (a) Velocity at 0.5 sec in Healthy Artery Tissue Region	45
4.6 (b) Velocity at 0.5 sec in Tumored Artery Tissue Region	46
4.7 Velocity Plots Which Show Comparisons of Velocities with respect to Diameter.....	47
4.8 Points Considered to Draw Plots with respect to Position.....	47
4.9 (a) Velocity Plots with respect to Position.....	48
4.9 (b) Pressure Variations in Blood Flow with respect to Position.....	49
4.10 (a) Velocity at 0.1 sec in Frontal Region of Reconstructed Brain.....	50
4.10 (b) Velocity at 0.1 sec in Mid-Section of Reconstructed Brain.....	50
4.11 (a) Velocity at 0.125 sec in Frontal Region of Reconstructed Brain.....	51
4.11 (b) Velocity at 0.125 sec in Mid-Section of Reconstructed Brain.....	51
4.12 (a) Velocity at 0.25 sec in Frontal Region of Reconstructed Brain.....	52
4.12 (b) Velocity at 0.25 sec in Mid-Section of Reconstructed Brain.....	53
4.13 (a) Velocity at 0.5 sec in Frontal Region of Reconstructed Brain.....	53
4.13 (b) Velocity at 0.5 sec in Mid-Section of Reconstructed Brain.....	54
4.14 (a) Velocity at Perpendicular Sectional Plane of Reconstructed Brain at 0.1 sec.....	55
4.14 (b) Velocity at Perpendicular Sectional Plane of Reconstructed Brain at 0.125 sec.....	55

Figure	Page
4.14 (c) Velocity at Perpendicular Sectional Plane of Reconstructed Brain at 0.25 sec.....	56
4.14 (d) Velocity at Perpendicular Sectional Plane of Reconstructed Brain at 0.5 sec.....	56
4.15 (a) Velocity at Rear Plane of Reconstructed Brain Tissue at 0.1 sec.....	57
4.15 (b) Velocity at Rear Plane of Reconstructed Brain Tissue at 0.125 sec	58
4.15 (c) Velocity at Rear Plane of Reconstructed Brain Tissue at 0.25 sec	58
4.15 (d) Velocity at Rear Plane of Reconstructed Brain Tissue at 0.5 sec	59
4.16 Velocity Distributions Plot at Sections of Brain.....	59
4.17 (a) Pressure at 0.1 sec in Reconstructed Brain.....	60
4.17 (b) Pressure at 0.125 sec in Reconstructed Brain.....	61
4.17 (c) Pressure at 0.25 sec in Reconstructed Brain.....	61
4.17 (d) Pressure at 0.5 sec in Reconstructed Brain.....	62
4.18 (a) Pressure at Perpendicular Sectional Plane of Reconstructed Brain at 0.1 sec.....	62
4.18 (b) Pressure at Perpendicular Sectional Plane of Reconstructed Brain at 0.125 sec.....	63
4.18 (c) Pressure at Perpendicular Sectional Plane of Reconstructed Brain at 0.25 sec.....	63
4.18 (d) Pressure at Perpendicular Sectional Plane of Reconstructed Brain at 0.5 sec.....	64
4.19 Points Considered to Draw Plots with respect to Position from the Reference.....	64
4.20 Pressure at Sectional Plot with Change in Position.....	65

Figure	Page
4.21 (a) Particle Velocity with 0.03 mL at 0.1 sec.....	66
4.21 (b) Particle Velocity with 0.03 mL at 0.125 sec.....	67
4.21 (c) Particle Velocity with 0.03 mL at 0.2sec.....	68
4.21 (d) Particle Velocity with 0.03 mL at 0.25 sec.....	69
4.21 (e) Particle Velocity with 0.03 mL at 0.3 sec.....	70
4.21 (f) Particle Velocity with 0.03 mL at 0.4 sec.....	71
4.22 (a) Particle Velocity with 0.05 mL at 0.1 sec.....	72
4.22 (b) Particle Velocity with 0.05 mL at 0.125 sec.....	73
4.22 (c) Particle Velocity with 0.05 mL at 0.2 sec.....	74
4.22 (d) Particle Velocity with 0.05 mL at 0.25 sec.....	75
4.22 (e) Particle Velocity with 0.05 mL at 0.3 sec.....	76
4.22 (f) Particle Velocity with 0.05 mL at 0.4 sec.....	76
4.23 (a) Particle Velocity with 0.08 mL at 0.1 sec.....	77
4.23 (b) Particle Velocity with 0.08 mL at 0.125 sec.....	78
4.23 (c) Particle Velocity with 0.08 mL at 0.2 sec.....	79
4.23 (d) Particle Velocity with 0.08 mL at 0.25 sec.....	80
4.23 (e) Particle Velocity with 0.08 mL at 0.3 sec.....	81

Figure	Page
4.23 (f) Particle Velocity with 0.08 mL at 0.4 sec.....	82
4.24 Particle Velocity Changes at Tissue-Tumor Region at 0.1 Time.....	83
4.25 Particle Velocity Changes at Tissue-Tumor Region at 0.125 Time.....	84
4.26 Particle Velocity Changes at Tissue-Tumor Region at 0.3 Time.....	85
4.27 Particle Velocity Changes at Tissue-Tumor Region at 0.4 Time.....	86
4.28 Line Probe of Particle Velocity Changes at Tissue-Tumor Region at 0.125 Time.....	87
4.29 Line Probe of Particle Velocity Changes at Tissue-Tumor Region at 0.3 Time.....	88
4.30 Line Probe of Particle Velocity Changes at Tissue-Tumor Region at 0.4 Time.....	89
4.31 Drug Distribution with Concentration Input with Cardiac Cycle Values.....	90
4.32 (a) Probe.....	91
4.32 (b) Concentration at Line Probe with Varying Dosage Levels.....	91
4.33 (a) Particle Velocity in Reconstructed Brain at 0.1 Time with 0.01 mL.....	92
4.33 (b) Particle Velocity in Reconstructed Brain at 0.125 Time with 0.01 mL.....	93
4.33 (c) Particle Velocity in Reconstructed Brain at 0.25 Time with 0.01 mL.....	94
4.33 (d) Particle Velocity in Reconstructed Brain at 0.5 Time with 0.01 mL.....	94
4.33 (e) Scaled Particle Velocity in Reconstructed Brain at 0.5 Time with 0.01 mL.....	95
4.34 (a) Particle Velocity in Reconstructed Brain at 0.1 Time with 0.03 mL.....	95

Figure	Page
4.34 (b) Particle Velocity in Reconstructed Brain at 0.125 Time with 0.03 mL.....	96
4.34 (c) Particle Velocity in Reconstructed Brain at 0.25 Time with 0.03 mL.....	97
4.34 (d) Scaled Particle Velocity in Reconstructed Brain at 0.5 Time with 0.03 mL.....	97
4.35 (a) Particle Velocity in Reconstructed Brain at 0.1 Time with 0.05 mL.....	98
4.35 (b) Particle Velocity in Reconstructed Brain at 0.125 Time with 0.05 mL.....	99
4.35 (c) Scaled Particle Velocity in Reconstructed Brain at 0.25 Time with 0.05 mL.....	100
4.35 (d) Scaled Particle Velocity in Reconstructed Brain at 0.5 Time with 0.05 mL.....	101
4.36 Velocity Distribution at the Tumor Region with Changed Concentrations	101
4.37 Variation in Drug Concentration at Tumor Site with Different Input Dosages.....	103
4.38 Penetration velocity with Change in Diameter.....	104
4.39 Penetration Velocity with Change in Density.....	105
4.40 Penetration Velocity with Change in Particle Size and Type.....	106
4.41 Concentration Variation with Change in Particle Size and Type.....	107

1. INTRODUCTION

1.1 Motivation

Nowadays improved medical technologies are available for efficient treatment for many dreadful diseases, including cancer. However, despite the efficient treatments, brain tumors are one of the leading cause of mortality. According to the statistical estimation of National Brain Tumor Society, the average mortality rate of adult malignant brain tumors is 3.3%. Brain tumors can originate with the growth of tumor cells within the brain or by tumor cells migrated from another part as a secondary tumor. Brain tumors come under a special category of cancers as the brain's blood-brain barrier offers resistance to the intake of external agents given as drugs to treat cancer in the brain.

Currently, extensive research is being conducted in the areas of treating brain tumors effectively crossing the barriers of the blood-brain barrier with direct administration of drugs through blood. However, administration of drug is to be in safe limits of dosage. Excess dosage given in an attempt to target the tumor reaching through blood-brain barrier may harm the healthy cells around the targeted area of the body. This study is on the development of a three- dimensional simulation analysis model of tumor-affected brain with a blood-supplying artery integrated to it and analyzing the drug particle movements with various parameters such as dosage, particle size, and estimate of the safe level of drug administration to treat the target area successfully.

Brain tumors occur in the brain with the growth of abnormal cells. Despite the advancements in medical technologies and treatments, the complex geometry of the brain impedes the treatment of tumors in brain. A promising and efficient drug targeting to the diseased regions with the limited dosage inputs is essential to reduce the risk of potential damage of healthy cells and tissues in the vicinity of tumor. Insertion of drug particles into the bloodstream through intravenous administration is one of the treatment methods available in treating tumor cells. In this method the tumor cells are directly targeted by the drug particles which flow with the blood. Typical dosages of drugs are administered to the patients depending on the extent of spread of tumor. Constant research is being carried out in improving the drug's targeting efficiency by changing parameters such as dosage increments and particle dimensions depending on the severity.

1.2 Literature Review

Jhunjhunwala et al. [1] studied analysis of pulsatile blood flow in healthy and atherosclerosis-affected artery. The study is carried out with changes in flow field. They compared both steady and transient flow of blood and the results showed that transient flow gives accurate results of analysis to the steady-state case. This study helped me in my work in setting the velocity inlet boundary condition for accurate results and also for reference in analyzing the results of the blood flow for given cardiac flow with varied velocities with respect to time.

Khaled and Vafai [2] mainly explain and derive various models available for setting porous medium for biological tissues. Using mass diffusion and different convective models,

transport in porous media is reviewed. Their study shows the applications of several models and suitability of flow models for various flow types. This study is useful to find the suitable flow model for the different regions of the human body. Using the list of suitability mentioned in this study, the Brinkman's model is considered for my case as it is the best fit of all the models for the tissues nearer to the capillaries as explained by their study.

Takami Yamaguchi et al. [3] studied fluid flow analysis on micro-scale and macro-scale hemodynamics. Their study includes analysis on arteries and capillaries using numerical methods. This paper mainly discussed the advantages and disadvantages of several methods such as bending element method and volume of method. This study is helpful in analyzing the flow in minor blood flow in minute vessels like capillaries.

Fuat Yilmaz and Gundogdu [4] have shown viewpoints on analysis of blood viscosity model and physiological flow conditions using experimental viscosity data. The set of experimental values of cardiac input is considered and the model is analyzed for pressure and velocities of blood flow making changes to viscosity models. They have explained that Carreau Yasuda model is appropriate for non-Newtonian flow of blood. For my work this paper is used as a basic guide to define accurate viscosity model for the given condition to avoid errors.

Arifin et al. [5] in their study explained the distribution of the drug in the brain tumor coupled to its physio-chemical properties. Their study includes design of a realistic three-dimensional tissue geometry extracted from MRI images of a brain tumor for analysis as a primary step and analyze the flow of blood in tumor considering the diffusion, reaction and convection models in which Darcy's law is used to account for the convective contribution of the interstitial fluid. This study is useful for analyzing the blood flow in realistic brain using

Darcy model.

Bello and Carroll [6] studied and evaluated the efficiency of combined chemotherapy drugs in treating the targeted area of human gliomas. But their study was initially limited to mice. They used carboplatin and etoposide as the two chemotherapeutic drugs. However their attempt caused several severe side effects with a decrease in tumor volume as an only added advantage of the study. This study has been used for my work in finding out the best drug for treating tumors.

Shafiullah [7] in his study analyzed the blood flow dynamics of three-dimensional straight artery with a branched structure with and without stenosis. A cardiac cycle for pressure waveform was derived from experimental data in the simulation analysis to evaluate the stented arteries. This study was helpful in setting up the physics of the present study and also used as a guide for analyzing the blood flow in unsteady case.

Narmada [8], in her study extended the Shafiullah's model of branched straight artery to a more realistic artery network derived from the CT scan of atherosclerosis patient. She also extended the model to include a porous medium based on Darcy's flow dynamics model for blood flow through artery network including a tissue region. This work is used in this study for setting up the porous media formulation for blood transport through tissue-tumor region.

1.3 Objective

The main objective of this study is to evaluate and optimize the effectiveness of the drug delivery to the internal targeted tumor region for different input drug parameters such as drug type, density and dose concentrations. The objective is to design the realistic three-dimensional artery network connected to a tumored tissue of the cerebral system and to analyze the blood

flow and drug concentration distribution in the artery- capillary cerebral network. For this study, the artery-capillary network with cerebral part is modeled and reconstructed using multiple CT and MRI scan images of a tumor-affected patient. The simulation model includes solution of governing equations of blood flow dynamics based on Navier-Stokes equations and mass species transport based on Lagrangian particle flow dynamics in the artery network and capillaries of the adjacent tissue-tumor regions subjected to typical cardiac cycle.

A computational analysis is performed to evaluate and analyze the blood flow and drug particle distributions around the targeted region. In this study the particle administration is assumed to be done directly through intravenous method and the administration is analyzed with varying concentrations and particle diameter to identify the possibilities of treating the targeted region effectively with prescribed safe level of dosage causing no harm to healthy cells around the target. The main objective of this study is to evaluate and optimize the effectiveness of the drug delivery to the internal targeted tumor region for different input drug parameters such as drug type, density and dose concentrations.

2. BLOOD FLOW IN BRAIN AND BRAIN TUMORS

In this chapter, brief description of the human body circulatory system, characteristics of the blood flow dynamics in artery-capillary network, cerebral network and details of brain tumor and its treatment methods are given.

2.1 Circulatory System

Human circulatory system consists of heart which acts as pump and the blood vessels which carry blood to and from the heart in respective cycles. This cardiovascular system's structure is designed to provide the body with oxygen, nutrients and also to remove waste from tissue cells.

Figure 2.1 gives the basic idea of the circulatory system.

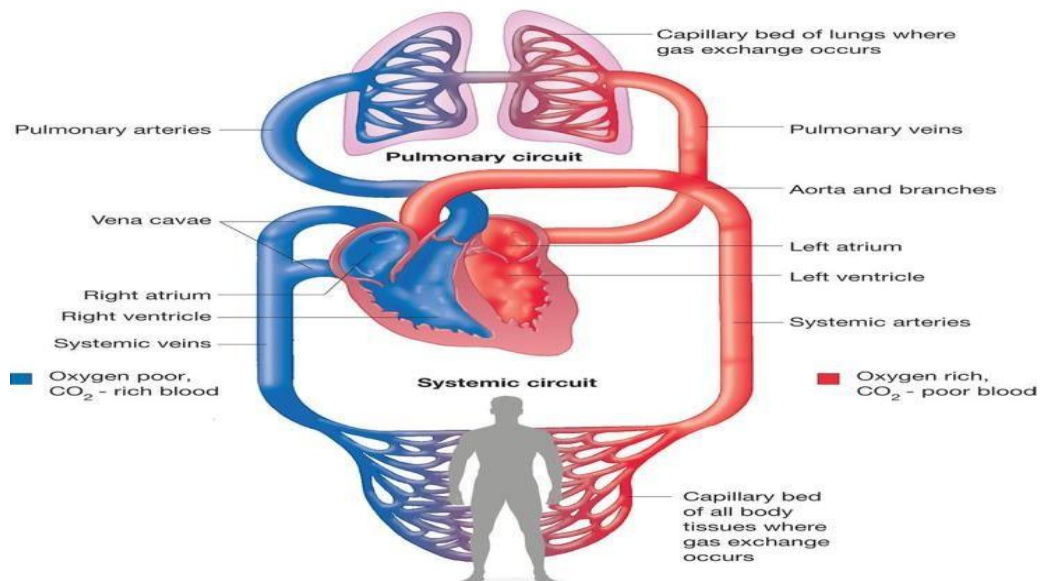


Figure 2.1 Circulatory system

(Source: <https://www.pinterest.com/pin/385761524304847833/>)

As shown in the Figure 2.1, blood flows into the heart through veins and flows away from the heart through arteries. However, flow of blood to various organs is worth noticing as it involves series of changes in flow diameter from start point to the target. The oxygenated blood carried by arteries is taken from the aorta, which is the biggest direct vessel connected to heart. From arteries, blood flows into smaller vessels called arterioles, which divide into even smaller vessels called capillaries [9]. The exchange of energies takes place from capillaries to the cells and deoxygenated blood merges into venules and then into larger veins.

2.2 Cardiac Cycle

Cardiac cycle explains the pumping mechanism of heart. Each cardiac cycle consists of a diastole and a systole phase. Blood leaves heart during systole with increased pressure in atria, whereas during the diastolic phase the ventricles relax leaving the pulmonary and aortic valves closed resulting in letting blood to the heart. The mitral, tricuspid, aortic and pulmonary valves of the heart, connected to arteries leaving the heart and the lower ventricles ventricle respectively, open and close in response according to pressure changes [9].

2.3 Blood

Blood is the fluid which flows through entire human body and provides necessary nutrients and energy to the tissues. It contains red blood cells, white blood cells and platelets in plasma. Blood flow exhibits non-Newtonian nature as it does not possess a constant viscosity at all flow rates. This nature of blood makes it one of the most experimented fluid in bio-engineering field. The other property of blood which is almost equally used in experimental applications is its constant mass density value, which is 1050kg/cm^3 [7, 8].

2.4 Blood Vessels

Blood vessels spread all over the body, originating from the heart to supply and draw blood from different body parts. The size of the vessels varies with the amount of the blood carried by them. There are three major types of blood vessels. The unique characteristics of each type of blood vessel is shown in Figure 2.2 below [7, 8].

2.4.1 Arteries and Arterioles

Arteries carry oxygenated blood from heart to all the body parts. The movement of blood exerts high pressure on arteries as most of the force is exerted by the blood while leaving the heart. To withstand this high pressure, artery walls are more elastic, thicker and muscular than all other vessel walls of the circulatory system. The high elasticity of arteries allows them to stretch and withstand higher pressures. Muscular nature offers smoothness to the arteries which allows them to expand and contract accordingly, resulting in regulating the blood flow [7, 8].

Similar to arteries, arterioles carry blood rich in oxygen to body parts. These are the subdivisions of arteries and are narrower than the arteries. They are thinner in size as they face less pressures than the arteries. However they are muscular in nature like the parent vessel (artery) and thus efficiently regulate the blood flow through a series of expansions and contractions whenever required [7, 8].

2.4.2 Capillaries

These are the smallest of all the blood vessels in the body and connect to all the various organs of the entire body. They have the thinnest structure with only a thin permeable layer called endothelium, which acts as the barrier between the tissues and the blood in capillaries. The permeability of the layer allows the blood to exchange the nutrients and oxygen as energy to the

tissues. Also the waste gases are in turn taken out from the tissue and carried away by the blood through this layer in capillaries. The exhaust derived from the tissues is carried to venules from capillaries [7, 8]. The Figure 2.2 gives an idea of the blood flow.

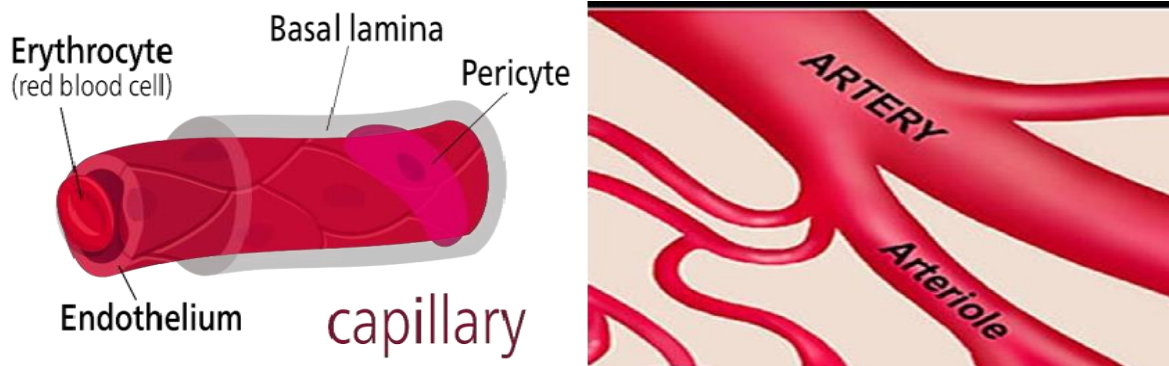


Figure 2.2 Capillary and artery-arteriole network

(Source: <https://en.wikipedia.org/wiki/Capillary>

http://www.medicalexhibits.com/medical_exhibits_image.php?exhibit=09079-36)

2.4.3 Veins and Venules

Deoxygenated blood from the capillaries is to be carried back to heart for repetition of cycle. This is done by veins in our circulatory system. Veins are thinner and less elastic in nature compared to arteries as they are under less pressures throughout the cycle. The underlying mechanism in pushing the blood back to the heart depends on the inertia, gravity and the muscle contraction force. This contraction force helps in forcing blood to the heart. Venules function similar to arteriole, but they collect and supply the deoxygenated blood back to the heart instead of supplying blood from the heart like arterioles [8].

2.5 Tissues

Tissues of the human body are made of series of discontinuous functional units connected together. Many capillaries combine and form the tissue. The outermost layer of tissues is made of muscles which are in turn made of blood vessels, capillaries and connective tissue [8].

2.6 Brain and Blood Flow

2.6.1 Brain

It is the most complex and heaviest organ of the human body responsible for the control over the action of the entire system. It weighs around three pounds and requires 746 ml of blood flow for every minute. Brain and spinal cord together constitute the central nervous system and function primarily as a unit that receives signals as inputs in the form of physical and chemical entities and interprets the information to control the body's response. Brain is also responsible for monitoring blood pressure and hormonal balances in the body. It has several parts with unique functionalities in controlling the bodily actions [10]. Table 1 gives the basic details on parts of brain and its functions.

Table 1: Parts of Brain and Their Functions

Cerebrum	Largest portion of brain	Controls physical reactions, behavior, mental ability
Cerebellum	Little brain	Controls Posture, structure and co-ordination of the body
Brain Stem	Mid-brain	Regulates body movement, vision and hearing
Medulla	Essential part of brain stem	Maintains heart rate and breathing

In this study CT scan image of basilar artery-capillary network is considered. So the study is basically the analysis of blood flow in tumored regions of posterior cerebrum.

2.6.2 Cerebral Blood Flow

Coronary artery arising from the heart divides into several branches to supply the blood in neck, throat and brain regions. The blood supply to the brain is carried by the two pair of arteries called internal carotid and basilar artery. These arteries originate from internal carotid artery and vertebral artery which branches from the coronary artery and subclavian artery of heart. These major arteries again branch into anterior, middle and posterior cerebral arteries to supply blood to various parts of the brain. The anterior cerebral artery supplies blood to the middle and front portions of brain and posterior cerebral artery supplies blood to brain stem and back portion of brain.

The Figures 2.3 and 2.4 show and explain various parts of brain and the path of blood flow.

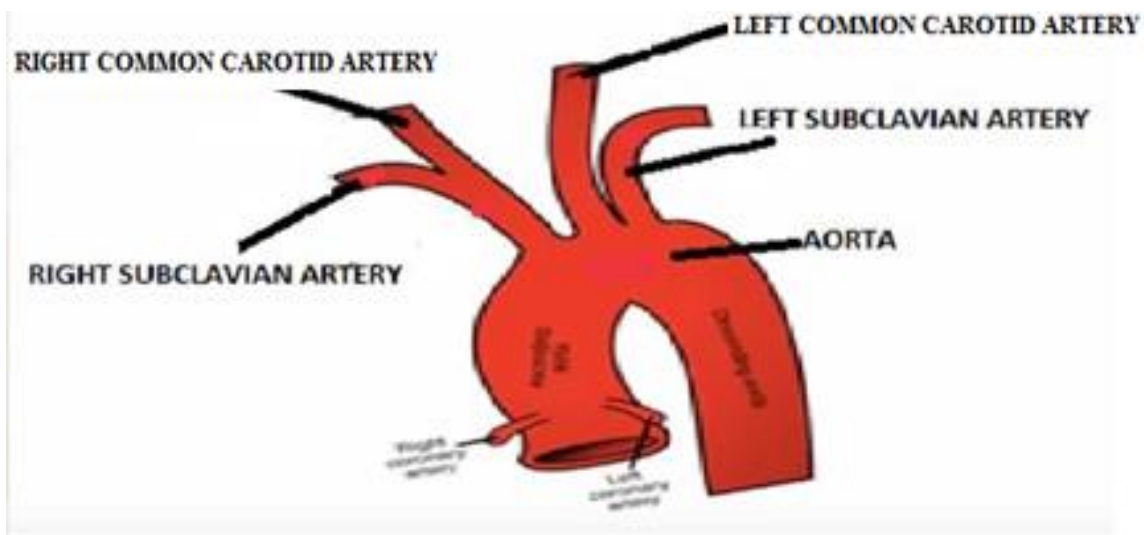


Figure 2.3 Path of blood flow to brain

(Source: Image snipped from a YouTube video)

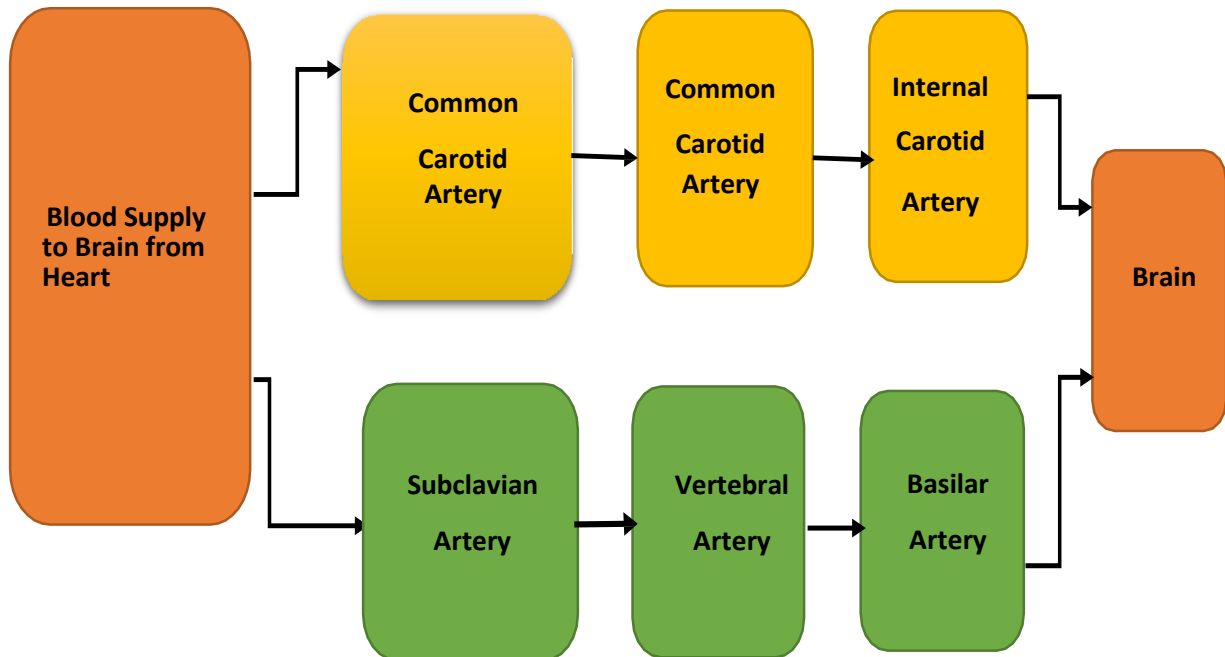


Figure 2.4 Cerebral Flow origin and flow chart of blood flow in cerebral arteries

2.7 Brain Tumors

Growth of abnormal cells in the tissues and other parts of brain leads to brain tumor. These tumors may originate within the brain or developed due to the transfer of tumor cells from another part of the body. These developed tissues avoid flow of blood and nutrients to the essential parts of brain resulting in functional abnormalities [10].

Brain tumors are classified based on the following:

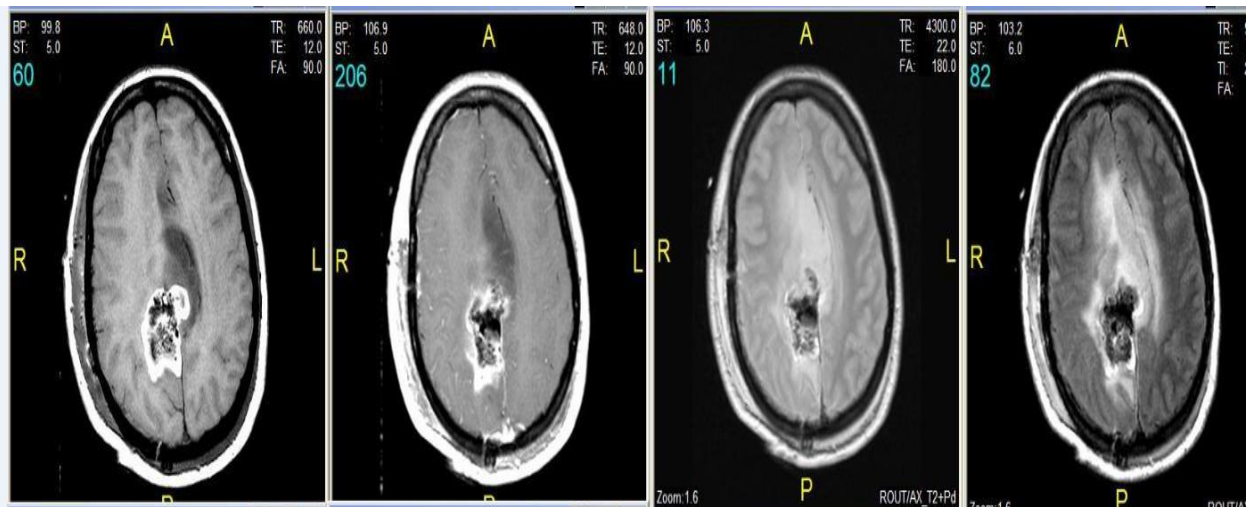
- Origin of tumor: Tumor's origin is the deciding factor to categorize them as primary or secondary tumors. Primary tumors originate within the brain, whereas the secondary tumors are derivatives of body tumors that finally reach the brain.
- The part of the brain being affected: Tumor types are decided depending on the type or part

of the organ where it arises. Brain can be affected with tumor in its tissues, brain stem and some other tiny parts within the brain. However, brain tumors which originate in the tissues are most common and are responsible for many deaths.

In this study tumor originated in the tissue of the brain connected to basilar artery is considered. The CT scan images considered in designing the model for analysis are shown below in Figures 2.5 and 2.6.

Figure 2.6 is of MRI scan image of a woman suffering from grade III astrocytoma. Astrocytoma arises from the cells called astrocytes which are the network of glial cells. The above scans show the area of existence of tumor and its extent of spread. From the scans both sagittal and axial, it is evident that the woman has an abnormal mass spreading from left to right [11]. Also the intensity of signals is shown predominantly in the right parietal lobe with an extension to corpus callosum.

Series of Axial Non-Enhanced and Contrast-Enhanced T1-Weighted, Proton Density-Weighted, and Fluid-Attenuated Inversion Recovery MRI:



(Source: <http://emedicine.medscape.com/article/336695-overview>, Fig 8)

Figure 2.5 MRI scan of diseased patient

Sagittal Non-Enhanced and Contrast-Enhanced T1-Weighted MRIs, Axial Diffusion-Weighted Images, and Axial Apparent Diffusion Coefficient Map:

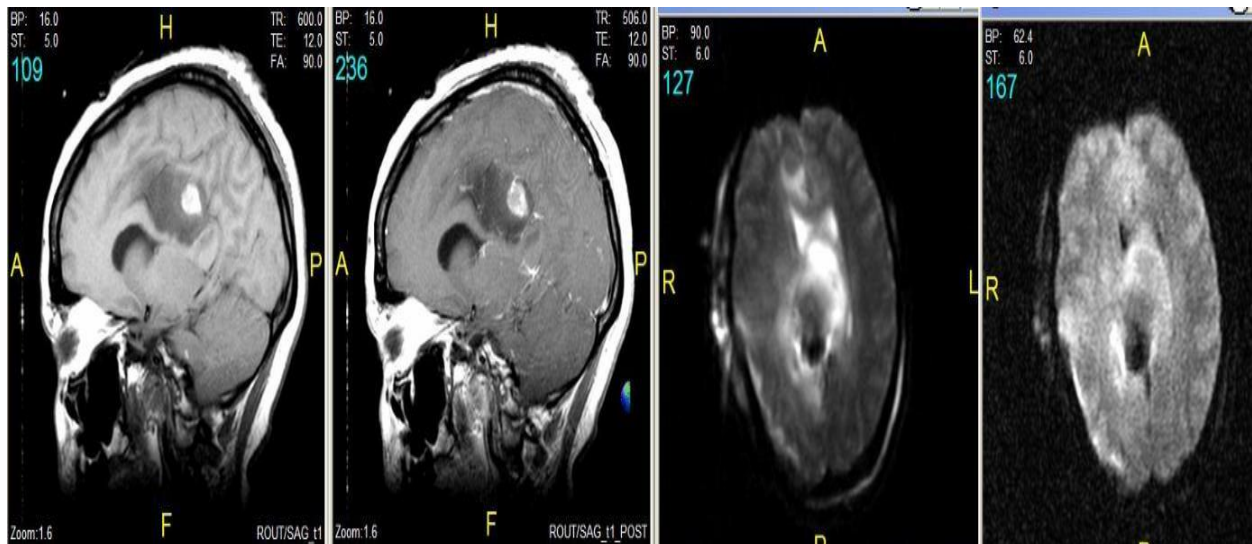


Figure 2.6 MRI scan of diseased patient

2.8 Treatment Methods

Several treatment methods are available for treating brain tumors; however, these methods depend on factors such as type, location and size of the tumor [10]. The following are the treatment options available:

- **Steroids:** These are the hormones given in fixed dosages for a fixed period of time to reduce the growth of tumors. Steroids cannot cure the tumor permanently, but they promote the growth inhibition.
- **Surgery:** It is the traditional treatment done as an initial attempt to remove abnormal mass from the brain. Surgery such as biopsy, partial removal or debulking is beneficial in treating tumors which are huge and hard to control. However risks include infections, blood clots and more recovery time.
- **Chemotherapy:** This process involves delivery of anti-cancer drugs travelling through the

bloodstream to reduce the tumor growth. This procedure offers promising results without the necessity of surgery with some potential risks like any other treatments.

- **Radiation Therapy:** This therapy involves treatment using external beam radiation to kill the cancer cells. This treatment is used to the parts of brain where surgery is not possible to perform. Unlike surgery it offers chance of avoiding seizures and infections through surgery.
- **Stereotactic Radiosurgery:** This is the new approach which is being used now-a-days. In this method radiation is targeted to the exact vicinity of the tumor thereby reducing the damage to the healthy tissues surrounding the tumor. This method also offers more flexibility and avoids surgery.

Table 2: Properties of Anti-Cancer Drugs

DRUGS	PROPERTIES
TEMOZOLOMIDE	Molecular Formula: C₆H₆N₆O₂ Density: 1.97gm/cm³ Molecular Weight: 194.15g/mol
AVASTIN	Molecular Formula: C₆₆H₃₈N₁₀O₂₁S₄ Density: 1.03gm/cm³ Molecular Weight: 149196.8162 g/mol
LOMUSTINE	Molecular Formula: C₉H₁₆ClN₃O₂ Density: 1.35gm/cm³ Molecular Weight: 233.6952 g/mol
CARMUSTINE	Molecular Formula: C₅H₉Cl₂N₃O₂ Density: 1.46gm/cm³ Molecular Weight: 214.05 g/mol

2.9 Anti-Cancer Drugs for Treating Tumors

In this paper, treating of brain's tumored tissue through injection of various concentrations of drug into the blood flow is observed. In this procedure several common intra venal anti-cancer drugs are used for analysis. Table 2 shows the list of drugs and general dosage levels used in treating glioma, a tumor that develops in brain tissues [6].

2.10 Blood-Brain Barrier

Some cells in the brain are connected with tight joints between them and have some electrical resistance. These are called endothelial cells. These cells of brain forms a barrier called blood-brain barrier which allows substances such as water, glucose and amino acids through diffusion while avoids entry of harmful toxins. Moreover all the capillaries which are passing in the brain are connected and surrounded by the cells of brain tissue and forms a strong barrier to avoid invasion of infective substances and other toxins. In this scenario even the drugs given to target the tumors in brain are being obstructed by the blood-brain barrier. Many studies have been made and many drugs are found and designed in the way to penetrate the brain's protective layer. However when compared to tumors in other regions of human body, treating brain is more difficult due to the existence of the powerful protective mechanism. In this study the drugs Carmustine, Temozolomide which are known for its ability of penetrating the blood-brain barrier was used.

2.11 Human Equivalent Dosage

Clinical trials on animals are done to evaluate the safe dosage for the extent of tumor spread in humans. The tumor cells of humans are placed and cultured in healthy animals such as mice and guniea pigs and the drugs are administered to find the power of drugs in treating the

tumor and also the optimum dosage that can be given to kill the tumor. The obtained dosage after the successful trial was converted to the human dosage using human equivalent dosage. In this study in order to convert the dosage from one of the referred papers, the following equation is used [6, 12]:

$$\mathbf{H.E.D = A.D * ((A.W)/(H.W))^{0.33}}$$

where

H.E.D: Human Equivalent Dosage.

A.W: Animal Weight in KG.

H.W: Human Weight in KG.

A.D : Animal Dose in (mg/kg).

2.12 Flows in Cerebral Arteries

Flow velocity of blood in the arteries and veins mainly depends on the flow area and therefore the circulatory system of the human body, which consists of blood flow with different velocities at different regions. Both coronary and carotid arteries which are less in size experience lesser flow velocities. Parameters such as Reynolds number and Womersley numbers are used to calculate and analyze the velocities in every part of the body. For instance, less Reynolds value of 300 and Womersley parameter of 4 in the carotid arteries considered in this study explain the presence of very low velocities in those, when compared to other major arteries [13].

3. MODELING OF FLUID FLOW AND DRUG DISTRIBUTION

In this chapter, details of geometry design, physics of the flow model, use of species transport equations, and boundary conditions are explained.

3.1 Design of Physical Model for Flow Analysis

One of the main objectives of this study is to design a three-dimensional artery connected to capillary and the tumor region of brain, using the CT and MRI scan images of tumor-affected patient. As it is difficult to model the geometry of capillaries with minute dimensions using general design software such as Creo, SolidWorks, expensive 3-D convertors and extensive design software are essentially needed for this task. However softwares such as Mimics and 3-D Doctor are also being extensively used in designing realistic models for research purposes today. They offer equal level of flexibility in design of complex geometries. Currently most research is being conducted in modeling the biomedical field geometries as the simulation analysis pathway to innovation of many technologies [14]. At the same time even some design software such as Space Claim can also perform well in doing necessary modification in design where there is a point of integrating two different entities subjected to study. In this study, a realistic artery- capillary system is designed using Space Claim software and is integrated with the tumor-affected human brain. The human brain is also modeled to the realistic dimensions using the MRI scans of the brain tumor-affected patients using the 3- D modeling software 3D-Doctor. However due to incomplete patient data in the form of numerous MRI slices, the design modeling software gave up the partially modeled brain with cavity at the tumor. So, the partially modeled data is taken into the design

software Space Claim and was reconstructed to the exact dimensions of complete brain with exact location of tumor using the raw data given by 3D-Doctor. The idea of this reconstruction was derived from one of the online forums on SolidWorks which explained the method of construction of brain using the scans. Also due to the incomplete data in design from the eight slices of scans considered in this study, some of the images at the ends of the brain were extracted from this to round out the complete brain obtained from the 3D-Doctor software. Using the raw data the design is developed in Space Claim software [15].

3.2 Design Procedure and Model Description

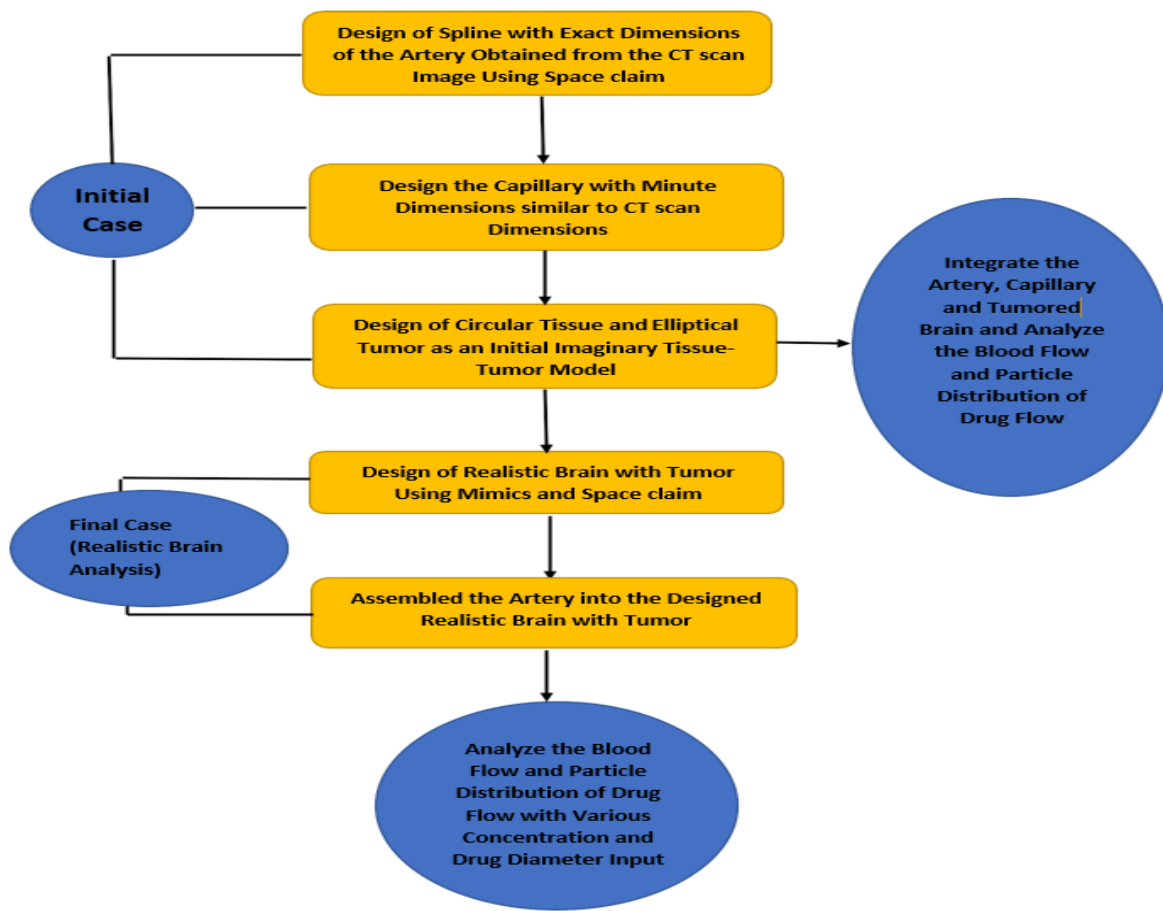


Figure 3.1 Flow chart of design

3.2.2 Procedure for Creating Designs

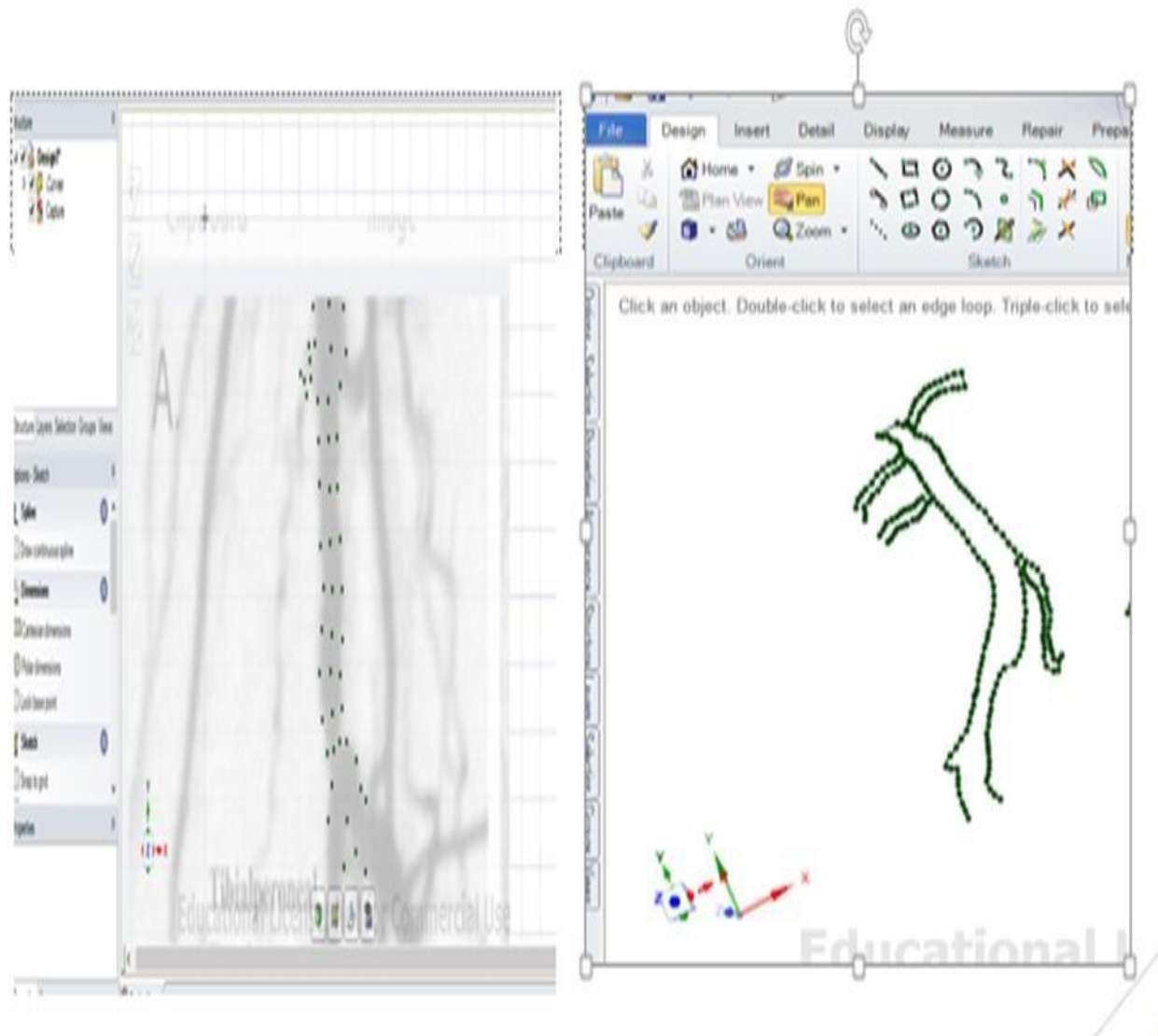


Figure 3.2 Steps of design

Initially the CT scan image of a 62-year-old adult is considered to model the above shown cerebral artery. The CT scan image shows several capillaries leading to various connections in the brain. However, for the simplicity of the design the partial part of the image is taken for modeling.

As the part of design process, the image is inserted into the design window and splines are carried out with respect to the image curvature. Then the splines are connected to a completed 2-D planar image. The design software Space Claim used for this construction has the unique feature of prompting the three-dimensional plane to the complex curvature. Using the three-dimensional plane and the sweep options, the 3-D model is prepared as shown in the Figure 3.3.

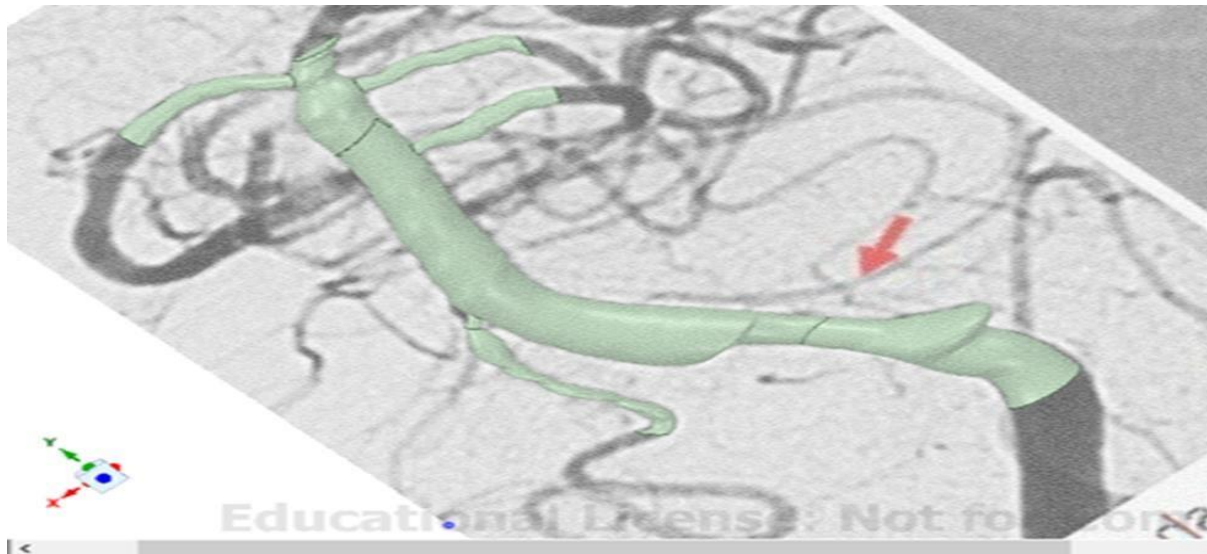


Figure 3.3 CAD design model constructed from CT scans

Now the above-obtained model was designed by dividing the artery into three divisions and each capillary into a separate division. The extrude option is used in joining the pieces of 3-D parts created separately. These can be done in Space Claim easily by dragging the images without using the assembly options. Figure 3.3 shows us the major cerebral artery of 14 mm diameter which flows into the brain with five capillaries leading to the tissues of the brain. The most complicated structures of capillaries which are 2mm in diameter can be seen at each outlet division.

Each capillary attached to the tissues is approximated to a certain length for making the design process simple. The connections at the major artery and capillary are done using the sweep extrude option of Space Claim which prompts insertion of the capillary to the major artery following the splines created as bounds for the extrusion. In this study the blood pumped by the heart to the cerebral arteries is considered as the inflow and the blood flows in the major artery followed by the smaller arteries and capillaries through the pump of heart called as systole phase.

3.2.3 Approximated Tumor in Tissue Connection

The artery-capillary unit designed in the Space Claim design module is taken into the meshing software Hyper Mesh to do the mesh. Using the constructive options in Hyper Mesh a circular tissue and an elliptical tumor is designed and integrated to the available three-dimensional artery. The Figure 3.4 explains the design of CT scan.

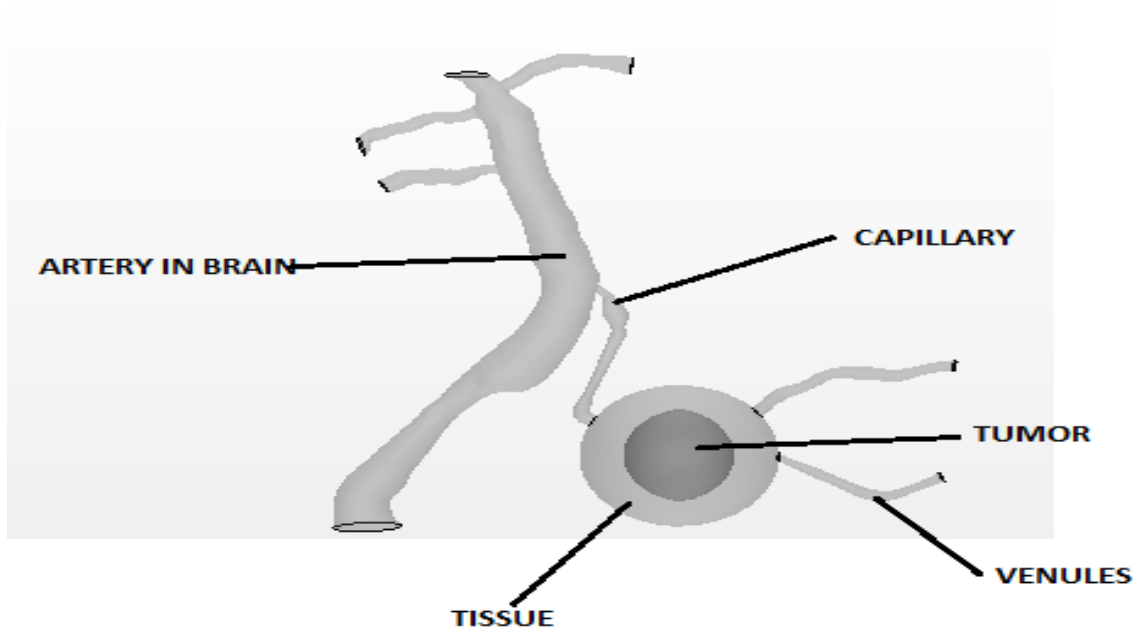


Figure 3.4 3D design from CT scan

3.2.4 Reconstructed Brain with Tumor

In order to obtain the three-dimensional model of the realistic brain from the available 3-D modeling software, we need to have the slices of the patient's complete brain which is taken as MRI scans. MRI scans, typically in the form of number of slices, provide the accurate geometric features of the patient complete brain. Many slices of brain in the form of MRI scans are needed to convert the MRI scans into a complete three-dimensional brain. The number of scans needed may vary from 80-120 depending on the accuracy of the model which has to be derived from the input scans. However due to difficulty in finding the specific patient's personal data through the online resources, in this study only eight slices of the MRI scans of a specific patient are considered in building up the three-dimensional model. The slices considered for this study consist of a tumor of volume 128.9 mm^3 at the distance of 13 mm and 7.3mm from the frontal part and the right side of the brain respectively. These slices are taken into the 3-D Doctor imaging software which prompts us to arrange the slices in the appropriate order of the human brain. It also allows us to copy the image repeatedly and arrange it an orderly manner. Now using the eight slices, the copies are made and arranged in an orderly manner to obtain the image with series of clicks. However due to the inadequate information in the form of slices, the image obtained in the imaging software was a partial one. Then the obtained feature is modeled into the complete brain using Space Claim features such as loft, sweep, etc. The final image obtained as the realistic brain is as shown in Figure 3.5.

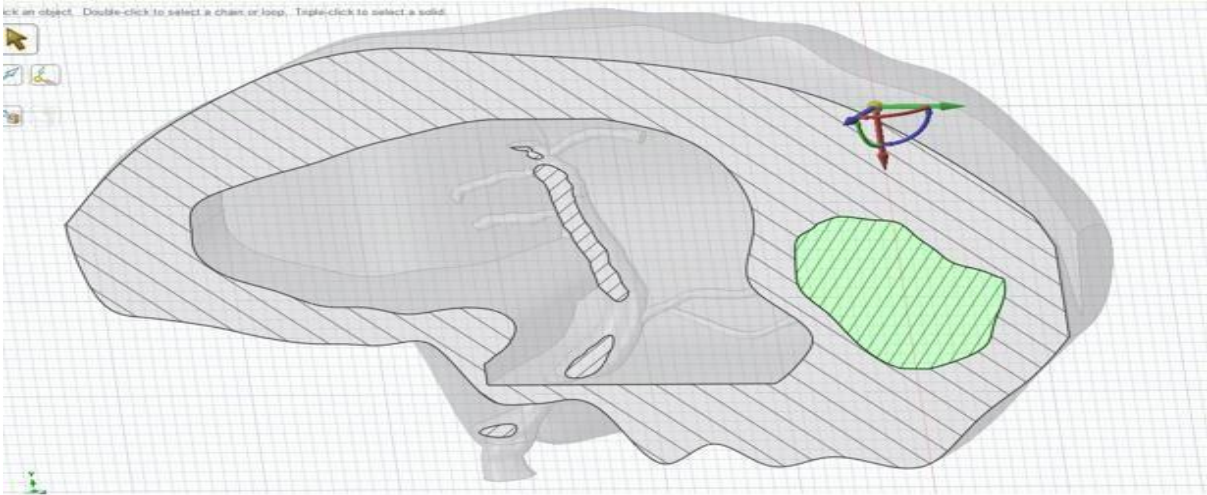


Figure 3.5 3D design of reconstructed brain constructed from the MRI scans

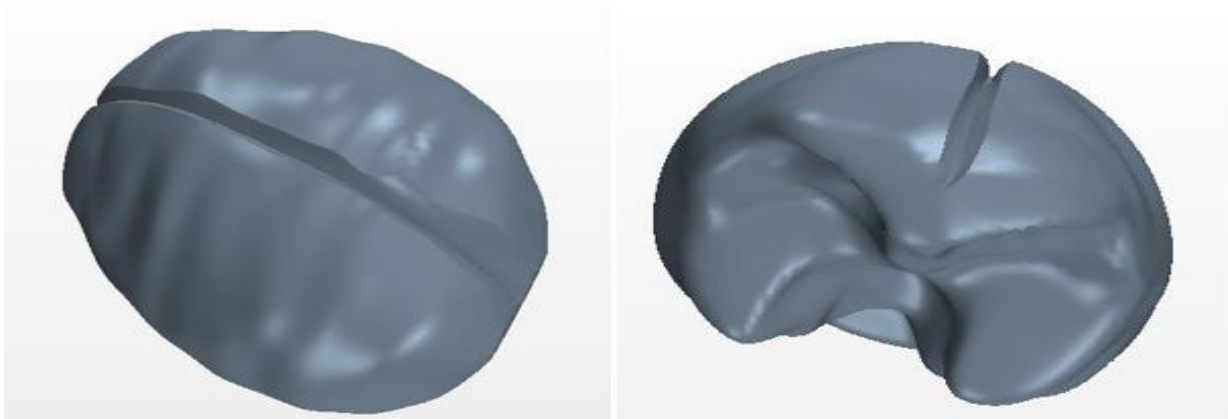


Figure 3.6 3D design model of reconstructed brain from MRI scan

Now the previously designed artery is integrated into the tumor-affected brain cavity which was left apart during its design due to inadequate data at certain central portions of the brain. Space Claim was again used for this job and the final unit of the brain with a cerebral artery-capillary network is shown in Figure 3.7.

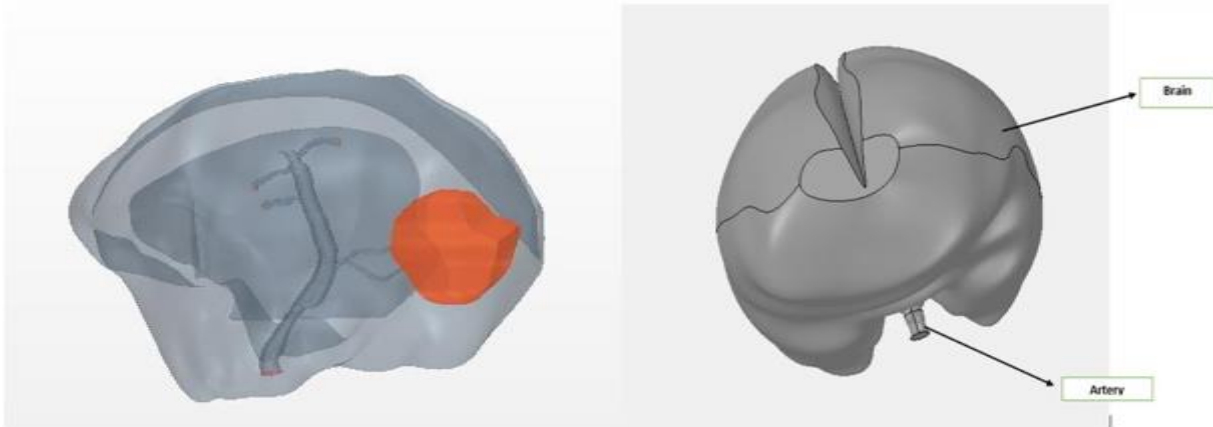


Figure 3.7 Transparent and opaque 3D design views

As an initial attempt, to the velocity and pressure variations during the blood flow to the brain and tumor region are analyzed in the imaginary circular tissue region with an elliptical tumor. Then the model of realistic brain shown above is used for analyzing the blood supply and drug administration which reflects the real case scenario. Table 3 shows the dimensions assigned to the two models considered for study.

Table 3: Physical Dimensions of the Computational Model

Parts	Initial Attempt 3D Model with an Imaginary tissue and tumor connection	Realistic 3-D Model with a Flow Path of Blood in Arteries and a Tumor Affected Brain
Artery	11mm Length,5mm Dia	11mm Length,5mm Dia
Capillary	5mm Length,1.5 mm Dia	5mm Length,1.5 mm Dia
Tissue	314mm²	3968mm²
Tumor	120mm²	35mm²,128.9 mm³

3.3 Selected Physics for Flow Model

Blood behaves as a non-Newtonian fluid. Also the real case scenario of modeling blood includes consideration of blood flow as two-phase flow as it contains red blood cells, white blood cells and corpuscles suspended in serum. However, due to the complexity in dealing with that real case flow of blood, the model in this study is initially simplified to Newtonian and then extended to non-Newtonian single-phase blood flow, which is further considered with drug inflow as another discrete phase. Table 4 details the physics assigned in modeling the blood and drug flow.

Table 4: Physics Assigned to the Model

Blood Flow	Newtonian with constant viscosity input, Implicit Unsteady, Constant density, Laminar, Segregated Flow	Non Newtonian with varying viscosity input, Implicit Unsteady, Constant Density, Laminar, Segregated Flow
Drug Flow	N/A	Multi-phase, Eulerian-Lagrangian Model, Injectors, Spherical Particles, Liquid, Density, Particle Dimensions

3.3.1 Newtonian and Non- Newtonian Fluid

Newtonian and non-Newtonian fluids are the fluids which obey and do not obey the Newton's law respectively. As Newton's law says that shear stress is directly proportional to shear rate, Newtonian fluids have the constant viscosity coefficient, whereas the other type of flow has varying viscosity coefficients as the shear stress and shear rates are not directly proportional to each other. Experiments on human blood vessels show the existence of Newtonian flow in large

arteries [1]. However, smaller arteries and capillaries show non-Newtonian behavior [8].

3.3.1 Viscosity of Flow Model

Several viscosity models are used for setting properties of the material for which the flow is calculated. However, in this study Carreau Yesuda model is used because of its known popularity in presenting the decreased velocity with applied shear strains, called shear thinning property. This model is suitable for non-Newtonian flow of blood in calculating the velocities at the wall [4, 8].

$$\eta_{\text{eff}}(\gamma) = \eta_{\infty} + (\eta_0 - \eta_{\infty})(1 + (\lambda\gamma)^2)^{\frac{n-1}{2}}$$

where:

η_0 = viscosity at zero shear rate

η_{∞} = viscosity at infinite shear rate

λ = relaxation time

n = power index

The values of 0.056 Pa-s, 0.004 Pa-s, 3.313 s, 0.3568 are used respectively for the above parameters [7].

3.3.2 Setting Porous Medium

The tissues of the brain are complex and exhibit porous nature. The nutrients carried by the blood will be delivered to the cells in the tissue in the form energy. The energy intake and waste disposals into the cells and venules are done by perfusion through the pores. In general, porous medium is defined as a group of closely bound particles which exhibit anti dispersible properties in the liquid through which it flows [8]. Mathematically it is given as follows:

$$s = \frac{\text{Total interface area}}{\text{Total Volume}}$$

$$\varepsilon = \frac{\text{Void Volume}}{\text{Total Volume}}$$

where S: Particular Surface

ε : Porosity

3.3.3 Brinkman's Flow Model for Porosity

Various models are utilized in analyzing the porous nature of biological tissues. Darcy model is one of the basic models used in analyzing flows in porous media. However, many other models such as Brinkman's and generalized Darcy models are derived by extending the Darcy model. These models are used in many experiments on analysis of mass transfer in porous medium and were tested for their suitability of usage in the regions of human body [2]. Results of experiments explain that Brinkman's porosity model could offer better results in analyzing the mass transport in arteries near tissues. Since in this study blood flow and drug distribution in two porous systems (i.e.,) tissue and tumor, are considered, Brinkman's model is used for defining porosity of the system.

3.3.4 Darcy and Brinkman's Models

According to Darcy flow model through a porous medium the drag force on the body is proportional to the viscosity of the fluid and velocity over the body, whereas Brinkman's model involves dealing with an extra term, comparable to the momentum diffusion term in the Navier-Stokes equation [2]. The following formula shows the mathematical representation of two models:

$$U = \frac{(G - \overline{\mu})\nabla^{(2)}U)K}{\mu}$$

where:

U=Velocity of Blood K= Porosity Parameter

$\overline{\mu}$ =Viscosity of Blood G= Pressure Gradient

In this study, due to complexity in solving the Brinkman's model, the modified form, Brinkman's Forchheimer equation, which takes care of inertial and viscous terms, is considered. The viscous and inertial terms are calculated using the Erguns empirical formula.

$$-\nabla P = \frac{\mu U}{K} + \beta \rho U^2$$

where $P_v = \frac{150\mu(1-\kappa)^2}{\kappa^3 D^2}$ and $P_i = \frac{1.75\rho(1-\kappa)^1}{\kappa^3 D^1}$

Here the change in pressure and variations of molecular viscosity in the above nonlinear equation are determined experimentally, whereas the porosity of the tissue and tumor regions is given as 0.3 and 0.2 as the white matter; tissue of brain has the porosity 0.3 [5]. Also the porous inertial and viscous resistance are assumed as 10500 kg/m⁴, 1.5E-3 kg/m^{-s} and 8000kg/m⁴, 1.5E-5kg/m^{-s} [5].

3.3.4 Drug Inflow Model

Fluid flow can be represented mathematically in Eulerian and Lagrangian flow. The basic difference these two flows is the Eulerian flow model tracks particles with respect to a fixed origin considering the particle phase as a continuum. The equations in Eulerian are developed using conservation equations on a control volume basis, where as in Lagrangian type of flow the particles are considered as the dispersed phase and the particle tracking with respect to its path is done individually. Because of this quality, Lagrangian model is a good fit for our objective of study to

trace the overall particle dispersion pattern. In this study the Lagrangian flow model is considered based on the objective of the study [16].

The Lagrangian equation for particle flow is given as:

$$(dU_p)/dT = F(U - U_p) + G(\rho_p - \rho)/\rho_p + F_1$$

where

U_p : Particle velocity vector

F_1 : Additional forces

F : Inverse of relaxation time

U : Fluid velocity

The above equation is analogous to Navier-Stokes equation and shows the force balance of the particle flow. The first term in the right hand side includes the drag force which is expected on the particle by the fluid. Here in this study the relaxation time includes the terms drag force and coefficient of drag which are derived from Stoke's law as it works best for flows with minute cross- sections. The Reynolds number is calculated for this study considering the slip velocity of particle which is the relative velocity between fluid and particle. The obtained Reynolds number guides us to choose the drag models for the fluid study. In this study the obtained Reynolds number demands the use of Nauman-Schiller equation which is one of the drag models. The second term of the equation takes care of the gravity force exerted by the fluid flow on the particle. The additional forces in the form of viscosity changes due to porosity responsible for changes in the

flow are also considered here. The below terms show the mathematical expressions considered in each term of the equation:

$$\text{Coefficient of drag } C_d = 24(1 + 0.15 R_{EP}^{0.687}) / R_{EP}$$

$$\text{where Reynolds number } R_{EP} = \rho \cdot v \cdot D / \mu$$

$$F = d^2 \rho / (18 \mu f_d)$$

$$\text{where } f_d = 0.5 c_d v_s^2 A \rho$$

3.4 Designed Simulation Model

3.4.1 Healthy Artery

The geometry of the healthy artery is shown in Figure 3.8. The length of the artery is 11mm and the diameter is 5mm. The capillary is of length and diameter 5mm and 1.5mm respectively. A tissue region assumed to be spherical with dimensions $320mm^2$ is also attached to the artery-capillary network. The geometry of the healthy artery-capillary system is as shown in the Figure 3.8.

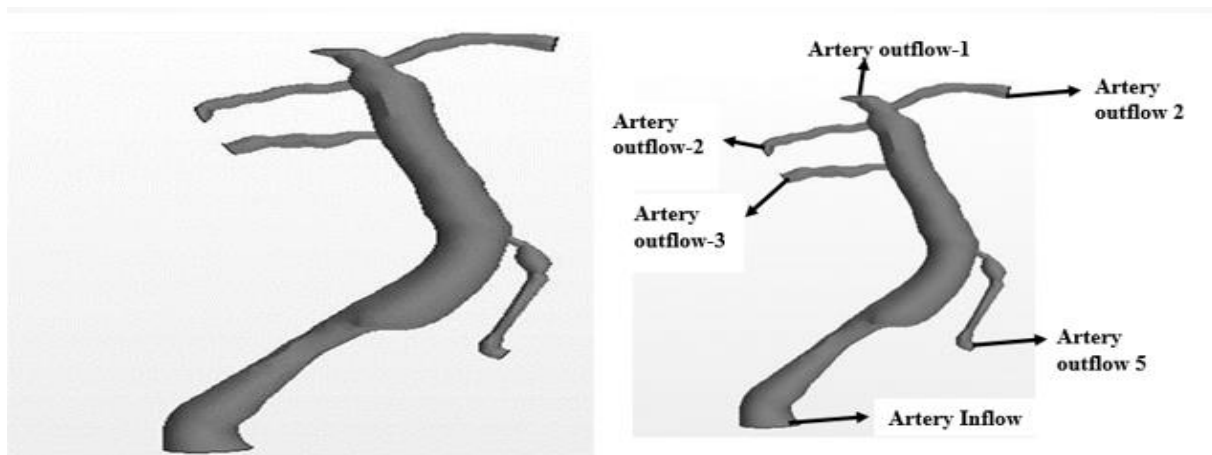


Figure 3.8 Geometry of the healthy artery-capillary network with healthy tissue

3.4.2 Artery-Capillary Network with an Imaginary Tumored Tissue

The geometry of the unhealthy imaginary tissue with artery-capillary network is as shown in the Figure 3.9. A tumor in elliptical shape is considered to be present in the spherical tissue.

The dimensions of the tumor are 120mm^2 .

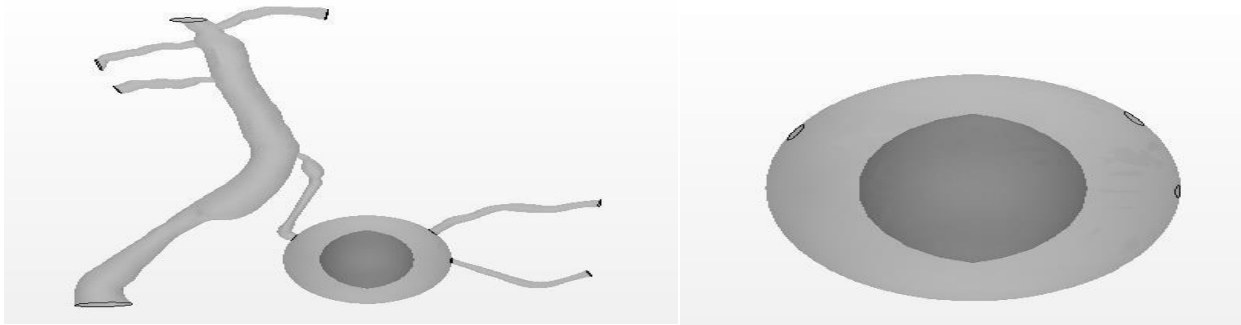


Figure 3.9 Geometry of the model with approximated tissue-tumor connection

3.4.3 Model with Realistic Brain Tissue

The geometry of the tumored brain is as shown in Figure 3.10. It has the average dimensions of 140 mm in length and 120 mm in width with the thickness of 110mm. Also the average dimensions of the tumor are 7.7 mm length, 4.65mm width and 3.6 mm thick.

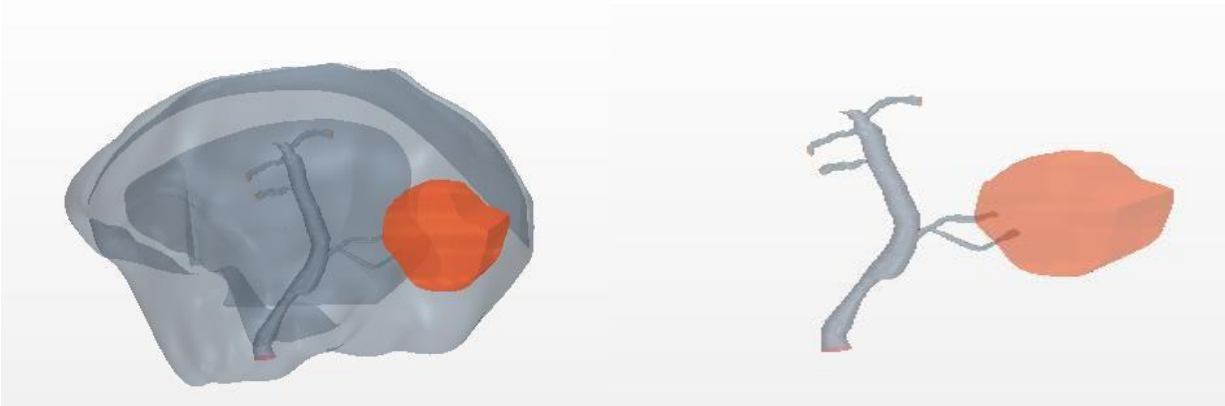


Figure 3.10 3D model with tumor view

3.4 Mesh Generation for Approximated Healthy Tissue with Artery-Capillary Network

The following are the mesh models considered for mesh. For this study Surface Remesher, Prism Layer Mesher and Trimmer are the mesh models used. The base size given is 0.03mm with three prism layers and 25% thickness of the base size.

Unhealthy Tissue Artery-Capillary System:

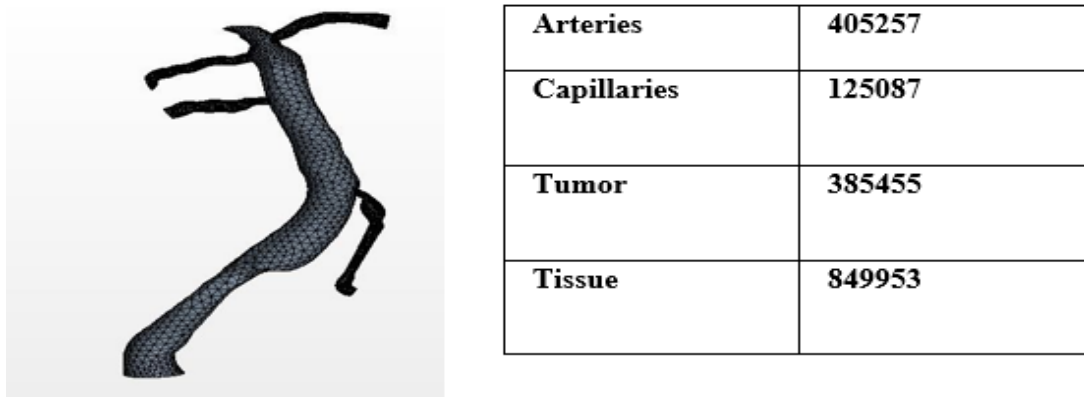


Figure 3.11 Artery mesh with node values

Figure 3.11 shows mesh Generation with number of cells for unhealthy approximated tissue artery-capillary system.

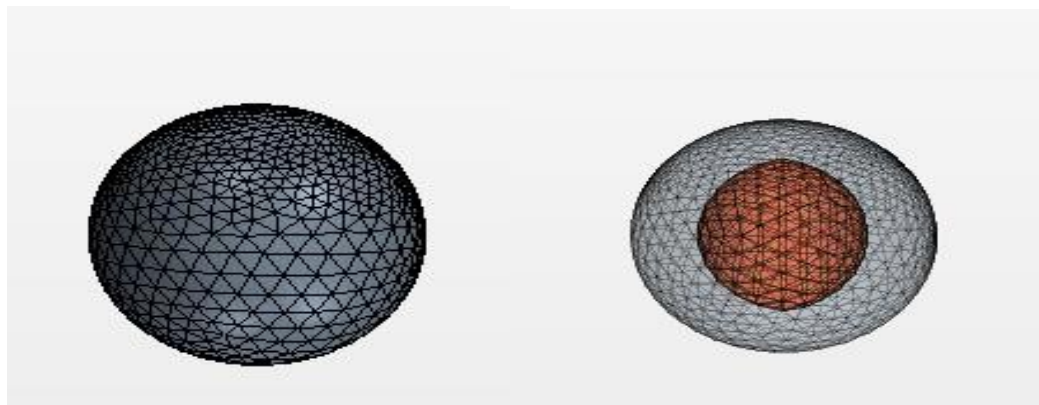


Figure 3.12 Unhealthy spherical-shaped approximated tissue with tumor

3.5 Mesh generation for Healthy and Tumor-Affected Reconstructed Brain Tissue with Artery Capillary Network

The mesh of the realistic brain is generated using Hyper Mesh. The base value is given as 0.01mm with three prism layers. The surface remeshing is done manually at the complex curvatures. The generated mesh for curved healthy and tumor-affected realistic brain tissue and artery system is shown in the Figure 3.13. The Figures 3.14(a) and 3.14(b) show the mesh and node values of artery. Also the Table 5 shows the mesh values of the entire brain.

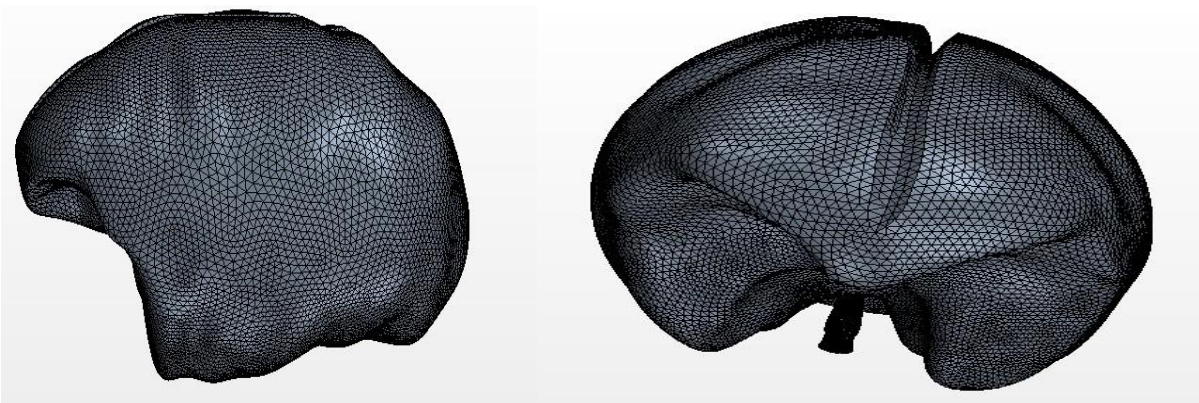
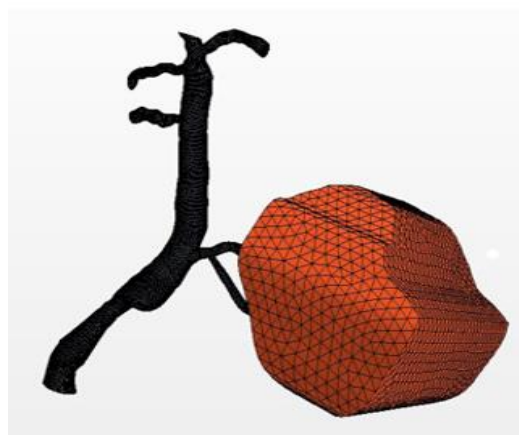


Figure 3.13 Mesh of Reconstructed Brain Tissue



3.14 (a) Mesh for approximated artery with the reconstructed tumor

Arteries	Cell:136870 Faces:258640 Vertices:3097
Capillaries	125087
Tumor	Cells :14831 Face:27986
Tissue	Cells:327935 Faces:627676 Vertices:6916

Figure 3.14(b) Mesh and node values of artery and tumor with reconstructed brain tissue

Table 5: Mesh Values of Two Models

Mesh	No of Cells	No of faces	No of Vertices
Healthy Artery Unit with Capillaries	505537	1116710	186467
Approximated Artery System with Tissues	733192	2934642	451485
Artery System with Tissues and Tumor	1118647	3582540	612988
Reconstructed Brain tissue	849953	627676	69162
Reconstructed Brain with tumor	864784	683648	72535
Reconstructed Brain with tumor with integrated cerebral artery	1370321	5582940	812688

3.6 Governing Equations

Navier-Stokes equation is used for analyzing and computing the dynamics of flow. However some assumptions are made in analysis depending on the requirement.

3.6.1 Blood flow

As in this study initially analysis is done for finding the flow velocities and pressures in arteries carrying blood from heart to brain, both Newtonian and non-Newtonian natures of blood were analyzed. For this the Navier-Stokes equation is considered as Newtonian incompressible and non-Newtonian incompressible respectively.

$$\rho \left(\frac{\partial \mathbf{u}}{\partial t} + (\mathbf{u} \cdot \nabla) \mathbf{u} \right) = -\nabla p + \mu \cdot \nabla^2 \mathbf{u}$$

The above equation is the general Navier-Stokes equation for incompressible flow. This equation remains the same for non-Newtonian flow analysis but it has to be modified for dealing with the other case. The modified equation is as shown below:

$$\rho \left(\frac{\partial \mathbf{u}}{\partial t} + (\mathbf{u} \cdot \nabla) \mathbf{u} \right) = -\nabla p + \nabla(\eta(\nabla \mathbf{u} + (\nabla \mathbf{u})^T))$$

Here in the above equation the viscosity and shear rate vary with time.

3.7 Boundary Conditions for Model

- **Velocity inlet with transient velocity data input:** The set of tabulated values is given as input velocity table for inlet of artery. This velocity table is observed from the waveform calculated by Hashimoto [17]. The changes of velocities with respect to time are shown in the Figure 3.15 in Table 6.

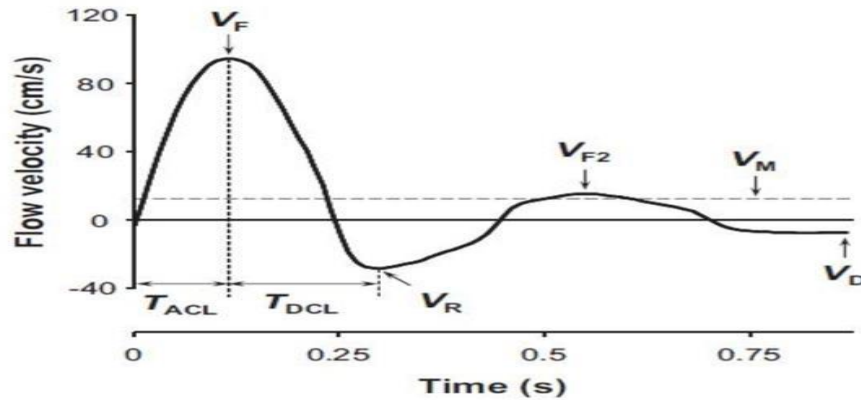


Figure: 3.15 Inlet velocity waveform

Table 6: Velocity Range with respect to Varying Velocities

Variable	Velocity range (cm/sec)
Systolic forward peak velocity (V_f)	69 ± 19
Diastolic reverse peak velocity	-19 ± 6
End diastolic velocity (V_d)	8 ± 4
Time-averaged mean velocity (V_m)	1 ± 3

- Pressure outlet at all the artery outputs and venules output:** The outlet boundary is set to zero pressure conditions.
- Porosity equation for tissue and tumor:** The tissue is considered spherical in shape in an initial case and then it is improved to the real-case brain tissue. In both the design models a tumor with imaginary shape is being enclosed in the tissues. A connection from artery and the tissue is taken care of by the capillary and the interfaces created at the connection points. These interfaces and the tissue and porous regions are assigned with different porosities 0.3 and 0.2 respectively. The other entities such as viscosity and inertia resistance required for the regions are tabulated in Table 7.

Table 7: Porosity Assigned for Different Regions of Brain

Porosity Parameters	Tissue Region	Tumor Region
Porosity	0.3	0.2
Porous Inertial Resistance	10500kg/m⁴,	8000kg/m⁴,
Porous Viscous Resistance	1.5E-3 kg/m^{-s}	1.5E-5kg/m^{-s}.

Input for drug flow model in multiphase Lagrangian flow: To set the particle flow for analyzing the drug concentration distribution, Lagrangian multiphase flow is considered. A separate physics is set for analyzing the particle flow in the artery-capillary-tissue-tumor network. The flow rate is given an inlet to the artery using Lagrangian injectors. Also particle specifications such as diameters and shape are specified. The Table 8 shows the flow input and particle specifications given to analyze the flow.

Table 8: Drug Particle Parameters

CONCENTRATION	PARTICLE DIAMETER	PARTICLE DENSITY
0.01mL	5.0MICRON	1460 Kg/M³
0.03mL		
0.05mL	0.5 MICRON	1960 Kg/M³
0.08mL		

3.8 Unsteady Computational Parameters

Simulations are carried out considering the segregated flow solver to solve the flow equations. The solution update in star ccm+ for the segregated model is done using the SIMPLE solver. Here in this study the first-order discretization is used to solve this problem and results are drawn at different time steps with the maximum physical time of 0.8sec, time step of 0.01sec and 50 inner iterations for each time step. Also under relaxation factors of 0.7 and 0.3 are considered for velocity and pressure respectively [7].

4. RESULTS AND DISCUSSIONS

The computational simulation model developed is used to determine the velocity and pressure changes in the flow of blood with respect to the cardiac cycle in the brain region with porous tissues. Further particle distribution of drug administered into the targeted tumor region is observed in terms of velocities with which drug reaches the target. Also the various concentrations administered are analyzed for particle velocity with changed particle size, density, concentration distribution and optimized concentration to determine the maximum safest drug dosage to treat tumor in brain.

4.1 Results for Blood Flow in the Artery with Approximated Tissue-Tumor Connection

Pressure Variations:

Pressure at 0.01 Sec:



Figure 4.1 (a) Pressure at 0.01 sec in healthy artery tissue region



Figure 4.1(b) Pressure at 0.01 sec in tumored artery tissue region

The Figures 4.1(a) and 4.1(b) show the pressure distribution of healthy and tumored regions of brain tissue connected to the artery-capillary network. Here in Figure 4.1(a) the pressure ranges from -701.9 pa to 2583.3 pa and in Figure 4.2 (b) it ranges from -49.9 pa to 641.72 pa. In specific, the tissue region of brain faces the pressure ranging from -44.86 pa to 612.18 pa in a healthy artery where increase in pressure range is observed in tissue region due to the presence of tumor.

Pressure at 0.1 Sec:



Figure 4.2 (a) Pressure at 0.1 sec in healthy artery tissue region

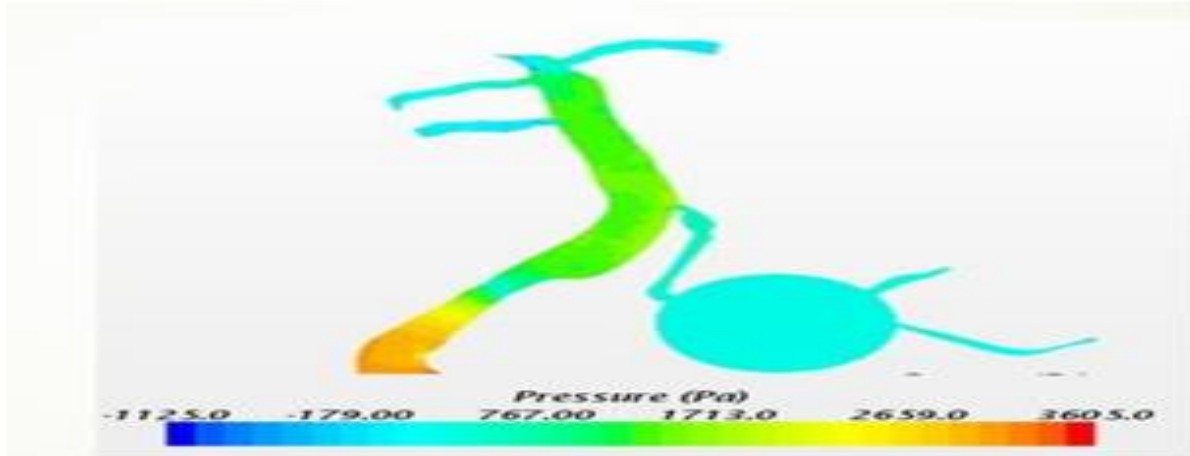


Figure 4.2 (b) Pressure at 0.1 sec in tumored artery tissue region

The Figures 4.2(a) and 4.2(b) show the pressure distribution of healthy and tumored regions of brain tissue connected to the artery-capillary network. Here in Figure 4.2(a) the pressure ranges from -985.90pa to 3180.3 pa and in Figure 4.2 (b) it ranges from -1125pa to 3605 pa. Here the tumored tissue region of brain faces the pressure ranging from -179 pa to 767pa in which there is an increase in pressure of 24% from the previous reading shown in Figure 4.1(a) and 4.1(b).

Pressure at 0.25 Sec:



Figure 4.3 (a) Pressure at 0.25 sec in healthy artery tissue region

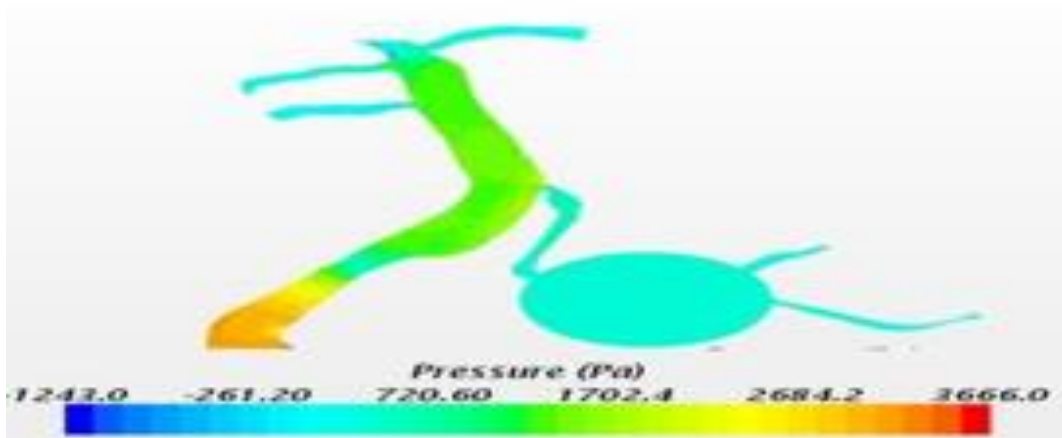


Figure 4.3 (b) Pressure at 0.25 sec in tumored artery tissue region

The Figures 4.3(a) and 4.3(b) show the pressure distribution of healthy and tumored regions of brain tissue connected to the artery-capillary network. Here in Figure 4.3(a) the pressure ranges from -905pa to 3620 pa and in Figure 4.2 (b) it ranges from -1243pa to 3666 pa. Here the tumored tissue region of brain faces the pressure ranging from -500 pa to 726pa which is comparatively 34% less than the pressures at 0.1 sec.

Pressure at 0.5 Sec:

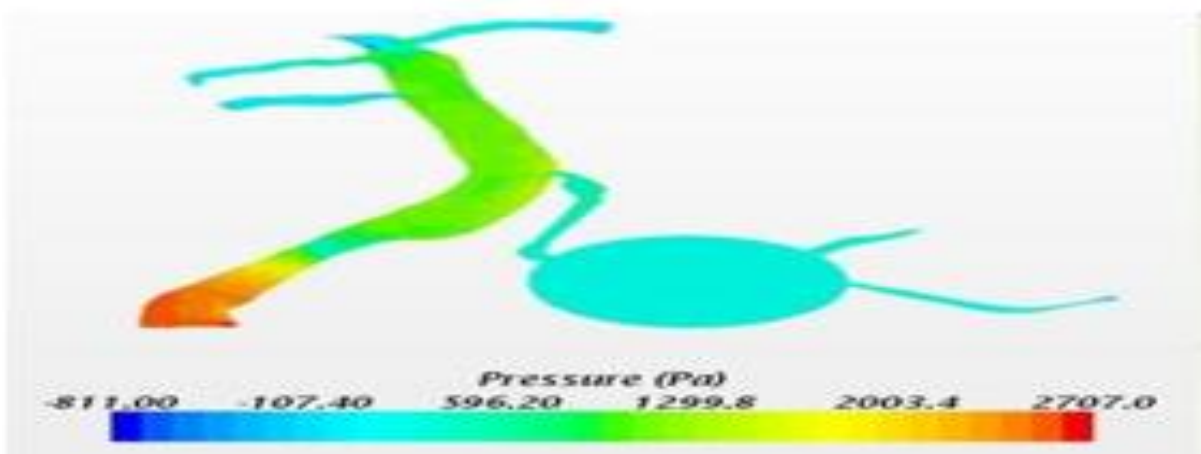


Figure 4.4 (a) Pressure at 0.5 sec in healthy artery tissue region

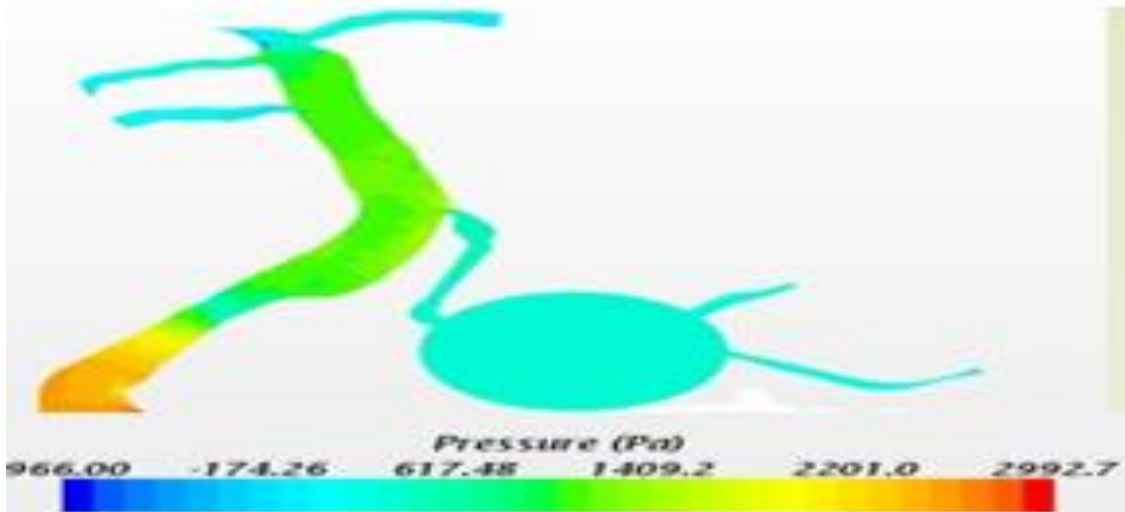


Figure 4.4 (b) Pressure at 0.25 sec in tumored artery tissue region

The Figures 4.4(a) and 4.4(b) show pressure ranges from -811 pa to 2707 pa and 966 pa to 2993 pa. Here the tumored tissue region of brain faces the pressure ranging from -175 pa to 615pa.

Velocity Variations:

Velocity at 0.1 Sec:

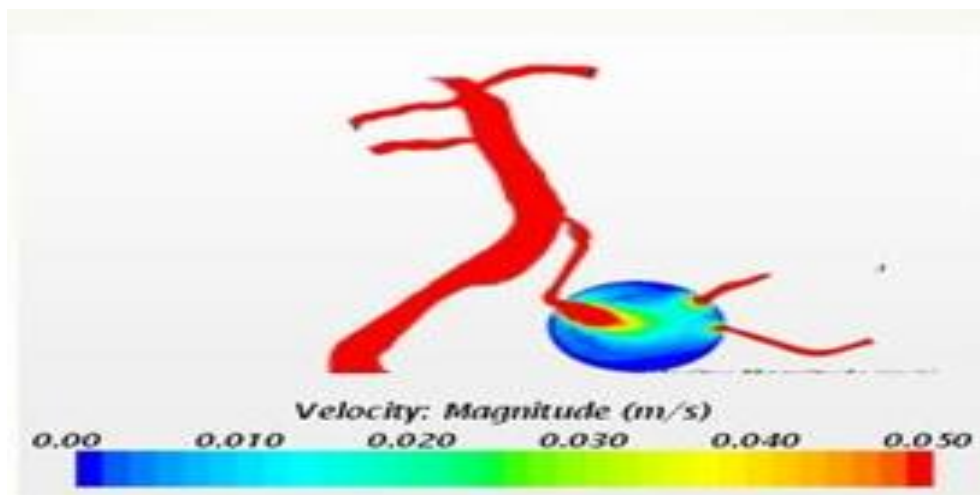


Figure 4.5 (a) Velocity at 0.1 sec in healthy artery tissue region

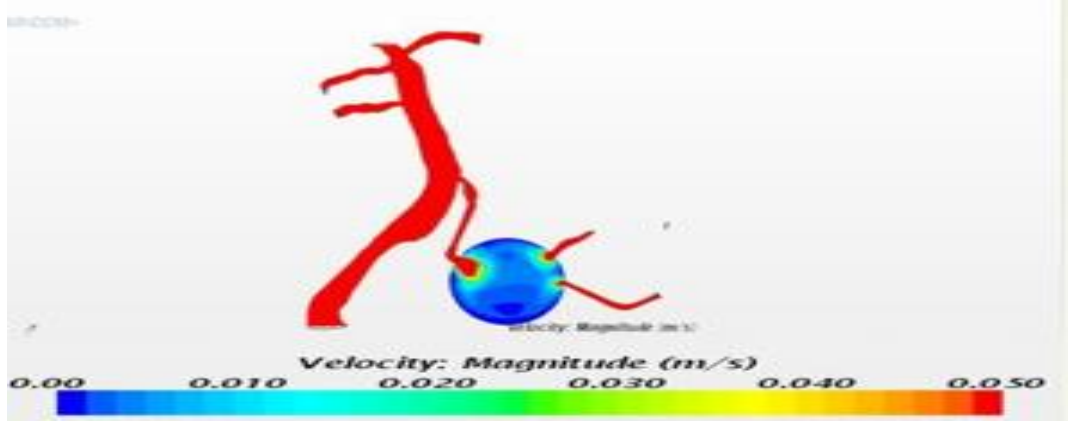


Figure 4.5 (b) Velocity at 0.1 sec in tumored artery tissue region

The Figures 4.5(a) and 4.5(b) show the velocity distribution of healthy and tumored regions of brain tissue connected to the artery-capillary network. The velocity ranges from 0 to 3.98m/sec in non-tumor case and 3.78m/sec in tumor case, with less velocity in regions of tumor and tissue. The above figure more precisely shows the values in closer range which is fixed to 0.05m/sec to show the tumor velocity. The above figures show the obstruction created by the tumor for the blood flow thereby reducing the velocity in the tumor tissue region.

Velocity at 0.5 Sec:

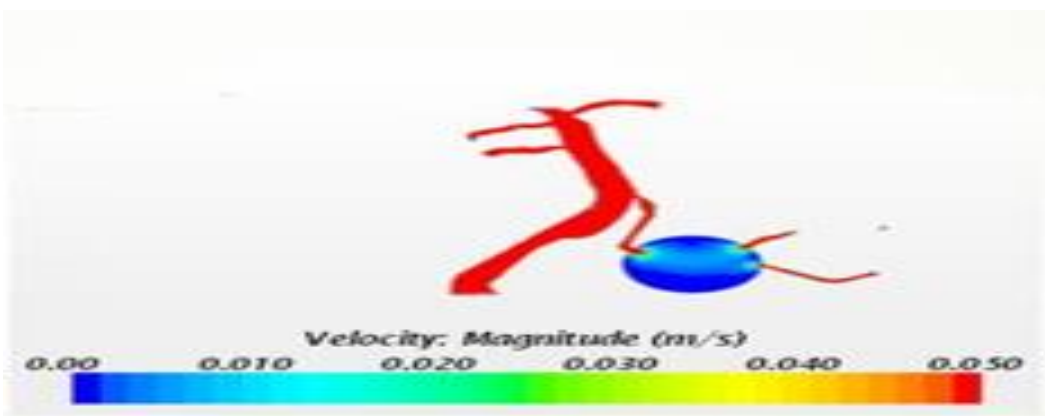


Figure 4.6 (a) Velocity at 0.5 sec in healthy artery tissue region

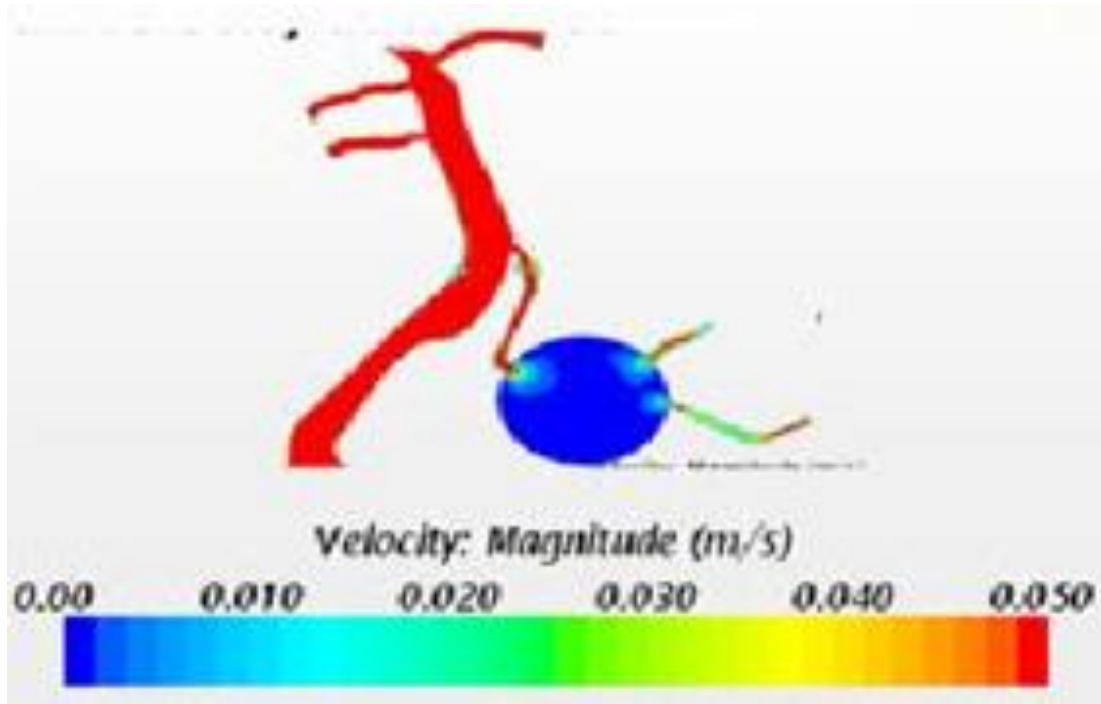


Figure 4.6 (b) Velocity at 0.5 sec in tumored artery tissue region

The Figures 4.6(a) and 4.6(b) show the velocity distribution of healthy and tumored regions of brain tissue connected to the artery-capillary network. The velocity ranges from 0 to 4.4m/sec in non-tumor case and 4m/sec in tumor case, with less velocity in regions of tumor and tissue. The above figure more precisely shows the values in closer range which is fixed to 0.05m/sec to show the tumor velocity. The Figure 4.6(b) shows the obstruction created by tissue for the blood flow and also changes venules with respect to the cardiac inflow as the cycle is being completed.

The plot in Figure 4.7 shows the velocity distributions at the 0.1 time step with respect to position. The x-axis is taken as the diameter of the artery tube and the y-axis shows the velocity values. The non-Newtonian velocity of tumored and healthy velocity lies in between the values of Newtonian velocity. Siebert says that Newtonian model cannot predict the

accurate values at the regions such as large and minor arteries [18]. Even in this study the Newtonian flow exceeded the values of porosity and boundary conditions assigned.

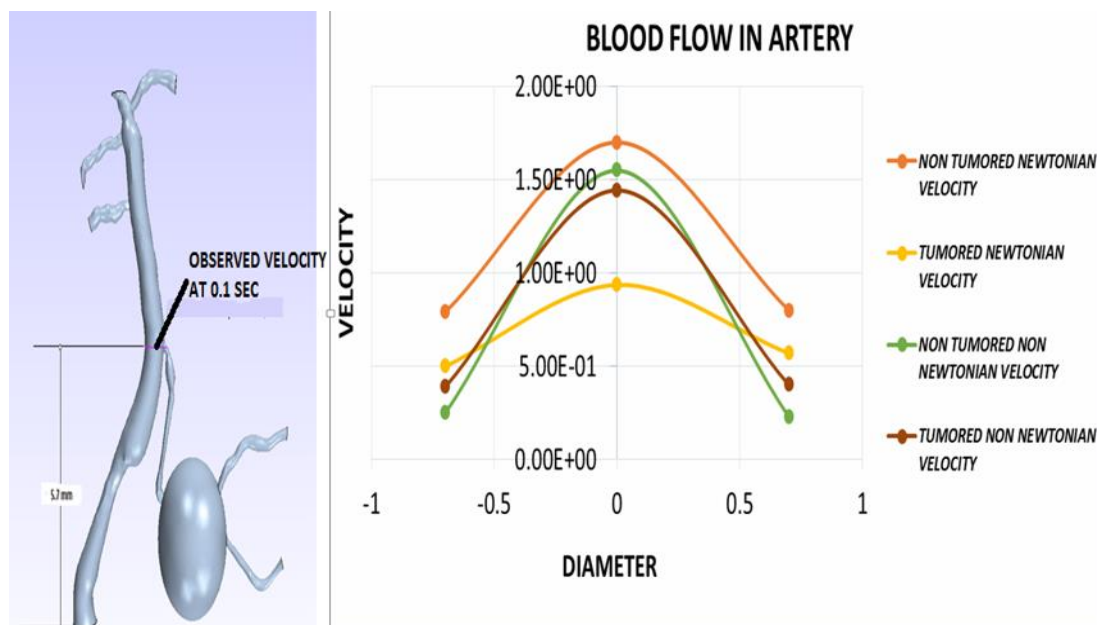


Figure 4.7 Velocity plots which shows comparisons of velocities with respect to diameter

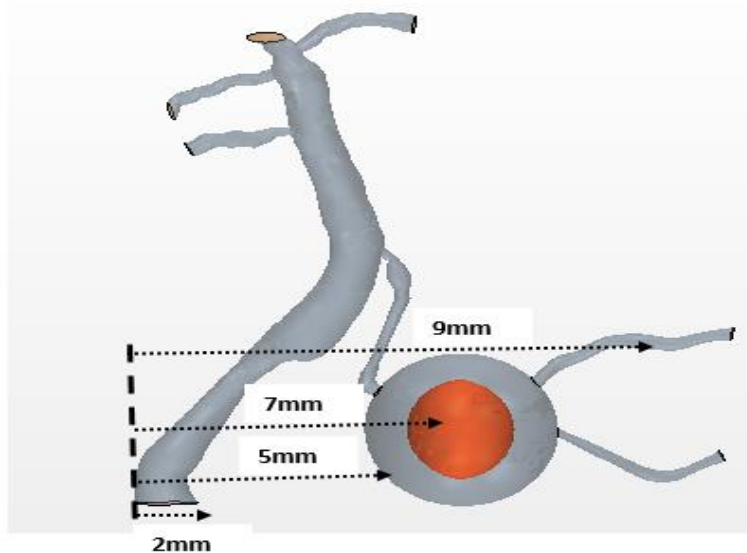


Figure 4.8 Points considered to draw plots with respect to position from the reference

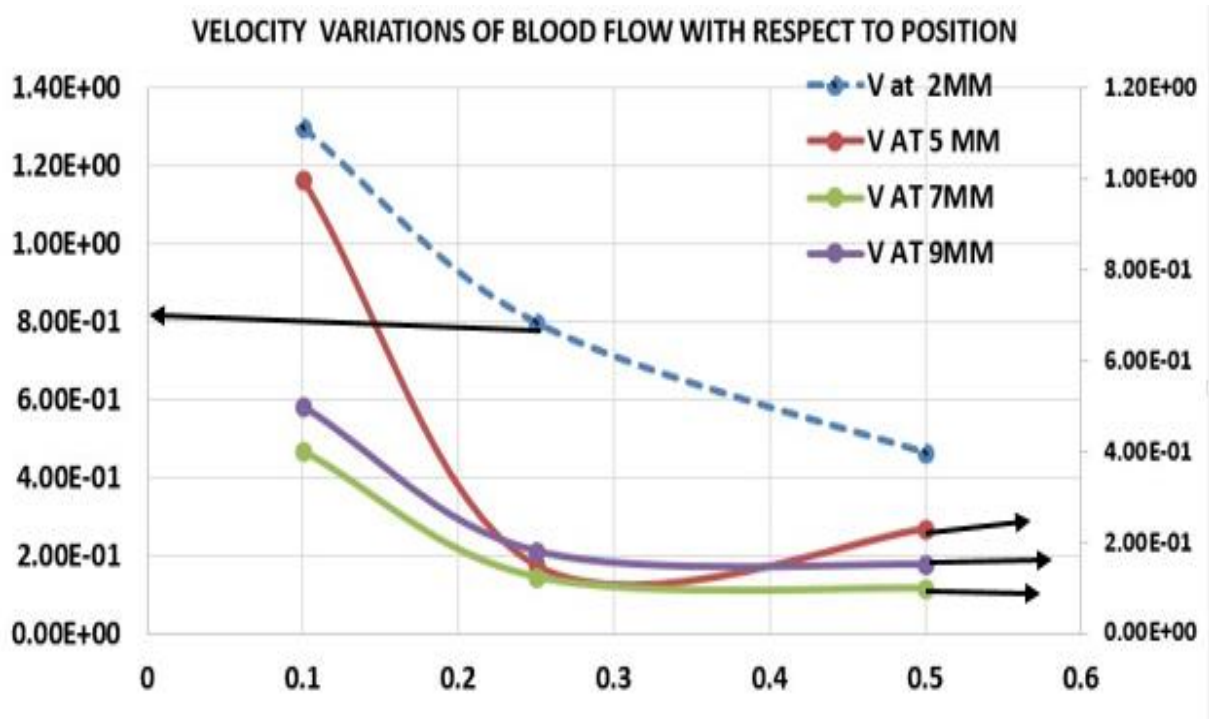


Figure 4.9 (a) Velocity plots with respect to position

The plots in Figure 4.9(a) show the velocity variation with respect to position of the artery. As we move from left to right with respect to position on x-axis as shown in Figure 4.8, the velocity decreases in the area of capillary due to higher resistance. The values vary from 1.4 m/sec in higher arteries to 0.18 and 0.15 at lower arteries. This shows the real mechanism of blood flow from heart to capillaries, which is generally lower to allow time for exchange of energy to tissues. Since the values are higher for major arteries, the plots shown above include two sets of values which shows both the flows in major arteries that are much higher than the other set of values in regions other than capillaries. In the above plot the lines obtained with the artery velocity is represented by the line with left-sided arrow, whereas the rest of the flow lines are shown with right arrows.

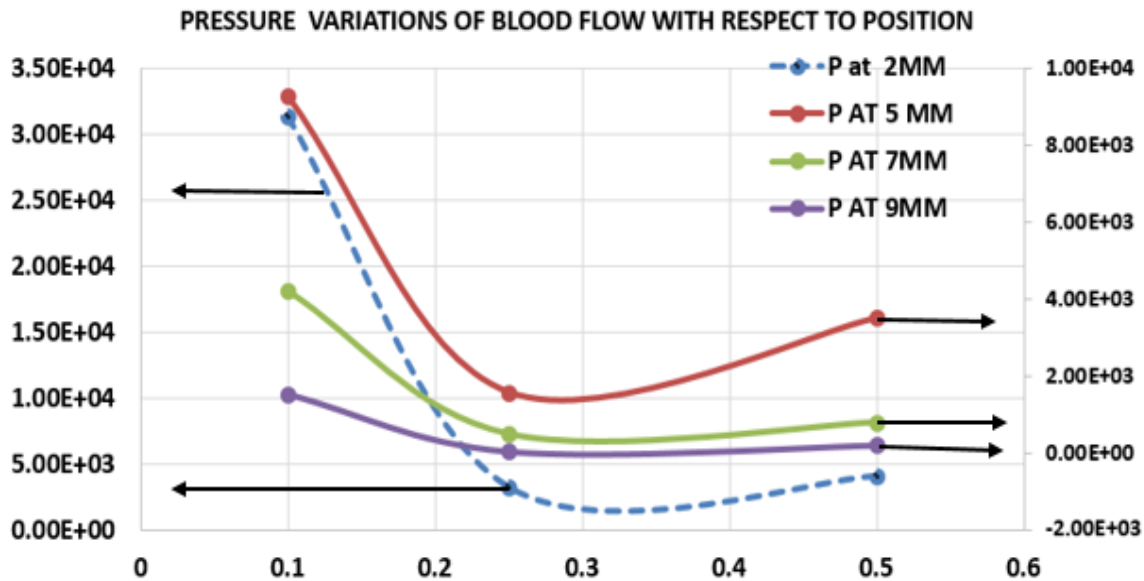


Figure 4.9(b) Pressure variations of blood flow with respect to position

The plot in Figure 4.9(b) shows the pressure distribution at 0.1, 0.25, 0.5 time. The pressure reduces with the resistance to flow due to obstruction, so there is a pressure variation in the tissue tumor region. The artery at 2mm shows the highest pressure as there is no obstruction to the flow, whereas the capillaries and tumor-tissue region have lower pressure. Then the outflows are shown with raised pressure due to the suction created at the heart valves demanding the next cardiac cycle to start and repeat. The plot here is also considering the points shown in Figure 4.8 as the points of interest to observe changes in pressures. However due to huge changes in values between the artery and the other areas, even here the secondary axis is taken to show the changes in the above plot. Here the dotted line with a left arrow marking shows the pressure changes with time in the major artery and the values shown at the side of left-handed arrow represent the respective values of major artery at different times, whereas the right-hand side values are the values of the rest of the regions at different time.

4.2 Results for Blood Flow in the Reconstructed Cerebral Artery-Brain-Tumor Connection

Velocity at 0.1 Sec:

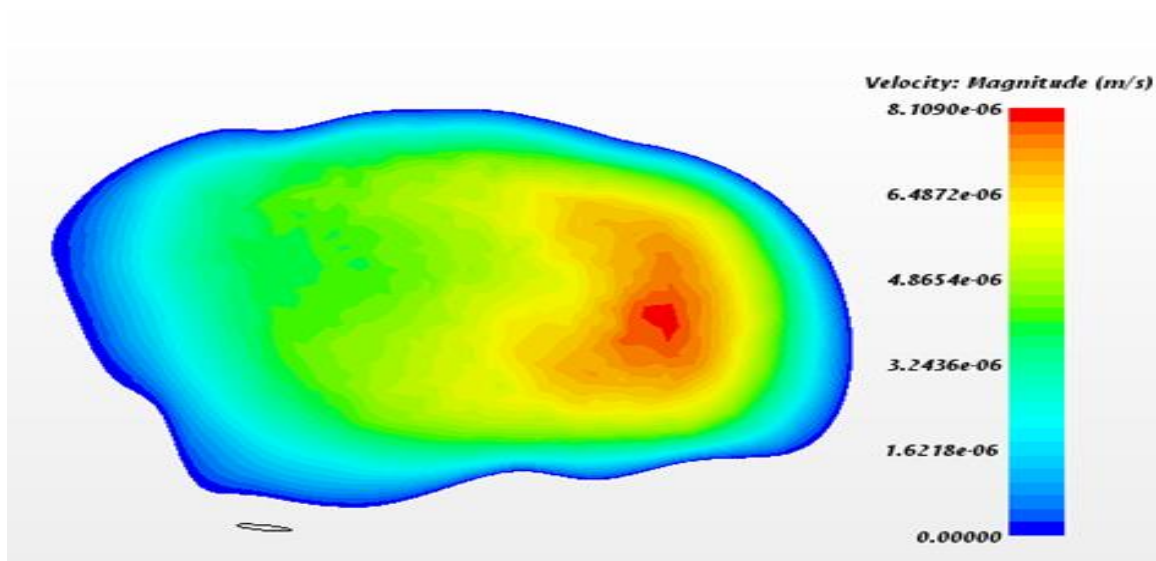


Figure 4.10(a) Velocity at 0.1 Sec in frontal region of reconstructed brain

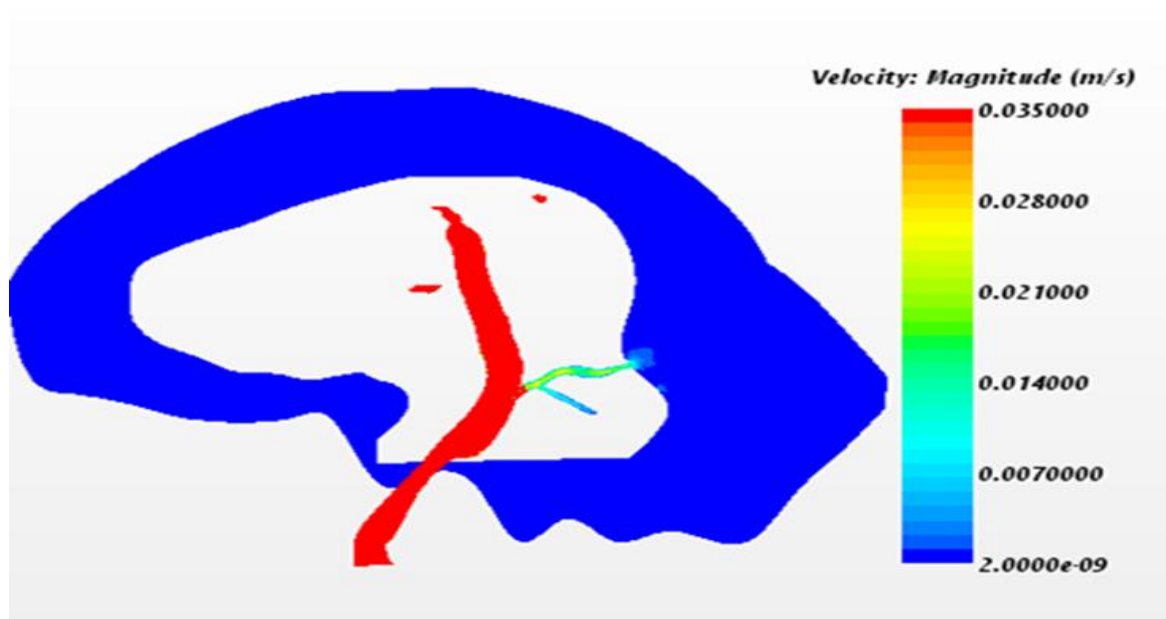


Figure 4.10(b) Velocity at 0.1 Sec in mid-section of reconstructed brain

The Figures 4.10(a) and 4.10(b) show the velocity distribution of the frontal and mid-sectional tissue regions of brain. The velocity ranges from 0 to $8E-6$ m/sec in frontal tissue region and $2E-9$ to 3.8 m/sec in mid-plane with tumor. The case (b) velocity is scaled to see the effect of flow in the plane of tumor. The above figures show the obstruction created by tumored tissue causes the less blood flow in the mid-plane. However the other parts of the brain shown in case (a) changes with higher velocity with respect to the cardiac inflow.

Velocity at 0.125 Sec:

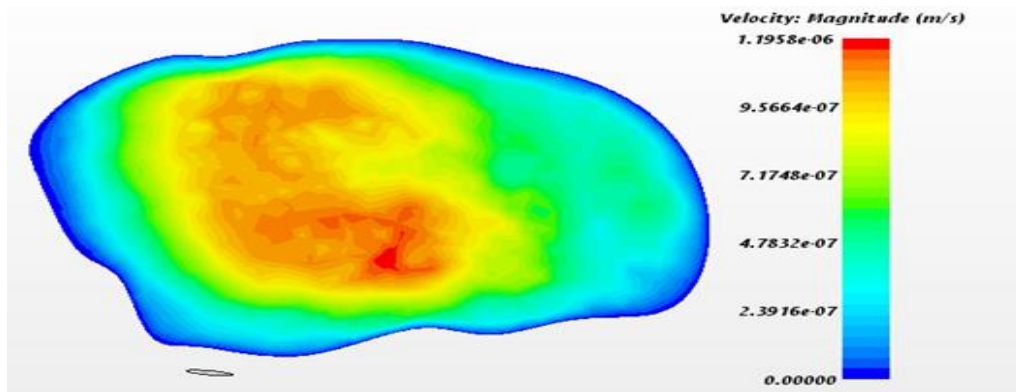


Fig 4.11(a) Velocity at 0.125 Sec in frontal region of reconstructed brain

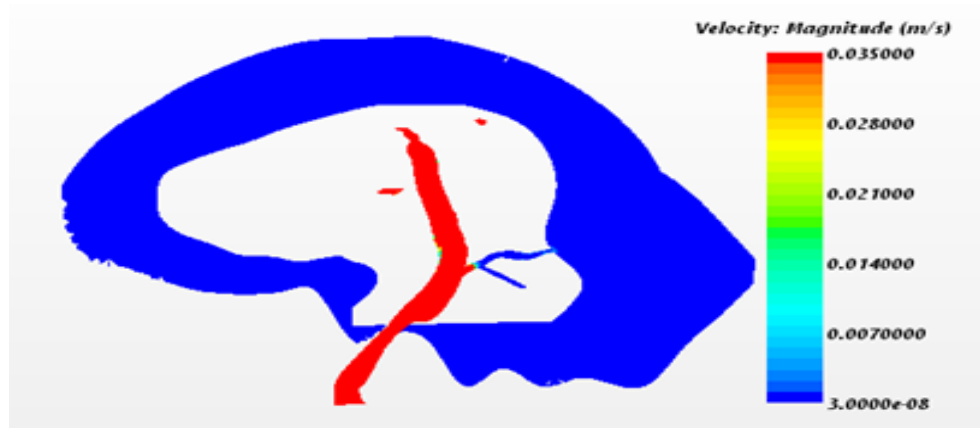


Fig 4.11(b) Velocity at 0.125 Sec in mid-section of reconstructed brain

The Figures 4.11(a) and 4.11(b) show the velocity distribution of the frontal and mid-sectional tissue regions of brain at point 0.125 time. The velocity ranges from 0 to 1.9×10^{-6} m/sec in frontal tissue region and 3×10^{-8} to 4.48 m/sec in mid-plane with tumor. The case (b) velocity is scaled to see the effect of flow in the plane of tumor. The above figures show the obstruction created by tumored tissue causes the less blood flow in the mid-plane. However the other parts of the brain shown in case (a) shows higher velocity than the mid-plane but 9% higher than the 0.1 time velocity. In this figure the inflow velocity being distributed from inflow to the tissue is observed clearly.

Velocity at 0.25 Sec:

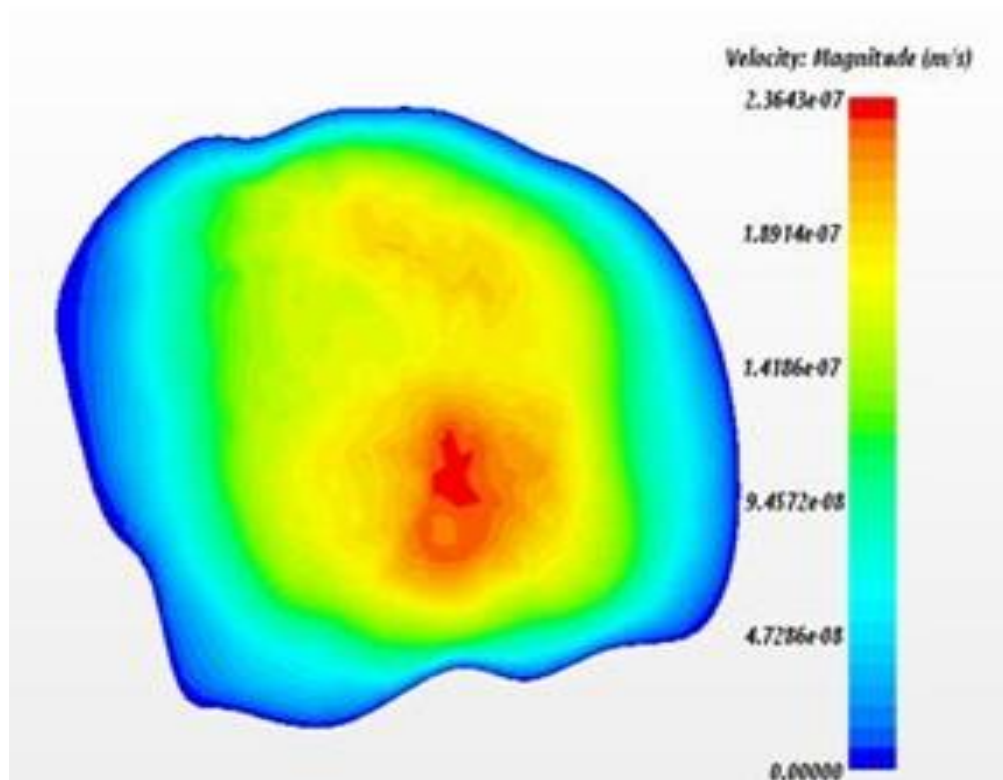


Fig 4.12(a) Velocity at 0.25 Sec in frontal region of reconstructed brain

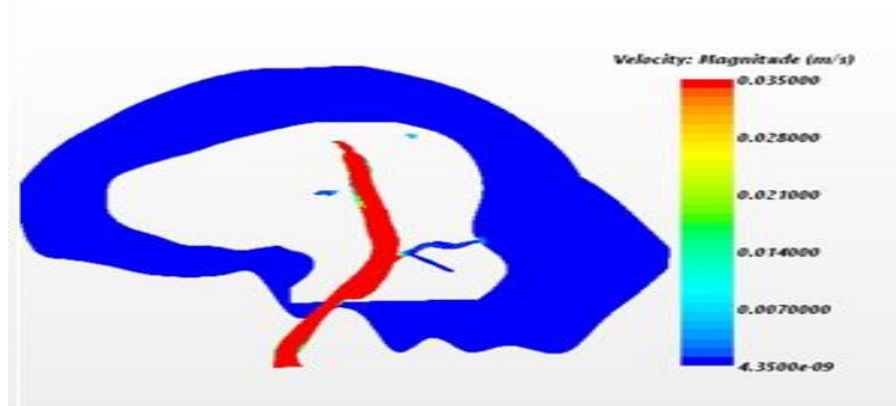


Fig 4.12(b) Velocity at 0.25 Sec in mid-section of reconstructed brain

The Figures 4.12(a) and 4.12(b) show the velocity distribution of the frontal and mid-sectional tissue regions of brain at point 0.25 time. The velocity ranges from 0 to $2.7E-6$ m/sec in frontal tissue region and $4E-9$ to 1.1 m/sec in mid-plane with tumor. The case (b) velocity is scaled to see the effect of flow in the plane of tumor. The above figures show the obstruction created by tumored tissue causes the less blood flow in the mid-plane. However the other parts of the brain shown in case (a) show higher velocity than the mid-plane.

Velocity at 0.5 Sec:

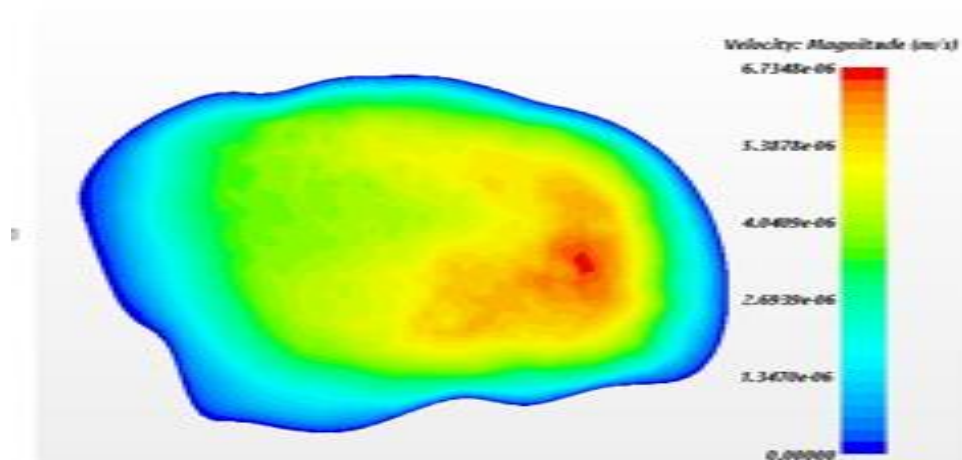


Figure 4.13(a) Velocity at 0.5 Sec in frontal region of reconstructed brain

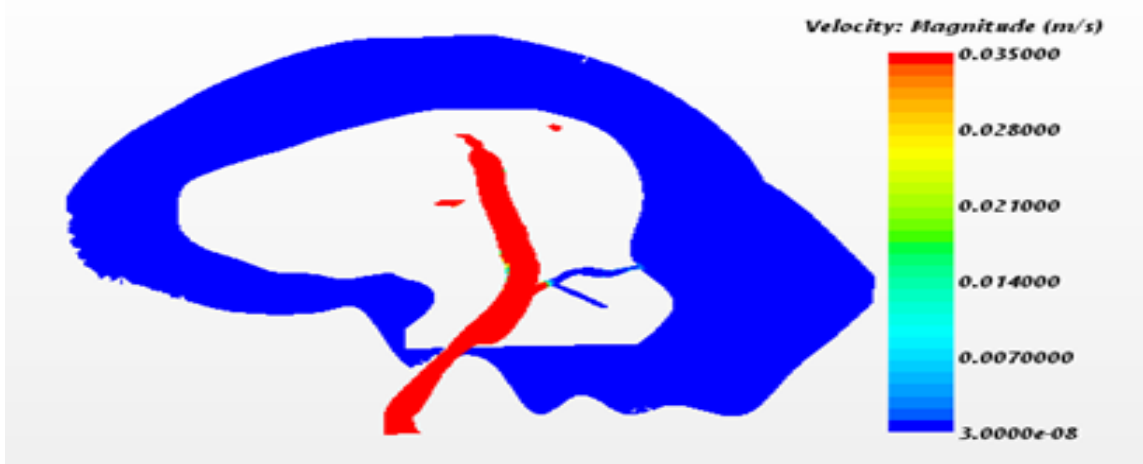


Figure 4.13(b) Velocity at 0.5 Sec in mid-section of reconstructed brain

The Figures 4.13(a) and 4.13(b) show the velocity distribution of the frontal and mid-sectional tissue regions of brain at point 0.5time. The velocity ranges from 0 to $6.736E-6$ m/sec in frontal tissue region and $3.5E-8$ to 1.237 m/sec in mid-plane with tumor. The case (b) velocity is scaled to see the effect of flow in the plane of tumor. The above figures show the obstruction created by tumored tissue causes the less blood flow in the mid-plane. However the other parts of the brain shown in case (a) show higher velocity than the mid-plane following the rise in cardiac cycle.

Now the velocities are analyzed with respect to planes. A two-sectional probe at the site of tumor and posterior parts of the brain is created to see the blood flow in both parallel and perpendicular planes. The perpendicular plane created at a distance of 105mm from the left of the brain at the origin of tumor is in Figure 4.14.

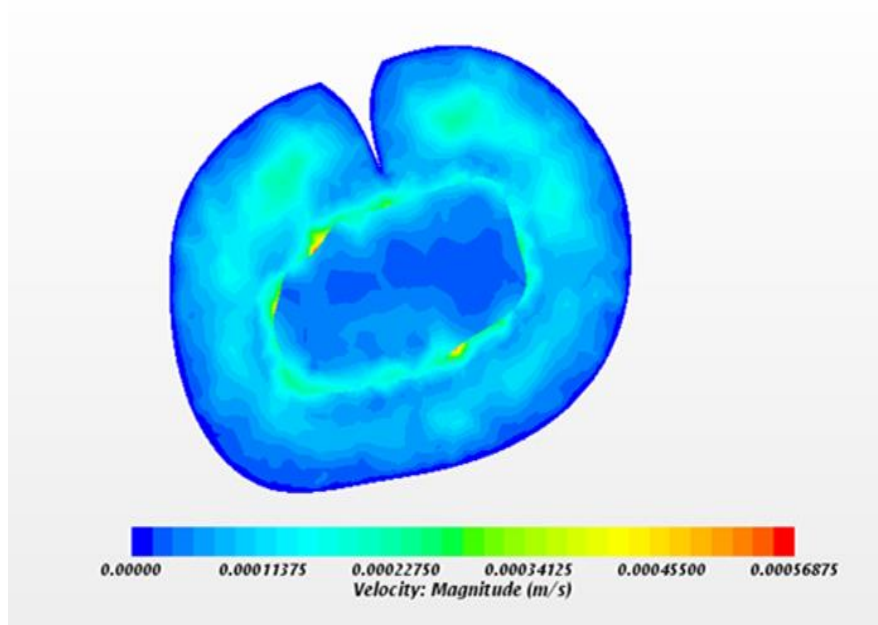


Figure 4.14 (a) Velocity at perpendicular sectional plane of reconstructed brain at 0.01 sec

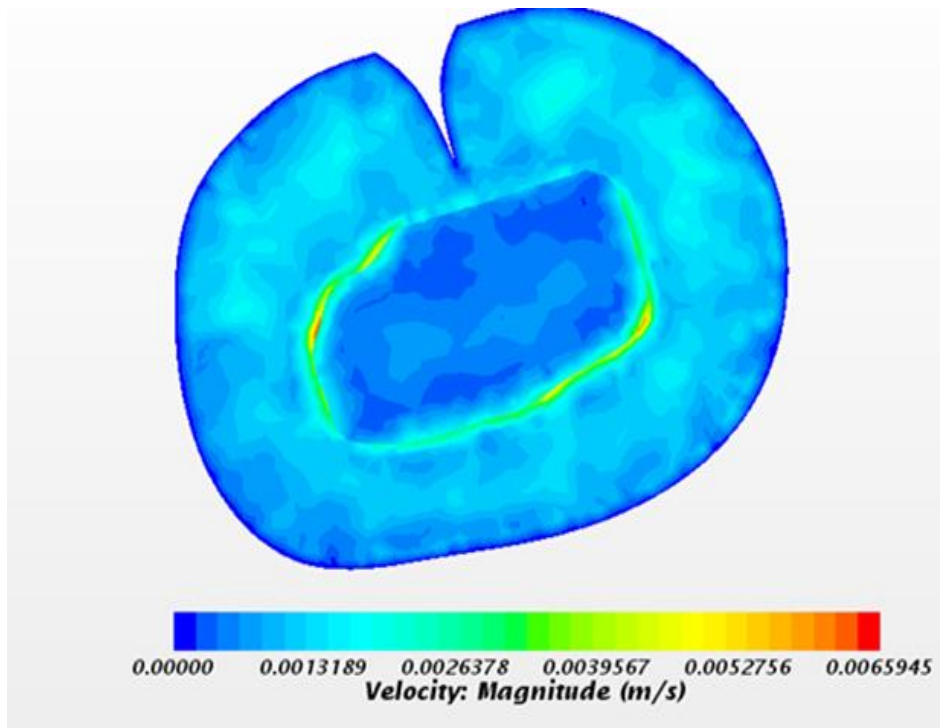


Figure 4.14 (b) Velocity at perpendicular sectional plane of reconstructed brain at 0.1 sec

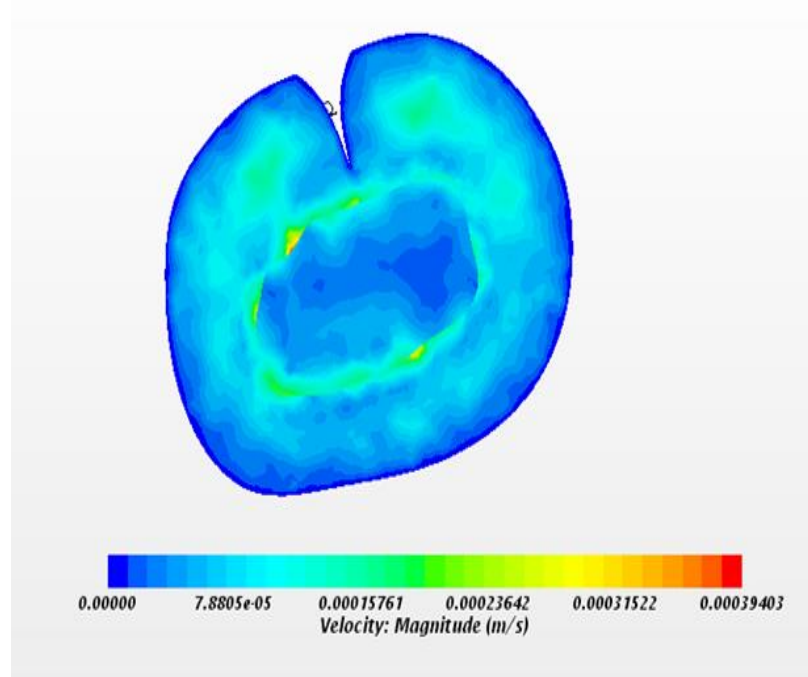


Figure 4.14 (c) Velocity at perpendicular sectional plane of reconstructed brain at 0.125 sec

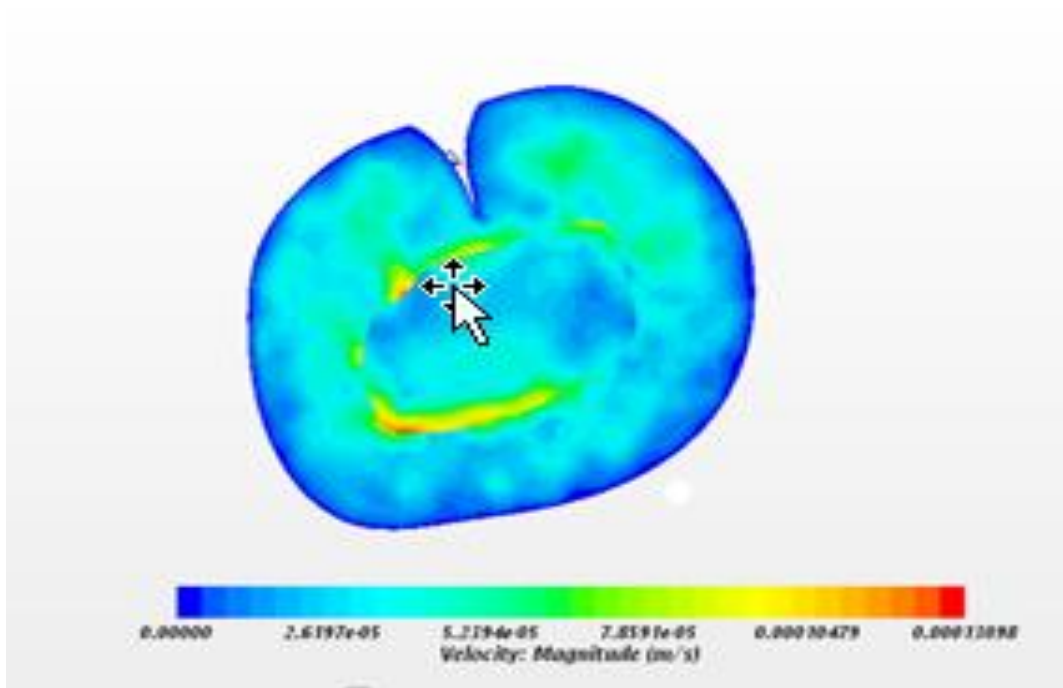


Figure 4.14 (d) Velocity at perpendicular sectional plane of reconstructed brain at 0.25 sec

The Figure 4.14(d) shows the blood flow velocity distribution at different time steps of the cycle. The value at 0.1 time starts from 0.0065m/sec as the highest velocity and 0.0013m/sec as lowest velocity. However the velocity at tumor site is even lower than 0.0013m/sec. Then with the rise in flow through the cycle there is an increase in velocity both at tumor and tissue regions to 0.002m/sec and 0.0056m/sec respectively shown in Figure (a) and (b). At time step 0.25, there is lower velocity due to negative rise in the velocity. Finally at the time 0.5 the velocity rises following the cardiac cycle.

Similarly a parallel plane is created at the posterior part of the brain. As shown in the frontal regions of brain the posterior planes also showed higher velocity when compared to the regions of the tumored mid-plane. However when compared to the parallel and perpendicular planes it shows different values due to differences in the distance from the capillary which supplies blood. For this reason, parallel and perpendicular planes are not compared but the changes are shown in this study.

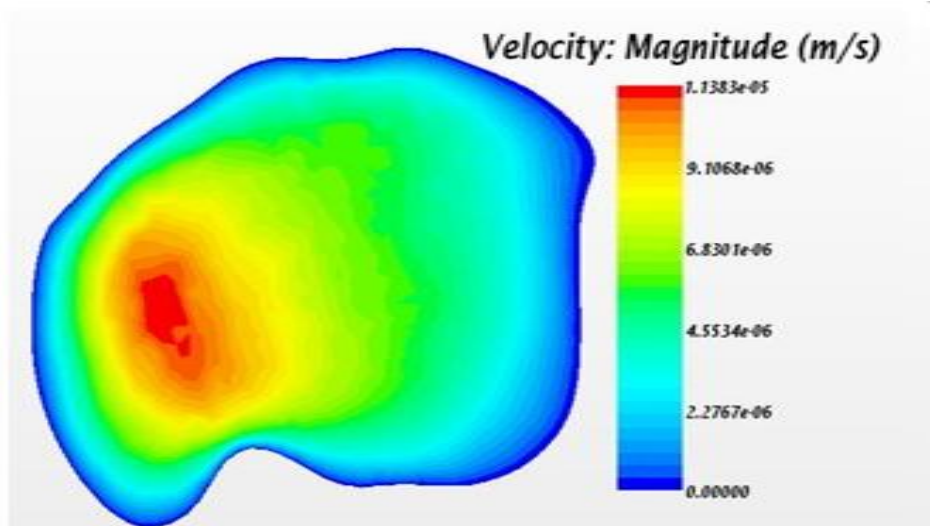


Figure 4.15 (a) Velocity at rear plane of reconstructed brain tissue at 0.1 sec

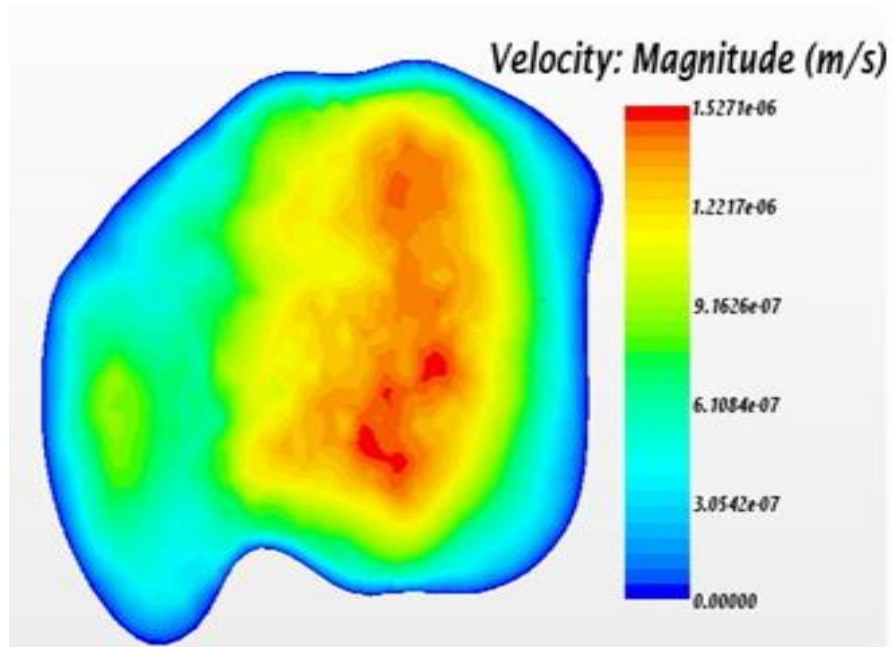


Figure 4.15 (b) Velocity at rear plane of reconstructed brain tissue at 0.125 sec

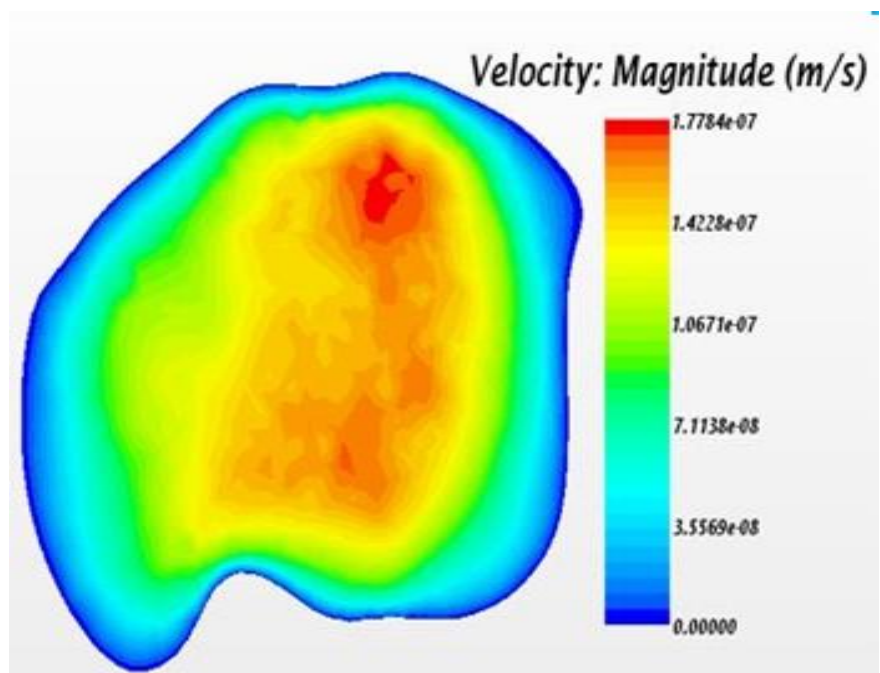


Figure 4.15 (c) Velocity at rear plane of reconstructed brain tissue at 0.25 sec

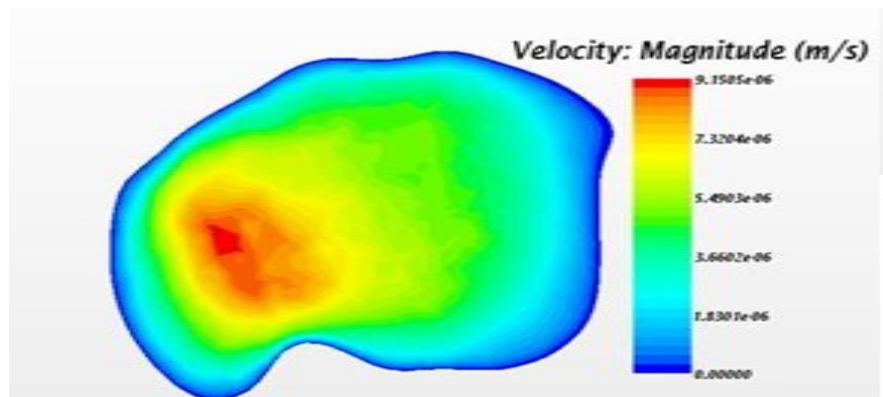


Figure 4.15 (d) Velocity at rear plane of reconstructed brain tissue at 0.5 sec

As shown in the Figure 4.15 the velocity follows the cardiac cycle. The velocity rises from 0.1 to 0.125 time step then it decreases to $1.77E-7$ and then rises to $9.7E-$ following the cycle. Figure 4.16 shows the velocity distributions at three different planes cut in parallel to the brain. The plots shows the highest velocities at both planes in the front and the back since there is no obstruction to the flow, whereas the velocity in the plane of tumor existence showed a less velocity of about 30% when compared to the other planes.

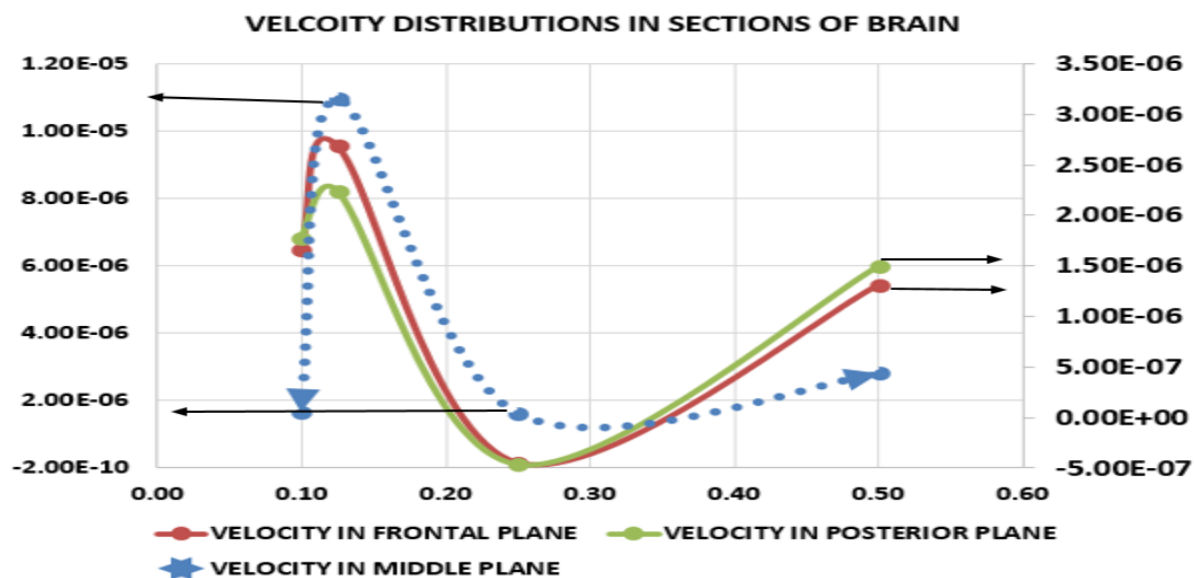


Figure 4.16 Velocity distributions in sections of brain

The plot in Figure 4.16 contains two different sets of values. So a secondary axis is chosen to show the velocity variations in the same plot. The dotted line shows velocity in the mid-section of the brain, whereas the rest of the regions show the velocity in frontal and rear regions of brain. The respective values of dotted and normal lines show the velocity with the arrows towards left and right respectively.

Pressure Variations:

Pressure at 0.1 Sec:

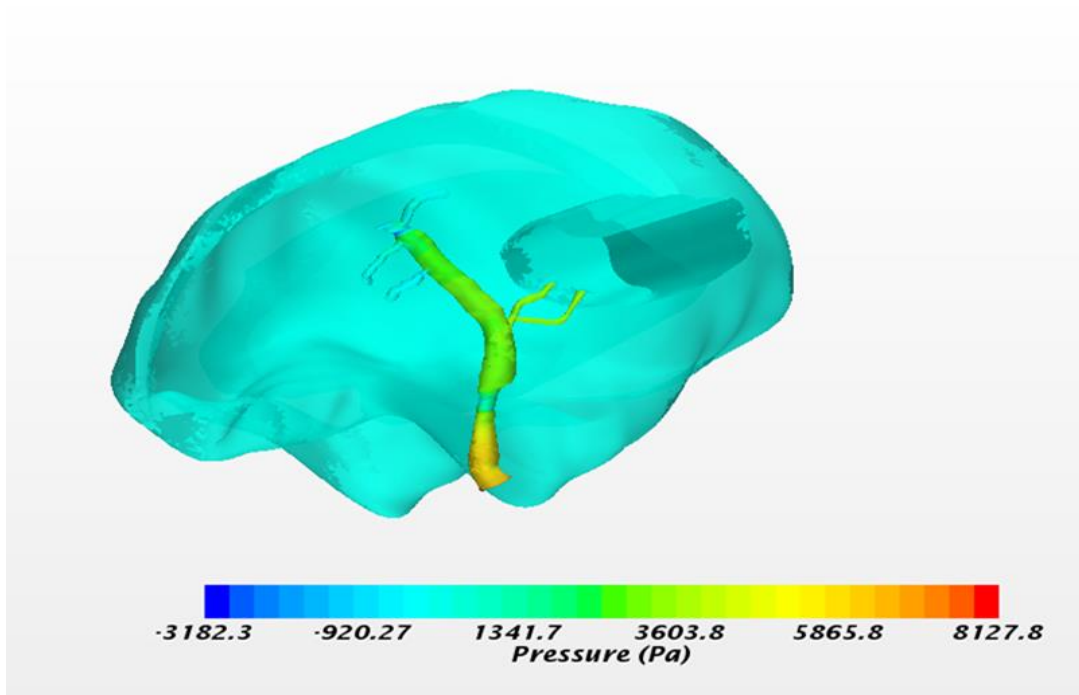


Figure 4.17(a) Pressure at 0.1 Sec of reconstructed brain

The Figure 4.17(a) shows the pressure distribution of healthy and tumored regions of brains tissue connected to the artery-capillary network. Here the pressure ranges from -3182.3 pa to 8127.8 pa. In specific, the tissue region of brain faces the pressure is 5865.8 pa in a healthy artery where increase in pressure range is observed in tissue region due to the presence of tumor.

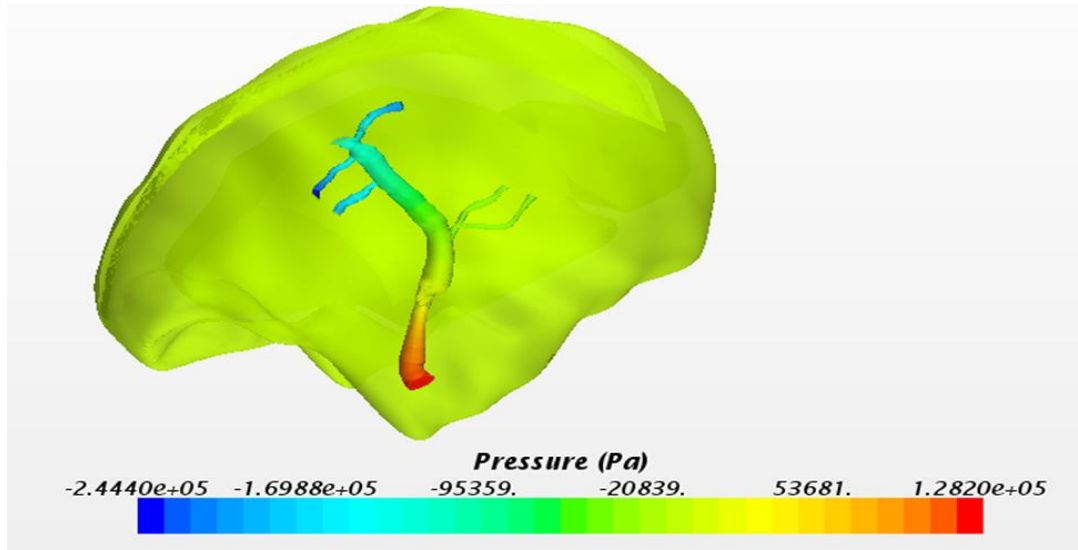


Figure 4.17(b) Pressure at 0.125 sec of reconstructed brain

The Figure 4.17(b) shows the pressure distribution of healthy and tumored regions of brain tissue connected to the artery-capillary network. Here the pressure ranges from -20839pa to 1.28E5pa. Here the tumored tissue region of brain faces the pressures that are being changed drastically with an increment by 15%.

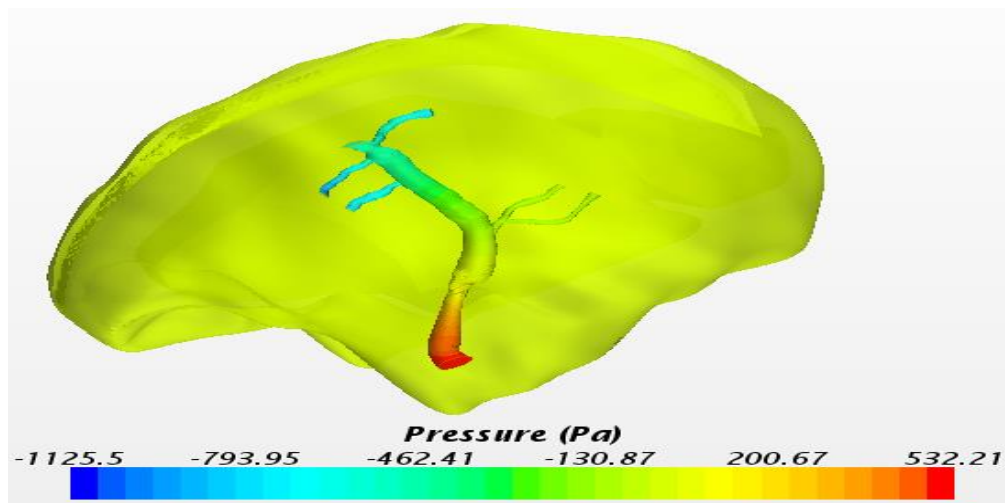


Figure 4.17(c) Pressure at 0.25 sec of reconstructed brain

The Figure 4.17(c) shows the pressure distribution of healthy and tumored regions of brain tissue connected to the artery capillary-network. Here the pressure ranges from -1125.5pa to 532.21pa. Here the tumored tissue region of brain faces the negative pressure analogous to cardiac input.

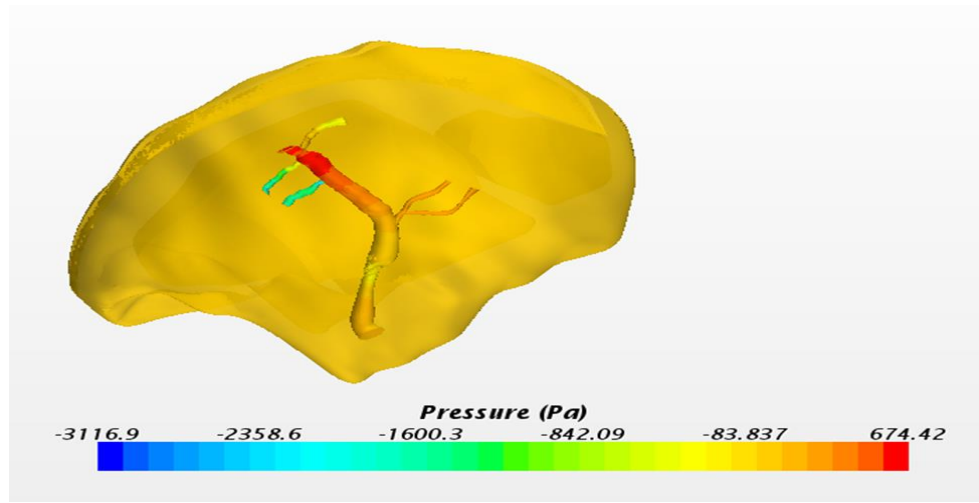


Figure 4.17(d) Pressure at 0.5 sec of reconstructed brain

The Figure 4.17(d) pressure ranges from -83pa to 674.2 pa and 88 pa to 966 pa following the rise in cardiac input.

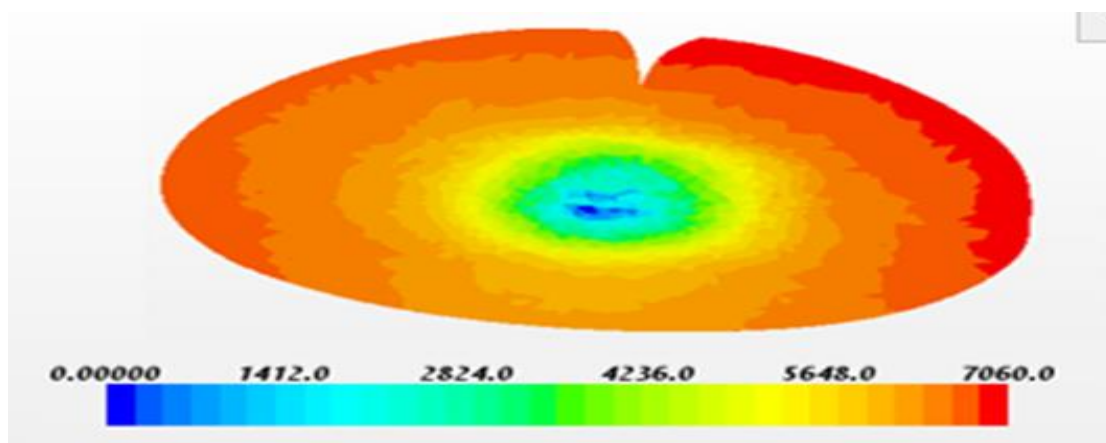


Figure 4.18 (a) Pressure at perpendicular sectional plane of reconstructed brain at 0.1 sec

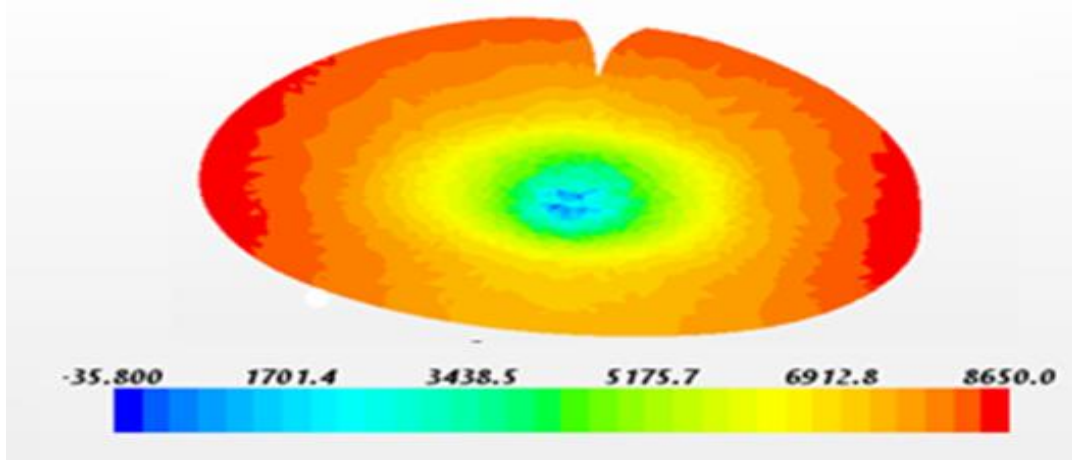


Figure 4.18 (b) Pressure at perpendicular sectional plane of reconstructed brain at 0.125 sec

The Figures 4.18 (a) and 4.18 (b) show the pressure distributions in the sectional planes cut perpendicular to the brain. At time 0.1 sec the pressure is higher in the regions of brain tissue where there is no tumor. The tumor region has lower pressure due to obstruction which causes the pressure drop. The pressure ranges from 1412 pa in tumor region and 7060pa in non-tumor regions, whereas at time 0.125 the pressure changes increase at the respective site by 10%.

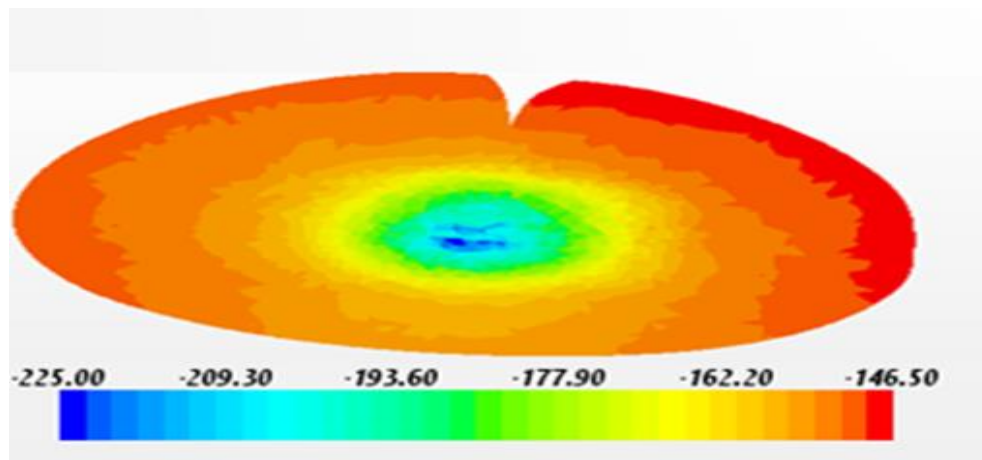


Figure 4.18 (c) Pressure at perpendicular sectional plane of reconstructed brain at 0.25 sec

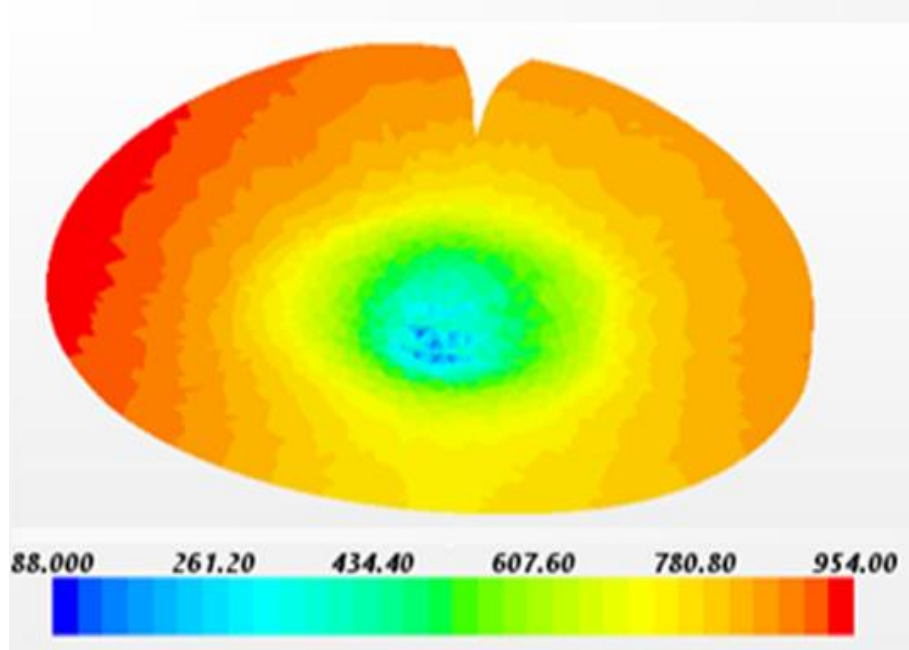


Figure 4.18 (d) Pressure at perpendicular sectional plane of reconstructed brain at 0.5 sec

The Figure 4.18(d) shows the negative pressure following the cardiac flow. Then the pressure rises at the time 0.5 sec by 6%.

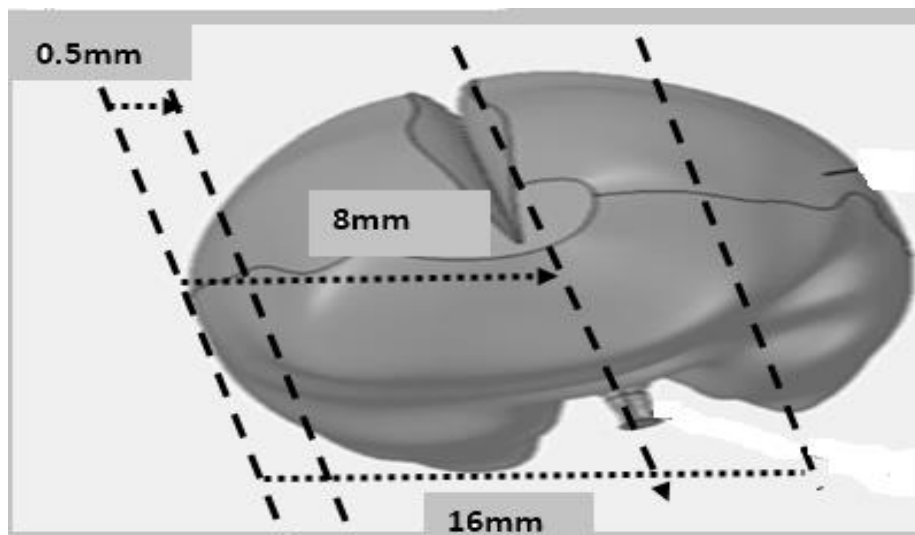


Figure 4.19 Points considered to draw plots with respect to position from the reference

The plot in Figure 4.20 shows the pressure distributions at a section plane cut in parallel to the brain. The plot shows the highest pressure at the ends of the brain and lowest pressures at the region of tumor existence due to the resistance to flow at each time. However a line probe is plotted to see the variation at each time with respect to the position of tumor. The variations are shown in the plot. The pressures are about 6000 pa at the initial time for both frontal and posterior planes, whereas the pressure is 3000 pa at the same time near the tumor. Even the other time steps following same trend can be observed from the plot.

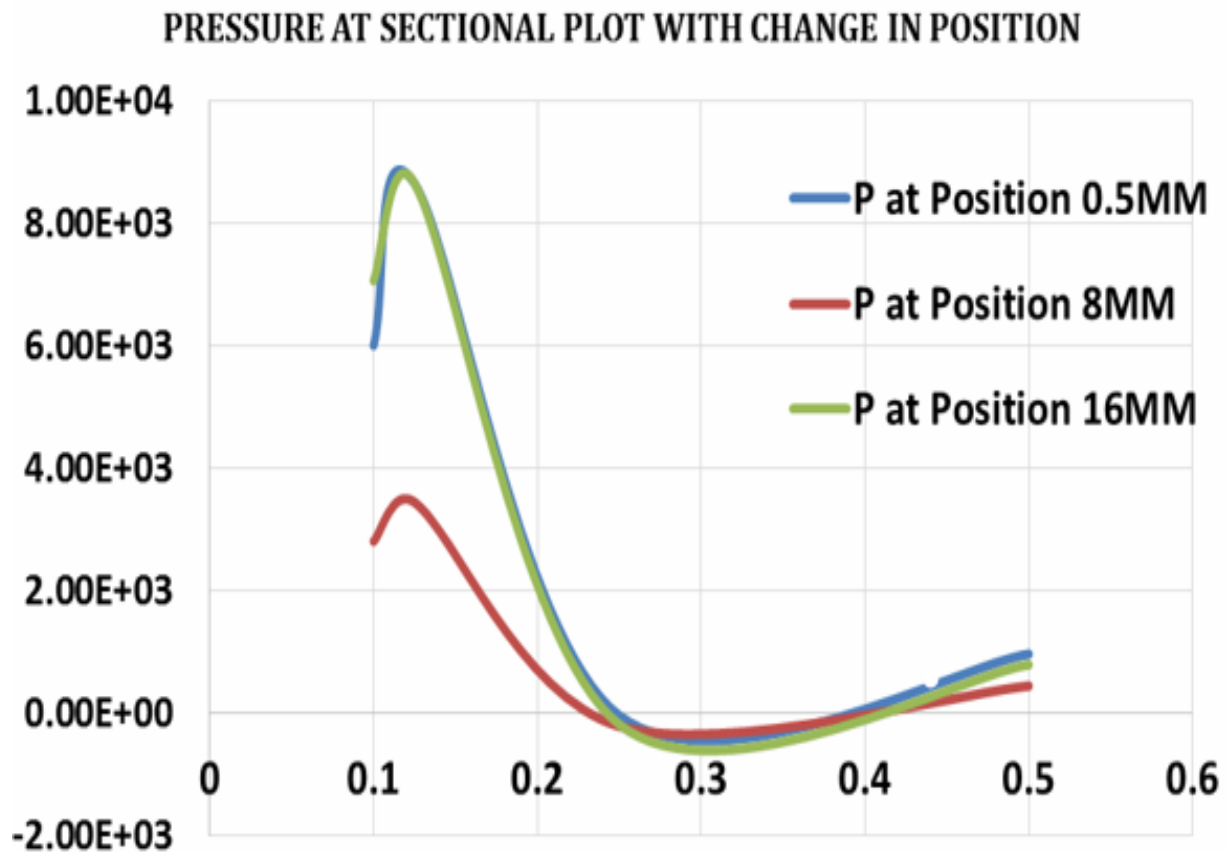


Figure 4.20 Pressure at sectional plot with change in position

4.3 Results for Drug Distribution in the Artery with Imaginary Tissue-Tumor Connection

For the initial case analysis, the drug Temozolomide is used with concentrations in safe range of 0.03 mL -0.08 mL using the advection diffusion principle in multiphase Lagrangian modeling of star Ccm+. In this initial case study particle velocities of drug with concentrations of 0.03 mL, 0.05mL, and 0.08mL are observed with changed particle dimension values of 5, 0.5 microns. The results below are obtained at times from 0.1-0.5 sec of cardiac cycle for the changed concentrations and changed particle dimensions.

4.3 Results with Dosage

Particle Velocity at 0.1 Time with 0.03 mL Concentration:

4.3.1 0.03 mL:

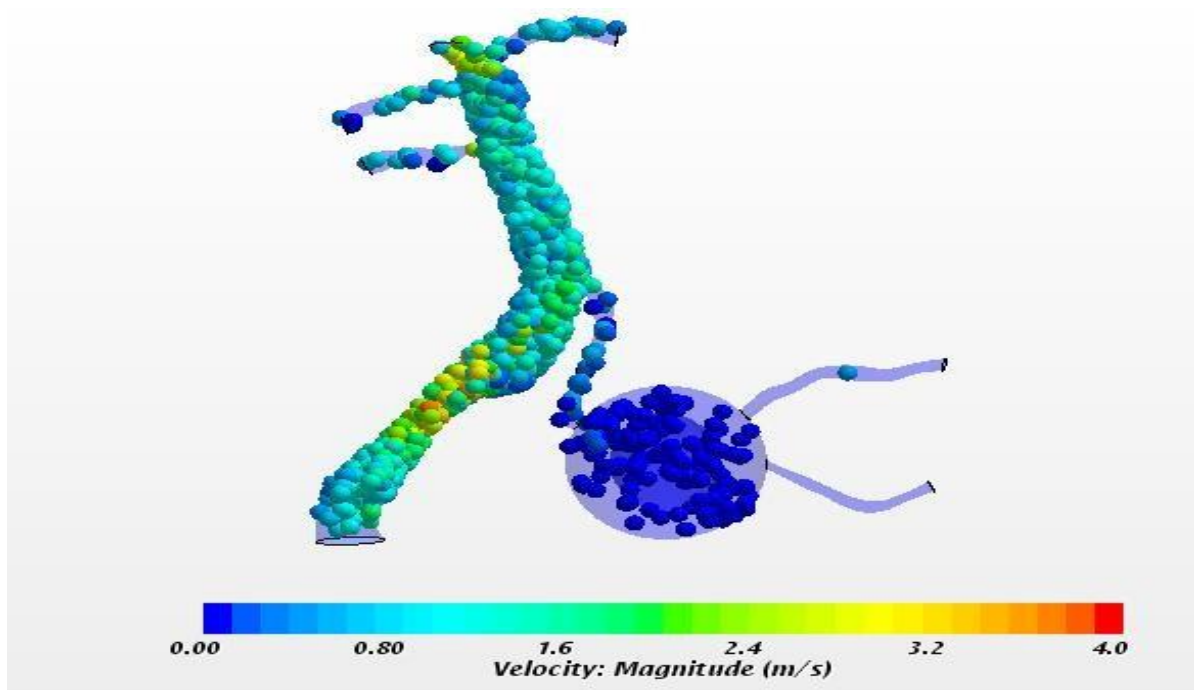


Figure 4.21(a) Particle velocity at 0.1sec

The Figure 4.21(a) shows the particle velocity at 0.1 time step when a dosage of 0.03mL is inserted into the blood stream. The highest velocity with which the particle flows is 4m/sec. However the tissue and the tumor regions receive blood flow with lesser velocities which is numerically not very clearly visible in this figure.

Particle Velocity at 0.125 Time with 0.03 mL Concentration:

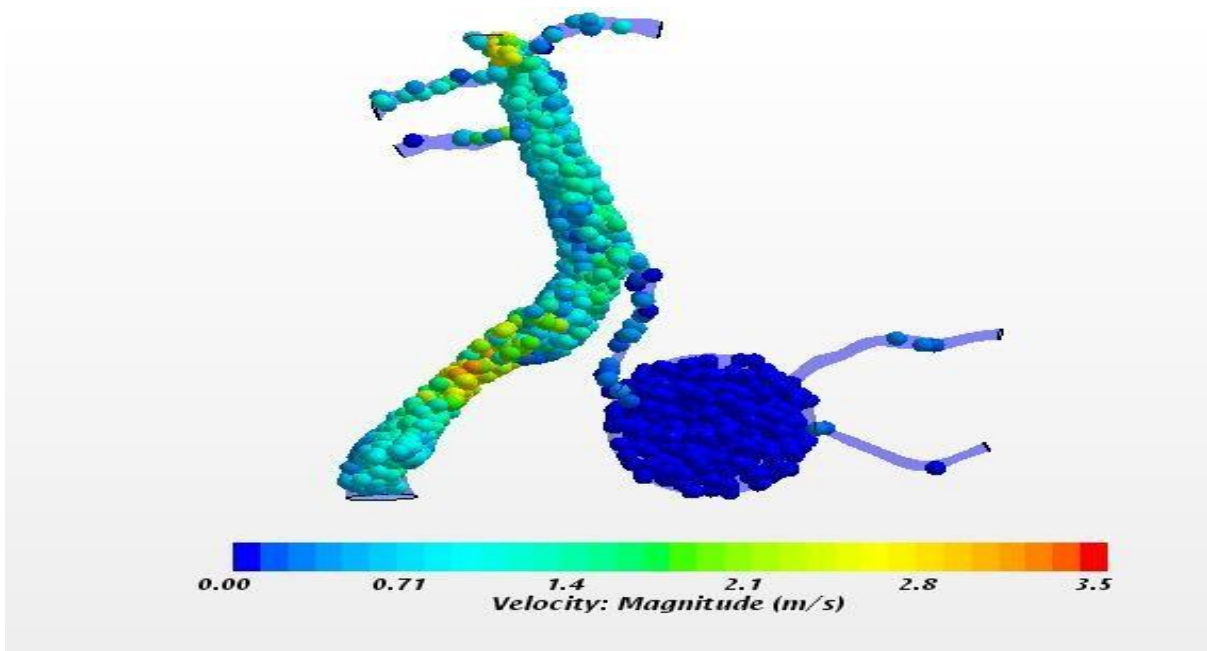


Figure 4.21(b) Particle velocity at 0.125sec

The Figure 4.21(b) shows the particle velocity at 0.125 time when a dosage of 0.03mL is inserted into the blood stream. The highest velocity with which the particle flows is 4.7m/sec. However the tissue and the tumor regions receive blood flow with lesser velocities which is numerically not very clearly visible in this figure. Also it is the highest velocity observed with in the cardiac cycle. We can also observe increased particle flow due to the increased cardiac input

into the tumor tissue region compared to previous and the other flows at various time steps shown.

Particle Velocity at 0.2 Time Step with 0.03 mL Concentration:

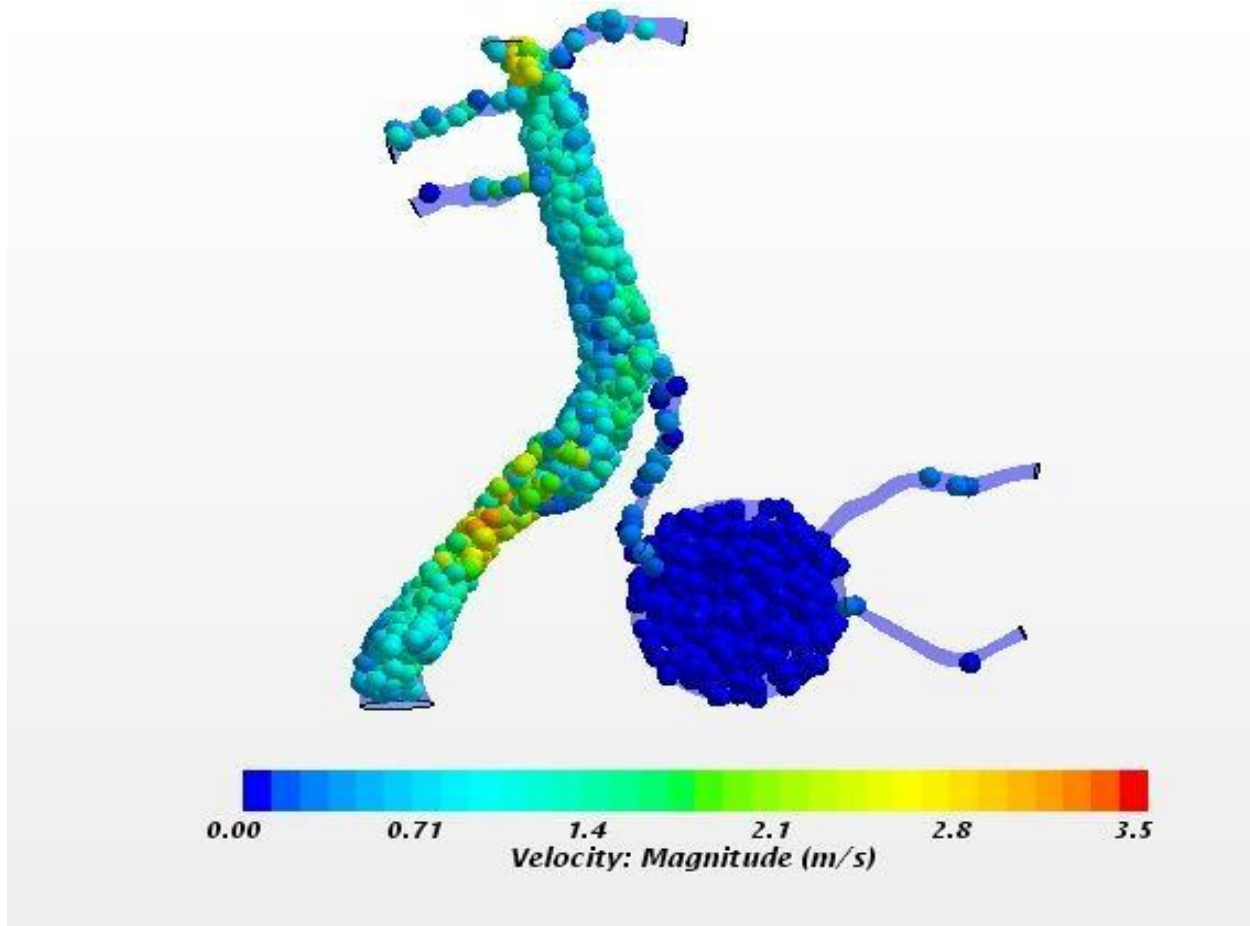
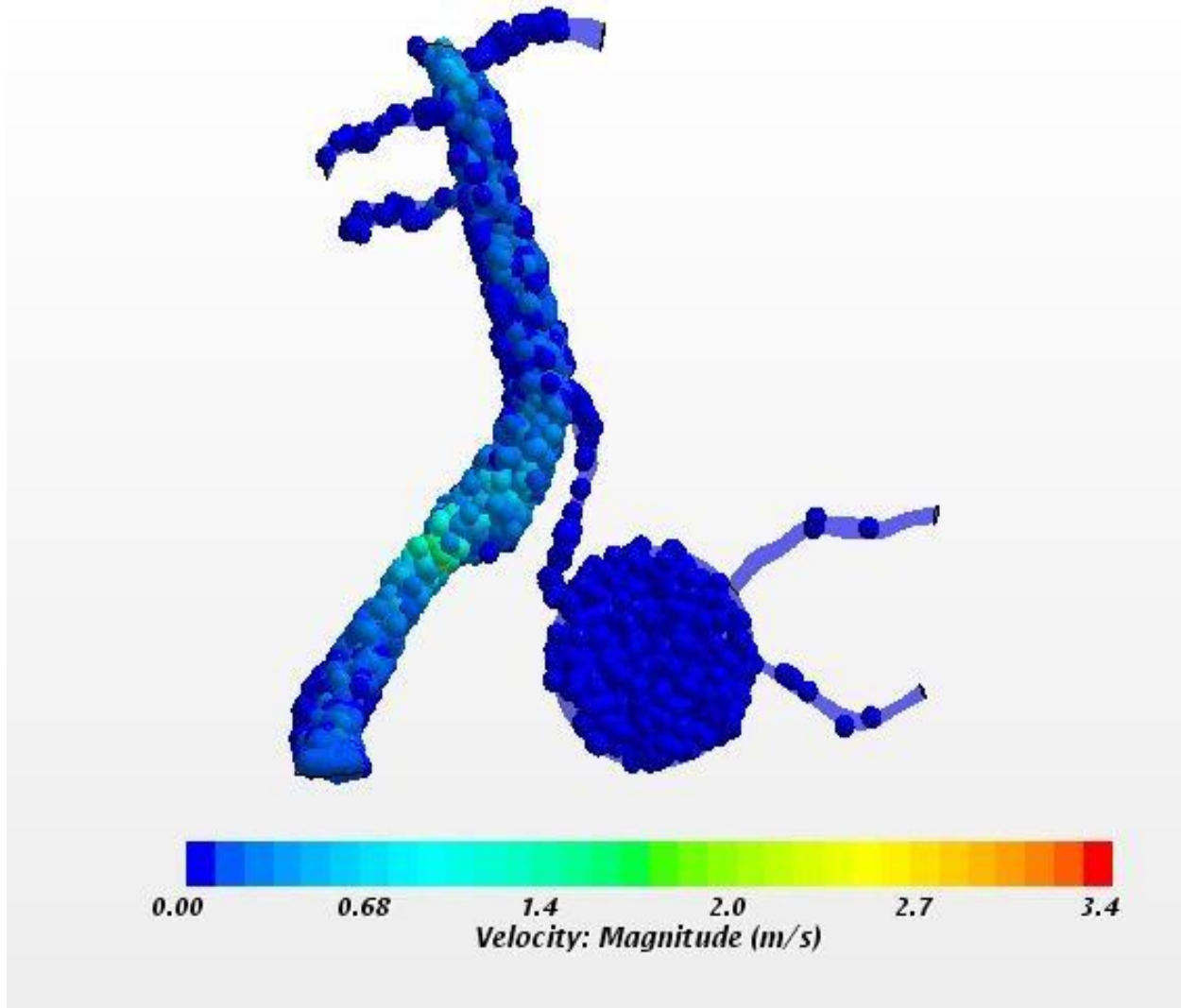


Figure 4.21(c) Particle velocity at 0.2sec

The Figure 4.21(c) shows the particle velocity at 0.2 time when a dosage of 0.03mL is inserted into the blood stream. Here the particle flows with a maximum velocity of 3.5m/sec. We can also observe a downfall of particle flow due to the change in cardiac input into the tumor tissue region compared to previous flow. However the particle concentration in the tumor tissue region appears almost similar to the case of 0.125 time.

Particle Velocity at 0.25 Time with 0.03 mL Concentration:**Figure 4.22(d) Particle velocity at 0.25sec**

The Figure 4.22(d) shows the particle velocity at 0.25 time when a dosage of 0.03mL is inserted into the blood stream. Here the particle flows with a maximum velocity of 3.4m/sec. We can observe at this stage majority of particle flow is very slow in velocity in both artery and tumor region compared to previous flow. However the particle concentration in the tumor

tissue region appears almost similar to the case of 0.125 and 0.2 time.

Particle Velocity at 0.3 Time Step with 0.03 mL Concentration:

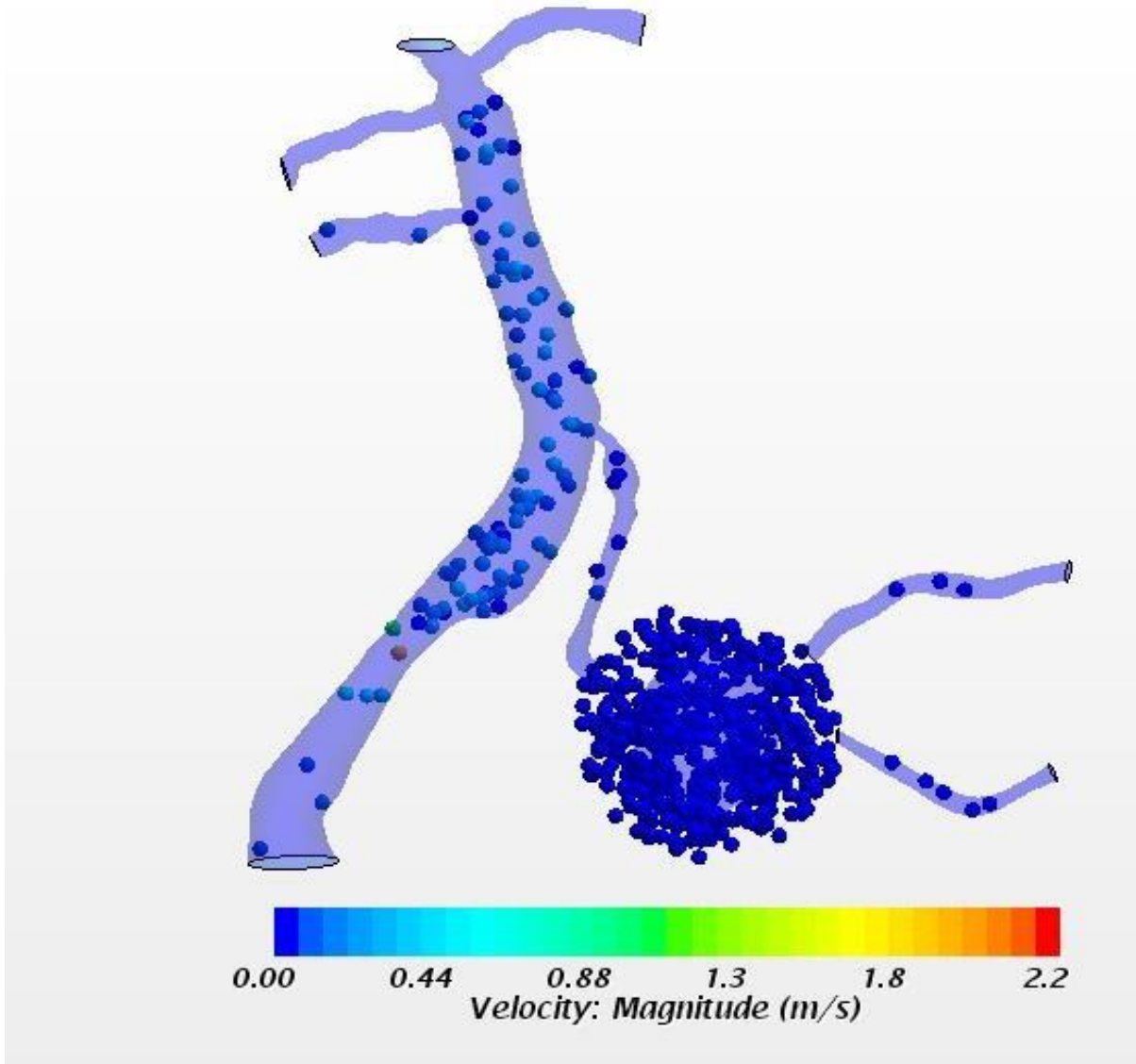


Figure 4.21 (e) Particle velocity at 0.3 sec

The Figure 4.21(e) shows the particle velocity at 0.3 time when a dosage of 0.03mL is inserted into the blood stream. Here the maximum particle flow velocity even drops to 2.2m/sec resembling the cardiac cycle. We can also observe less flow in the arterial region compared to

the tumor tissue regions are the half cycle is completed at this stage.

Particle Velocity at 0.4 Time with 0.03 mL Concentration:

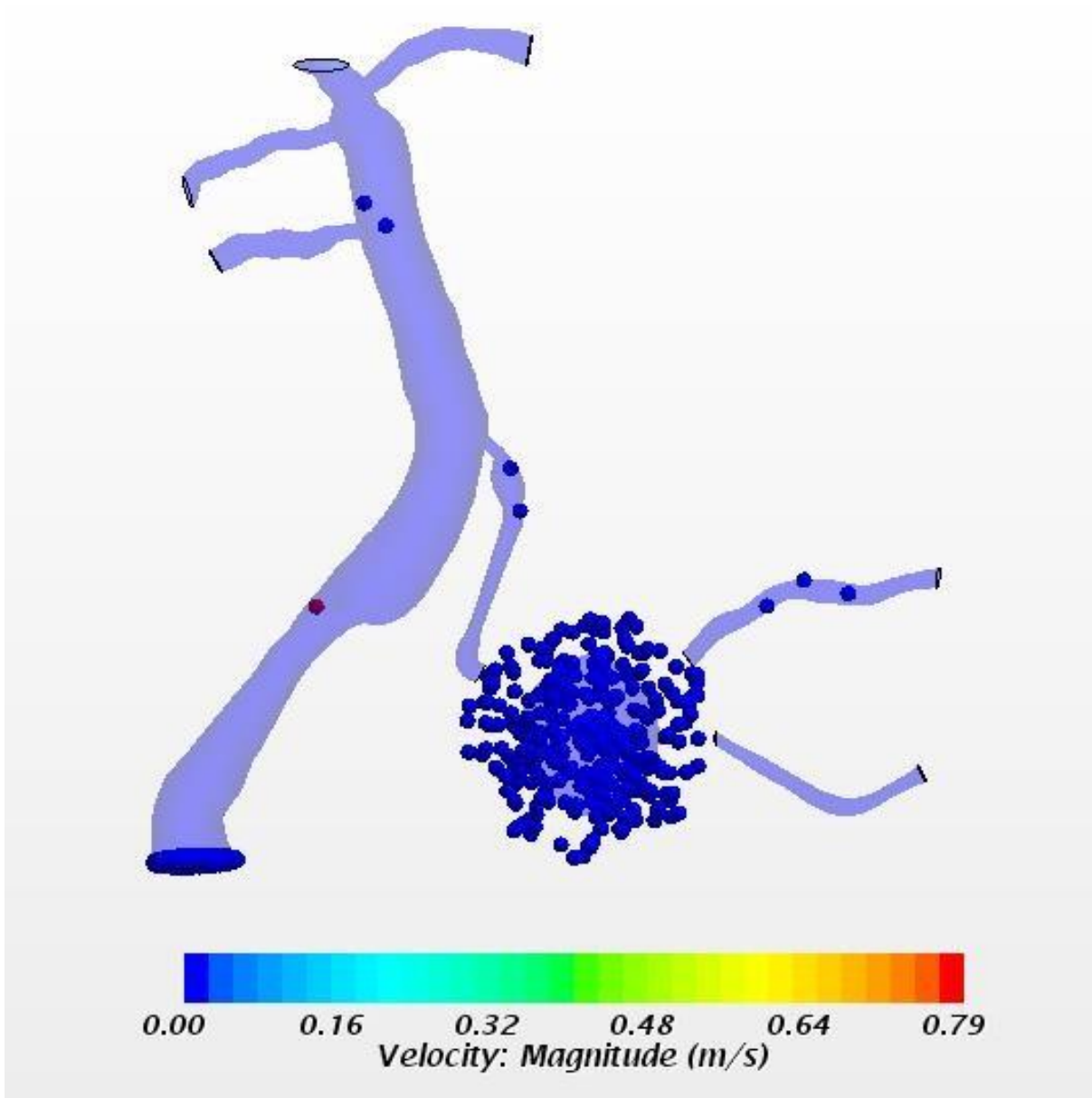


Figure 4.21(f) Particle velocity at 0.4sec

The Figure 4.21(f) shows the particle velocity at 0.4 time when a dosage of 0.03mL is

inserted into the blood stream. The values obtained at this time step is 0.79m/sec. Also only a few particles are observed in the artery regions as the cycle is being finished.

4.3.2. 0.05 mL:

Particle Velocity at 0.1 Time with 0.05 mL Concentration:

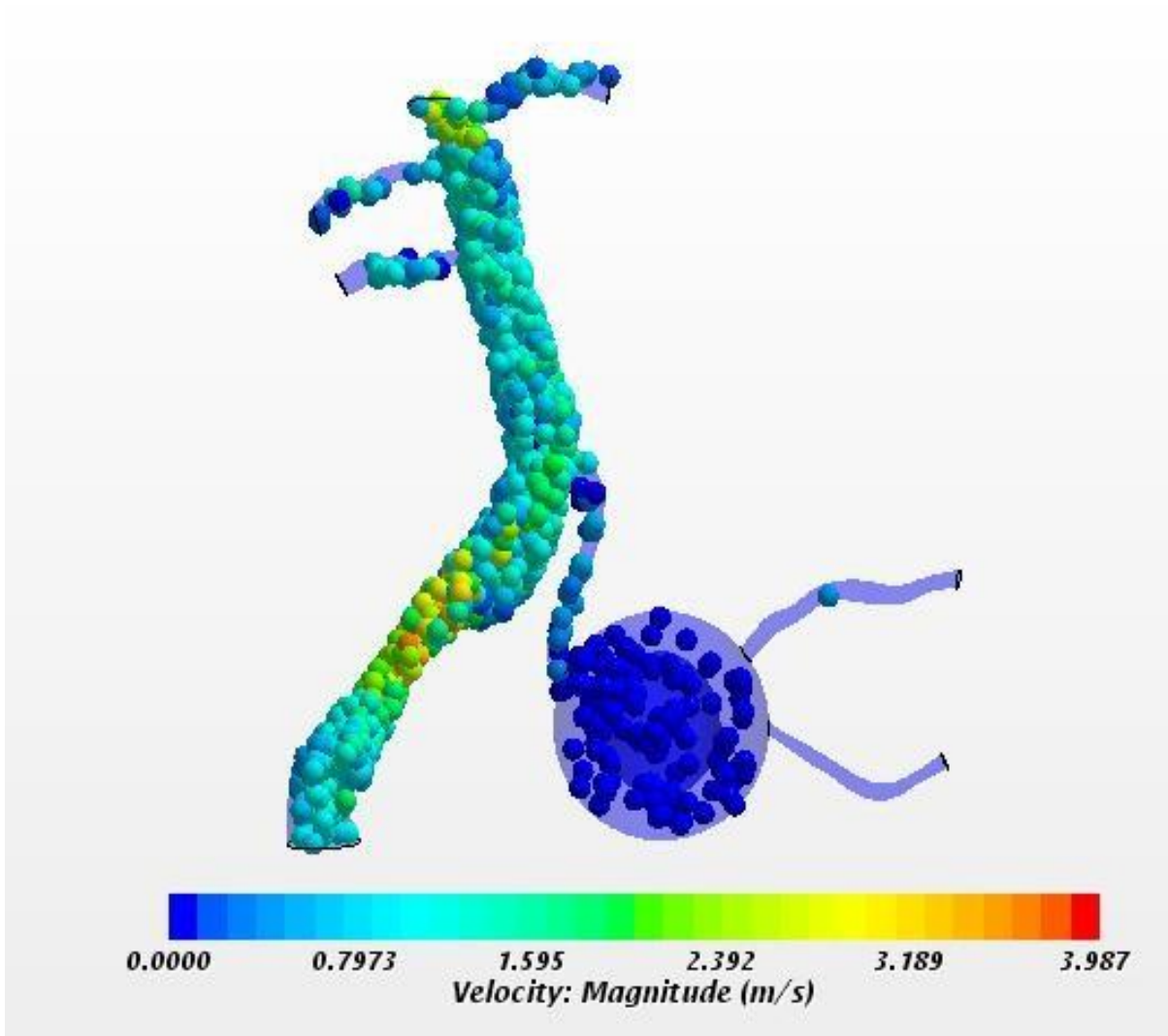


Figure 4.22(a) Particle velocity at 0.1sec

The Figure 4.22(a) shows the particle velocity at 0.1 time when a dosage of 0.05mL is inserted into the blood stream. The value obtained at this time step is 3.987m/sec, which is the

maximum value observed at the arterial flow. However the tissue and tumor regions are shown with semi- filled particle flow with lower velocities ranging from 0 to 0.7973 m/sec. Also only a few particles are observed in the artery regions as the cycle is being initiated.

Particle Velocity at 0.125 Time with 0.05 mL Concentration:

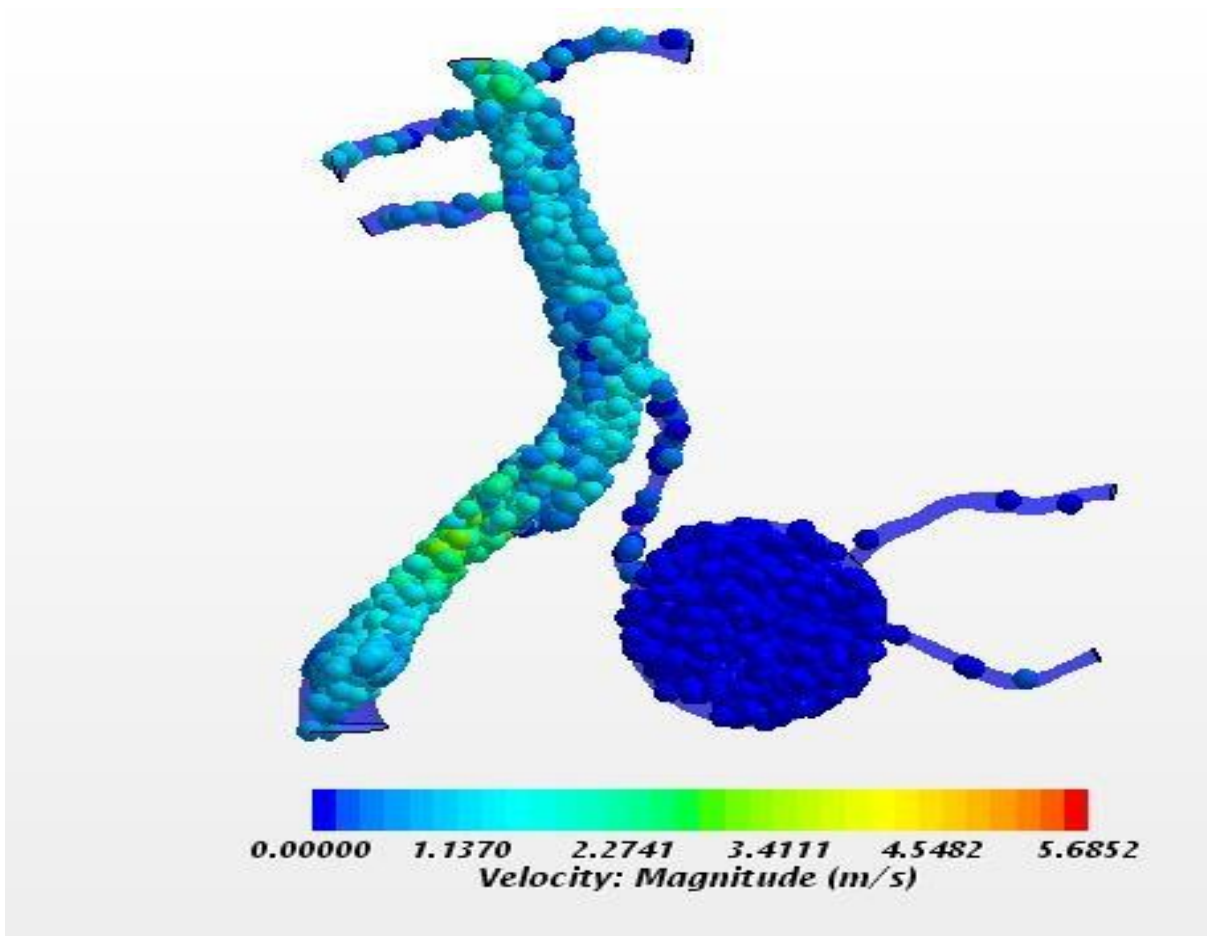


Figure 4.22(b) Particle velocity at 0.125sec

The Figure 4.22(b) shows the particle velocity at 0.125 time step when a dosage of 0.05mL is inserted. The highest velocity is obtained at this time step and the observed velocity is 5.6852 m/sec. However the tissue and tumor regions are shown with completely filled particle

flow with lower velocities ranging from 0 to 1.1370 m/sec. Also increased concentration of particle inflow is observed at this time step.

Particle Velocity at 0.2 Time with 0.05 mL Concentration:

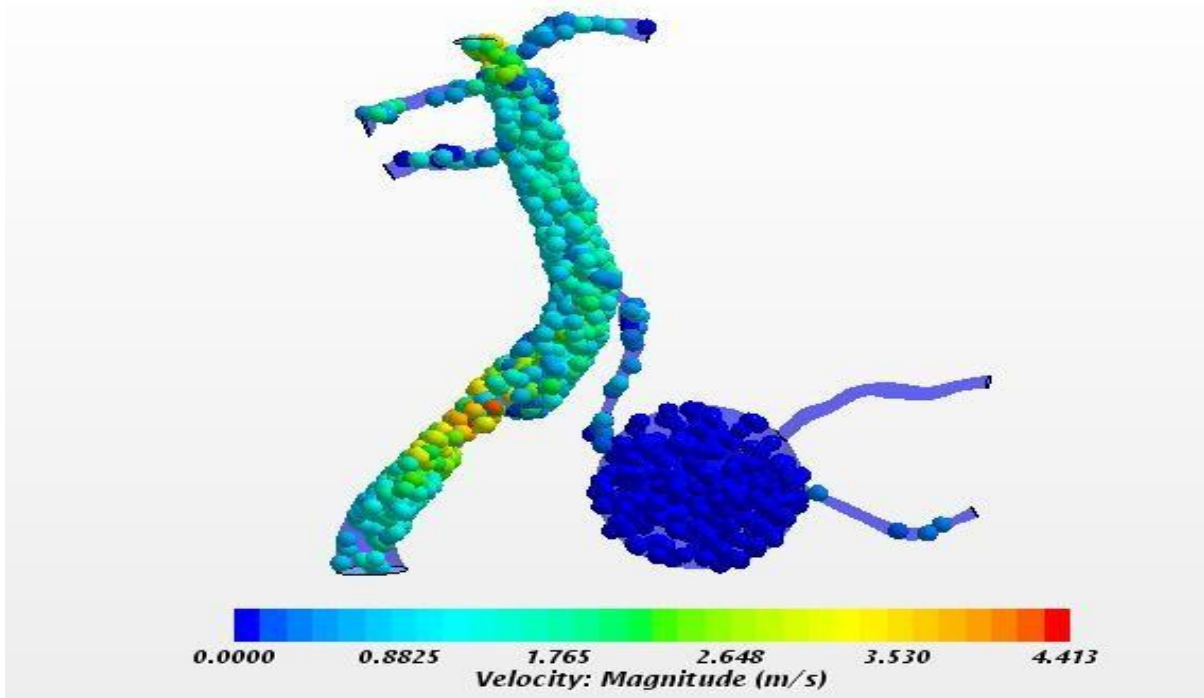
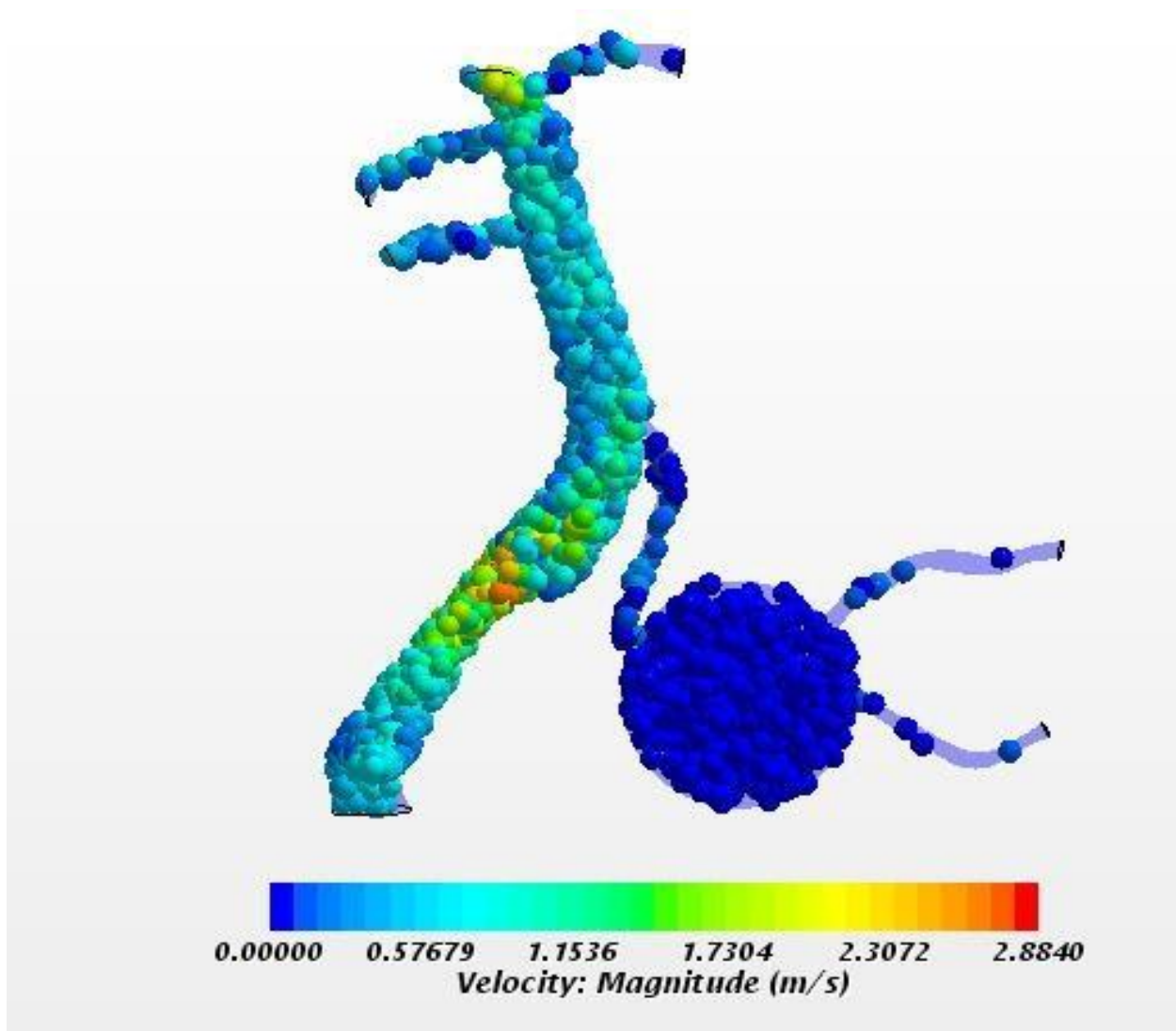
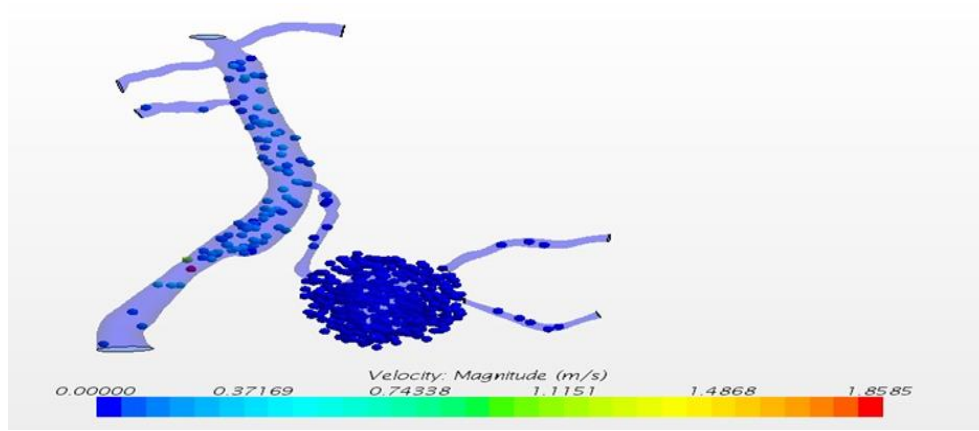


Figure 4.22(c) Particle velocity at 0.2sec

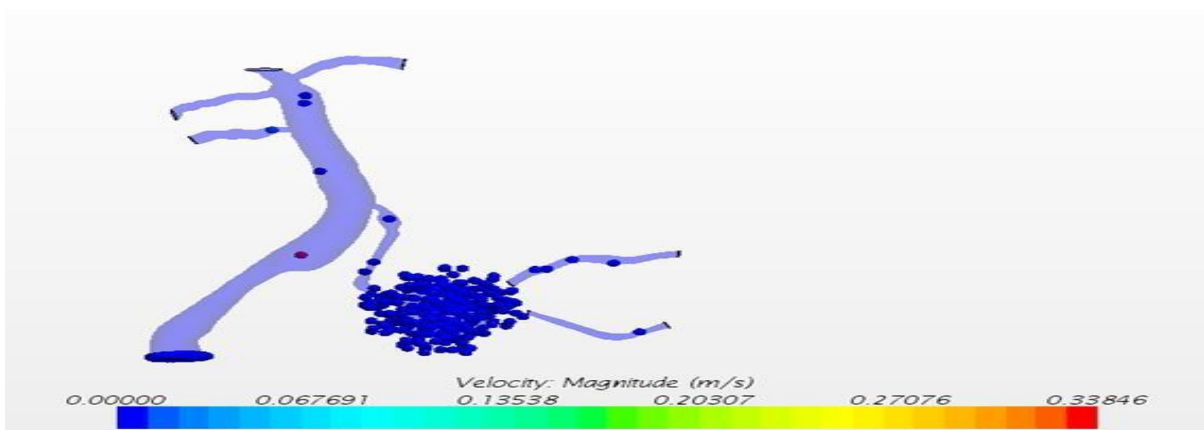
The Figure 4.22(c) shows the particle velocity at 0.2 time when a dosage of 0.05mL is inserted. The highest velocity is obtained at this time step and the observed velocity is 4.41 m/sec. However the tissue and tumor regions are shown with completely filled particle flow with lower velocities ranging from 0 to 0.8825 m/sec. Also increased concentration of particle inflow is observed at this time.

Particle Velocity at 0.25 Time with 0.05 mL Concentration:**Figure 4.22(d) Particle velocity at 0.25sec**

The Figure 4.22(d) shows the particle velocity at time 0.25 time with a dosage of 0.05mL. The highest observed velocity at this time is 2.8840 m/sec. However the tissue and tumor regions are shown with completely filled particle flow with similar concentrations to the previous time.

Particle Velocity at 0.3 Time with 0.05 mL Concentration:**Figure 4.22(e) Particle velocity at 0.3sec**

The Figure 4.22(e) shows the particle velocity at time step 0.3 time with a dosage of 0.05mL. The highest observed velocity at this time step is 1.85 m/sec. However the tissue and tumor regions are shown with completely filled particle flow and the arteries show less particle flow.

Particle Velocity at 0.4 Time with 0.05 mL Concentration:**Figure 4.22(f) Particle velocity at 0.4sec**

The Figure 4.22(f) shows the particle velocity at time step 0.4 time with a dosage of 0.05mL. The highest observed velocity at this time is 0.33846 m/sec. Here the tissue and tumor regions are shown with completely filled particle flow with similar concentrations to the previous time, but there is much less particle flow in arterial region.

4.3.3 0.08 mL:

Particle Velocity at 0.1 Time with 0.08 mL Concentration:

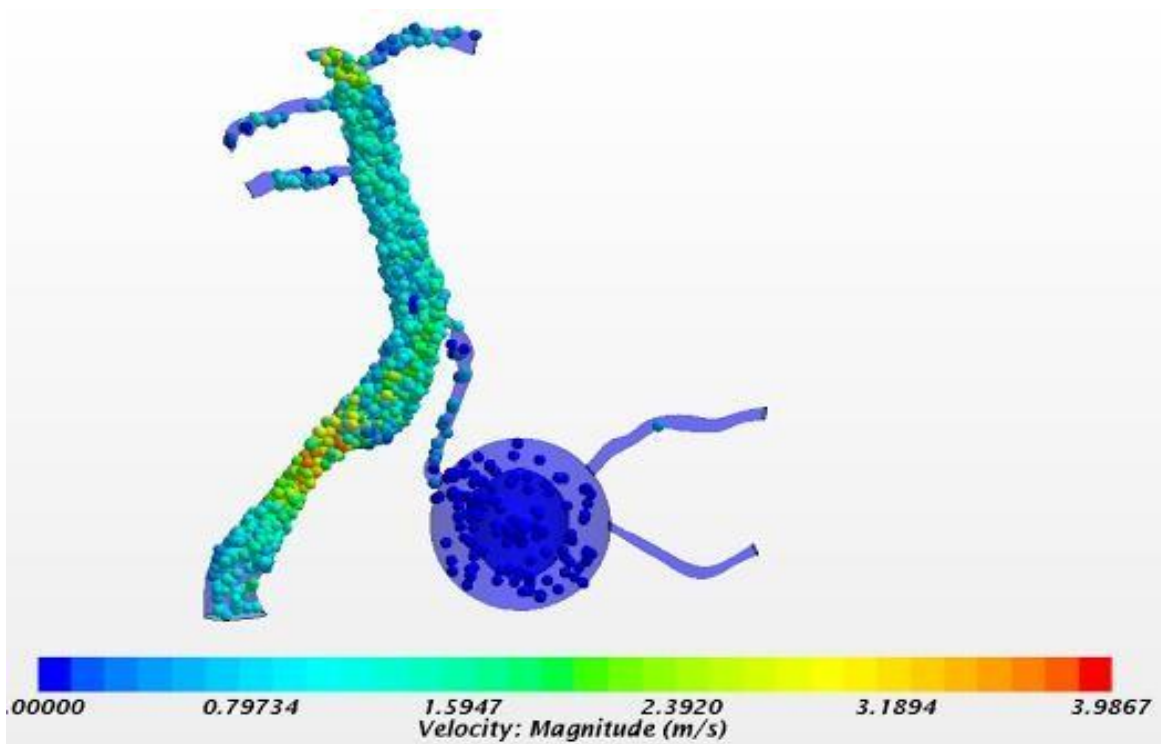
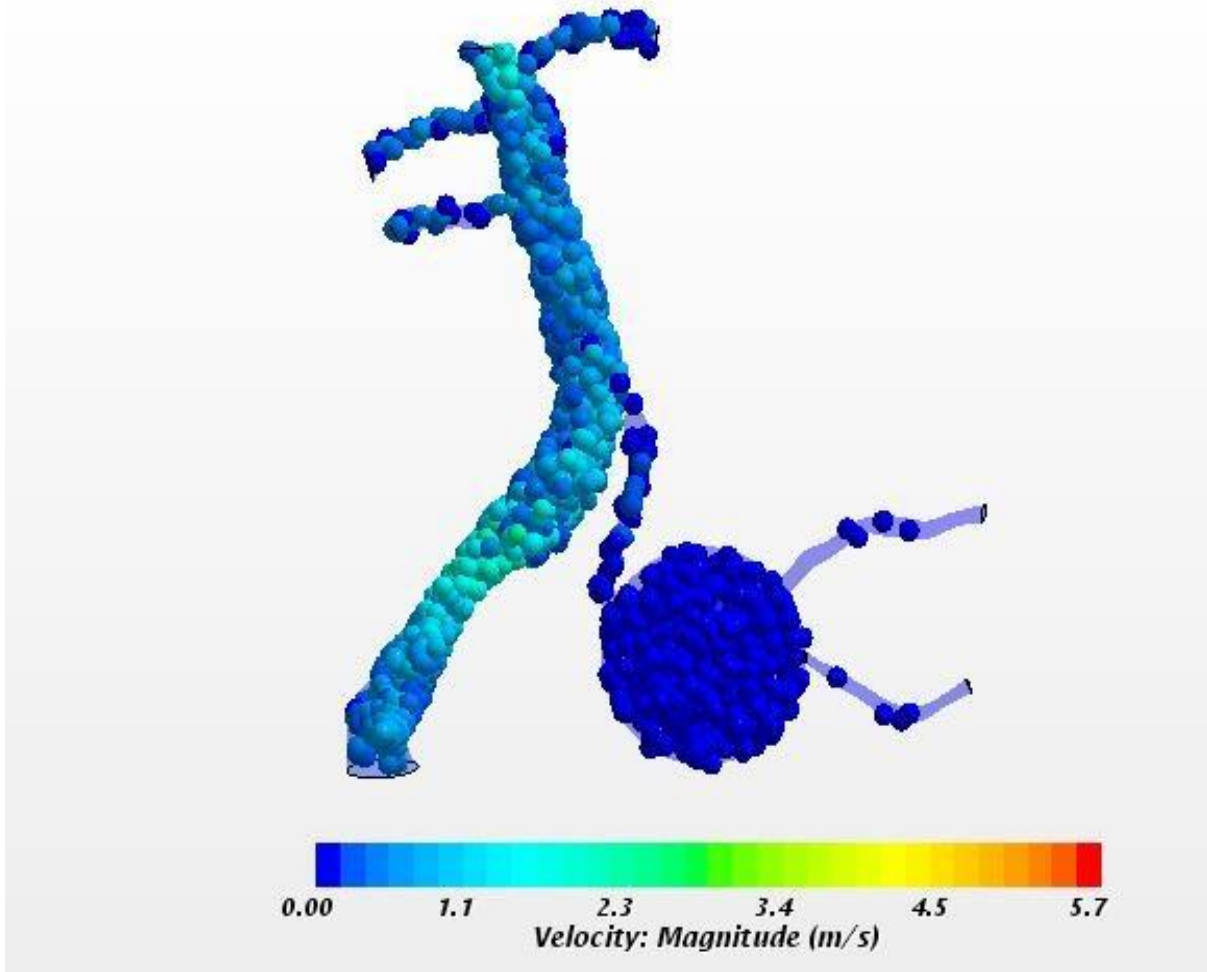
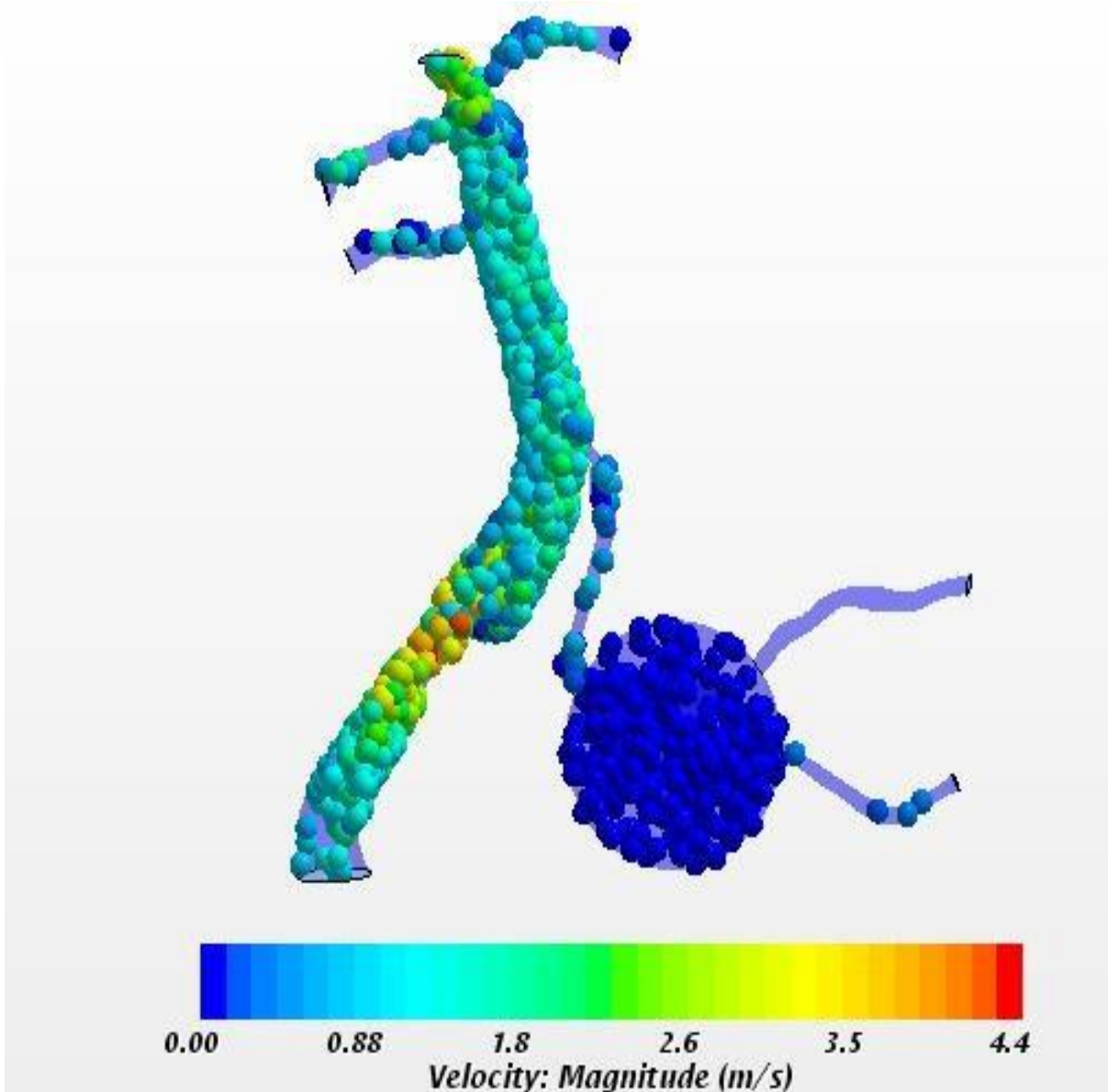


Figure 4.23(a) Particle velocity at 0.1sec

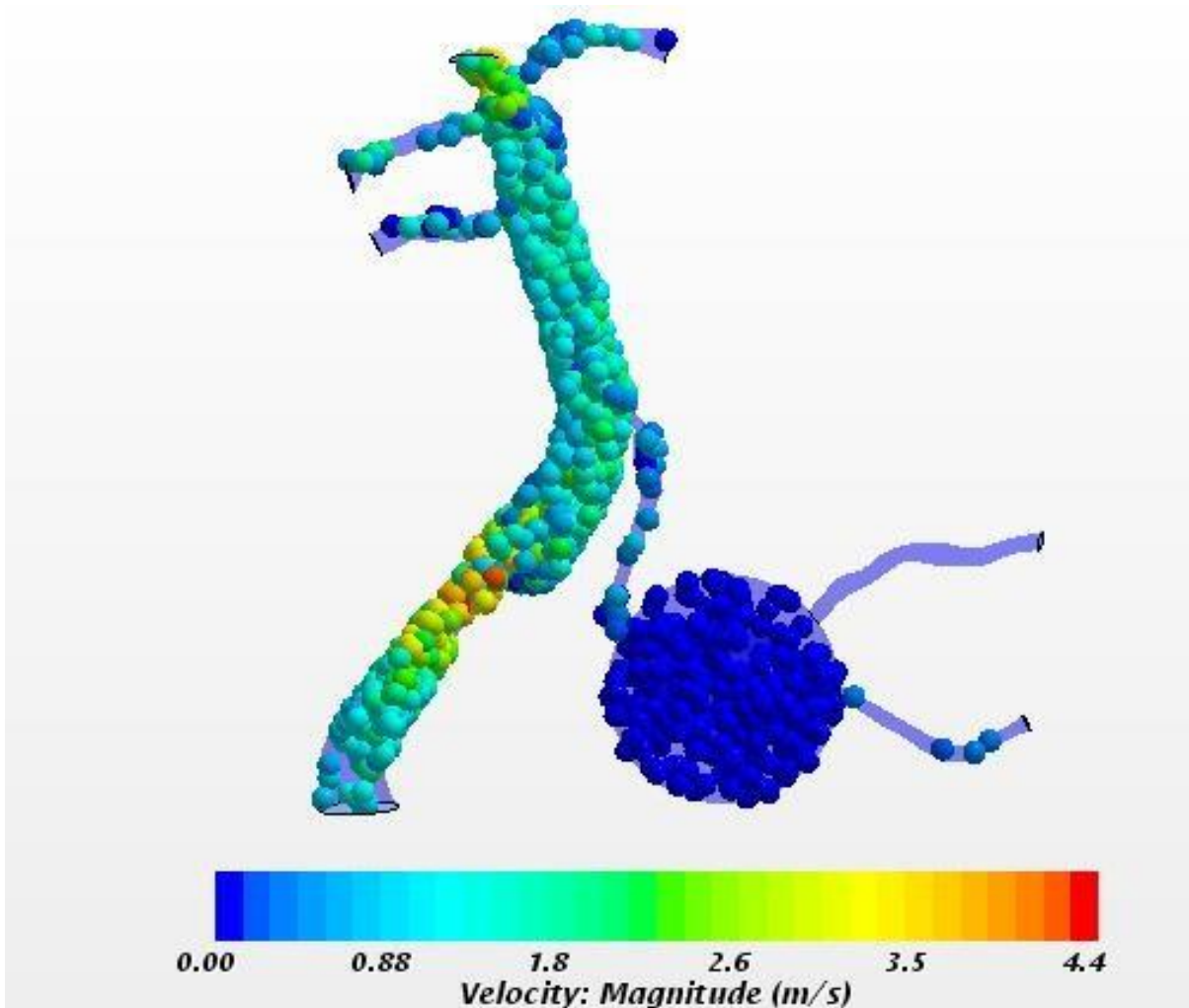
The Figure 4.23(a) shows the particle velocity at 0.1 time when a dosage of 0.08mL is given to blood flow through intravenous administration into the blood stream. The value obtained at this time step is 3.987m/sec, which is the maximum value observed at the arterial flow. Only a few particles are observed in the artery regions as the cycle is being initiated.

Particle Velocity at 0.125 Time with 0.08 mL Concentration:**Figure 4.23(b) Particle velocity at 0.125sec**

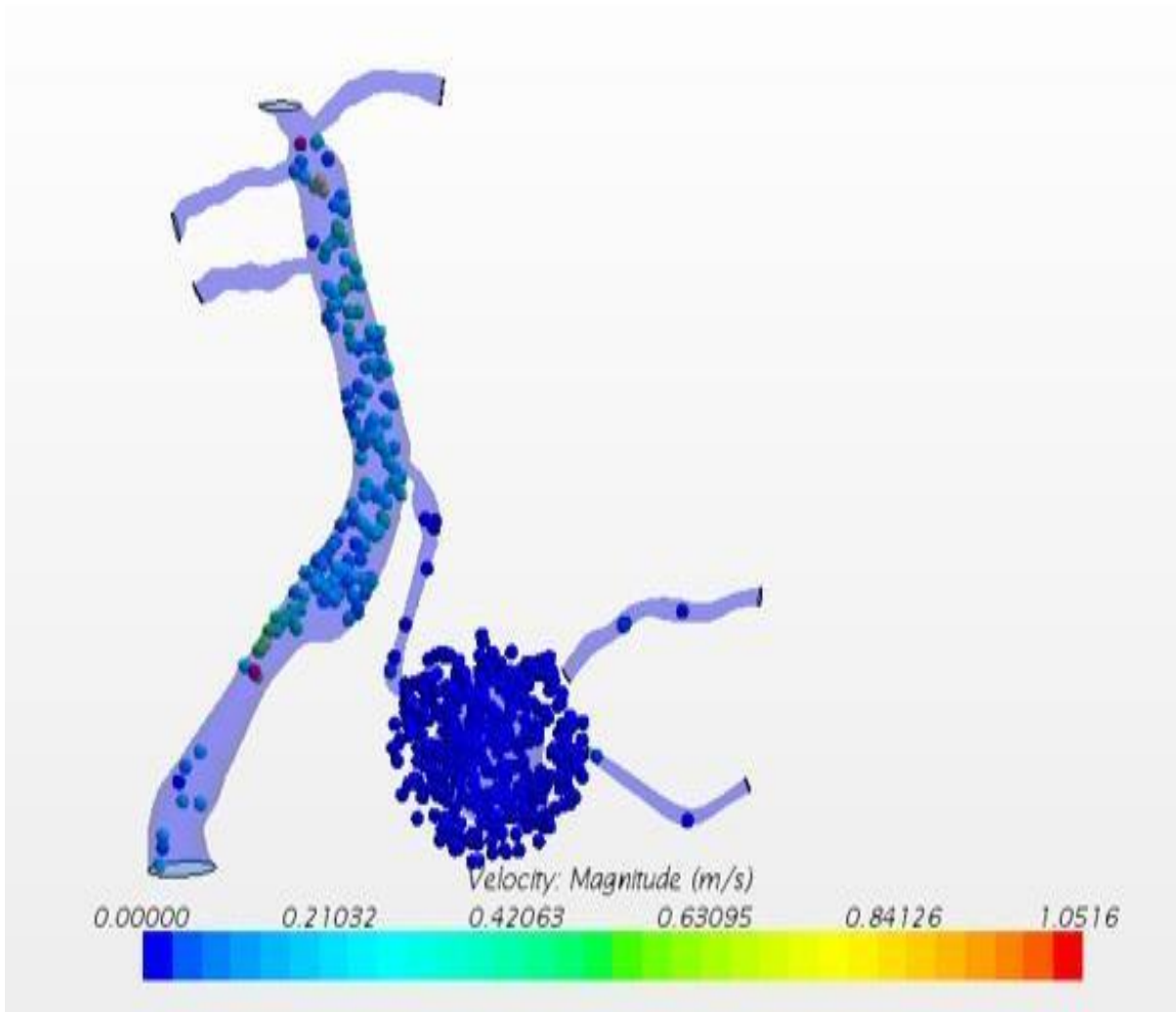
The Figure 4.23(b) shows the particle velocity at 0.125 time when a dosage of 0.08mL is inserted. The highest velocity is obtained at this time step and the observed velocity is 5.7m/sec. However the tissue and tumor regions are shown with completely filled particle flow with lower velocities ranging from 0 to 1 m/sec.

Particle Velocity at 0.2 Time with 0.08 mL Concentration:**Figure 4.23(c) Particle velocity at 0.2sec**

The Figure 4.23(c) shows the particle velocity at 0.2 time when a dosage of 0.08mL is inserted. The highest velocity is obtained at this time and the observed velocity is 4.4 m/sec.

Particle Velocity at 0.25 Time with 0.08 mL Concentration:**Figure 4.23(d) Particle velocity at 0.25sec**

The Figure 4.23(d) shows the particle velocity at time step 0.25 time with a dosage of 0.08mL. The highest observed velocity at this time step is 4.5 m/sec. However the tissue and tumor regions are shown with completely filled particle flow with similar concentrations to the previous time.

Particle Velocity at 0.3 Time with 0.08 mL Concentration:**Figure 4.23 (e) Particle velocity at 0.3sec**

The Figure 4.23(e) shows the particle velocity at time step 0.3 time with a dosage of 0.08mL. The highest observed velocity at this time is 1.056 m/sec. Here likewise the previous cases the tissue and tumor regions are shown with completely filled particle flow and the arteries show less particle flow.

Particle Velocity at 0.4 Time with 0.08 mL Concentration:

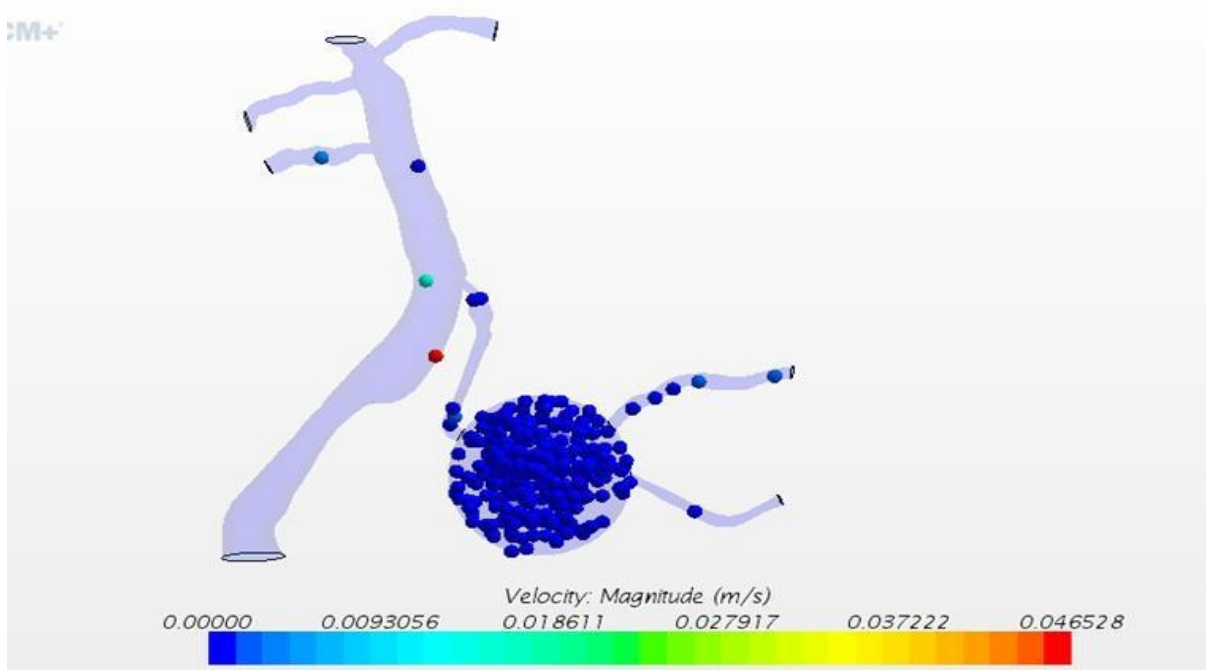


Figure 4.23(f) Particle velocity at 0.4sec

The Figure 4.23(f) shows the particle velocity at time step 0.4 time with a dosage of 0.08mL. The highest observed velocity at this time is 0.046528 m/sec. Even here like the previous concentration, results of the tissue and tumor regions are shown with completely filled particle flow with similar concentrations to the previous time step, but there is much less particle flow in arterial region.

In the above results with different concentration input, the velocity in the overall system looks similar with the concentrations of 0.05mL and 0.08 mL. However in order to predict the velocity and concentration at the tissue tumor region the velocities are scaled and snapped to the regions of tissue and tumor and analyzed for better penetration velocities as shown below.

4.4 Comparison of Velocities with Respect to Concentration in Increasing Order

0.1 Time:

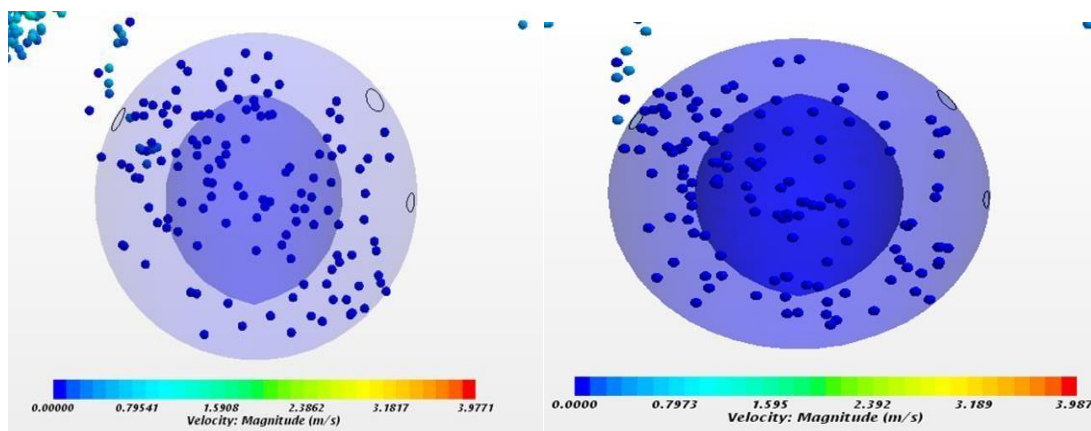


Figure 4.24 (a) 0.03mL

Figure 4.24(b) 0.05mL

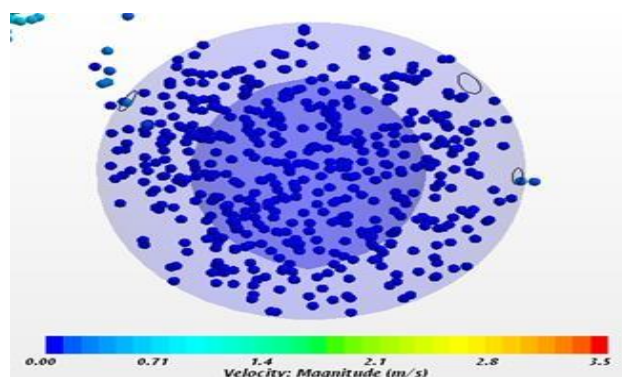


Figure 4.24(c) 0.08 mL

Figure 4.24 Particle velocity changes at tissue-tumor region at 0.1 time

The Figure 4.24 shows the particle velocity change at time step 0.1 time step with a change in dosage from 0.03mL to 0.08mL. The highest observed velocity at this time is 3.9 m/sec for 0.03mL and least for 0.08mLas 3.5 m/sec. Then the velocity decreased with increase in concentration.

0.125 Time:

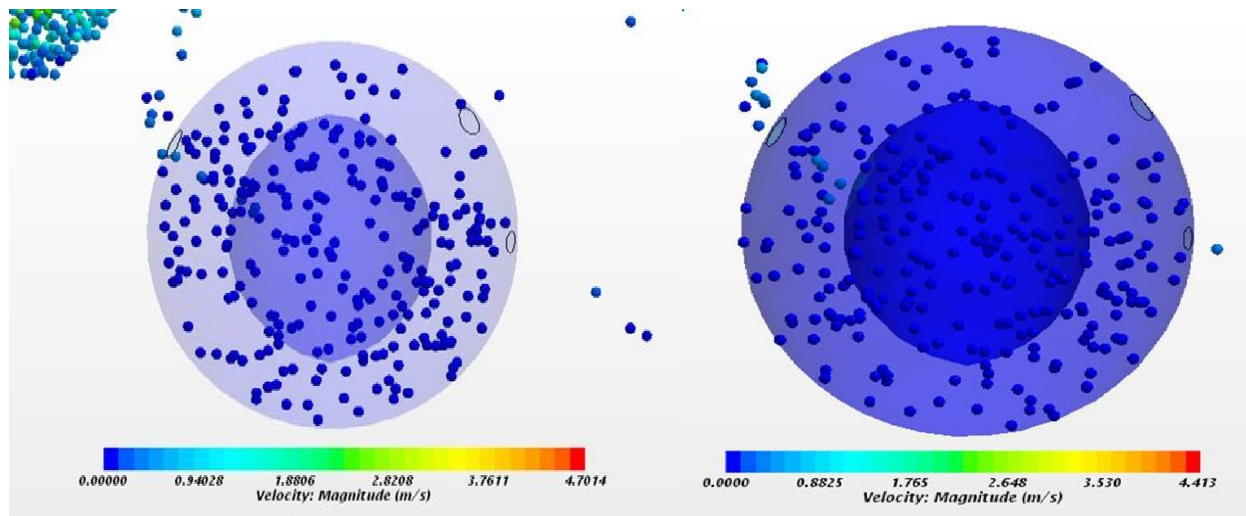


Figure 4.25(a) 0.03mL

Figure 4.25(b) 0.05mL

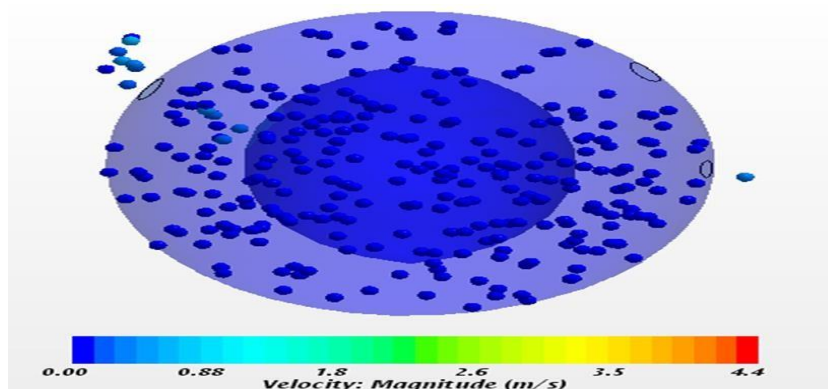


Figure 4.25(c) 0.08mL

Figure 4.25 Particle velocity changes at tissue-tumor region at 0.125 time

The Figure 4.25 shows the particle velocity change at time 0.125 with a change in dosage from 0.03mL to 0.08mL. The highest observed velocity at this time is 4.7 m/sec for 0.03mL. Then the velocity decreased with increase in concentration.

0.3 Time:

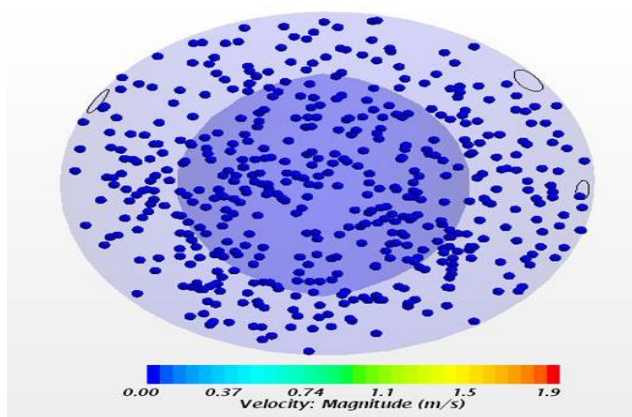


Figure 4.26 (a) 0.03mL

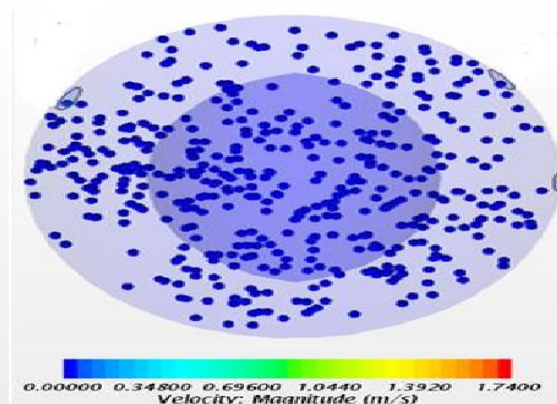


Figure 4.26(b) 0.05mL

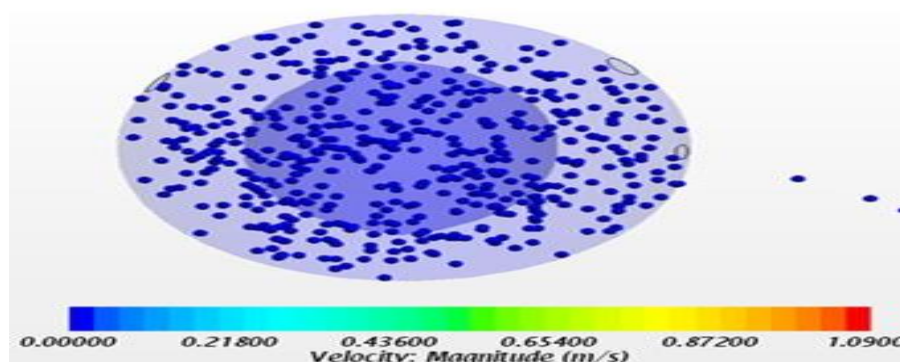


Figure 4.26 (c) 0.08 mL

Figure 4.26 Particle velocity changes at tissue-tumor region at 0.3 time

The Figure 4.26 shows the particle velocity change at time step 0.3 time with a change in dosage from 0.03mL to 0.08mL. The highest observed velocity at this time is 1.9 m/sec for 0.03mL and least for 0.08mL as 1.09 m/sec. Then the velocity decreased with increase in concentration.

0.4 Time:

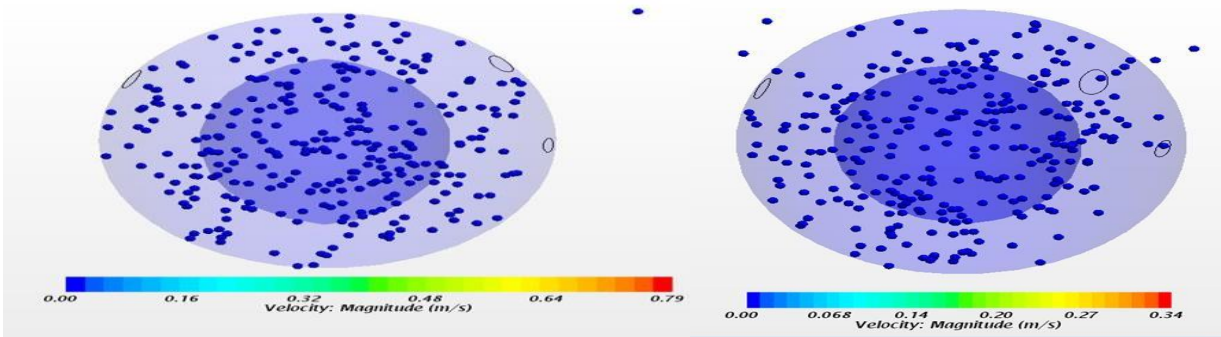


Figure 4.27 (a) 0.03mL

Figure 4.27 (b) 0.05mL

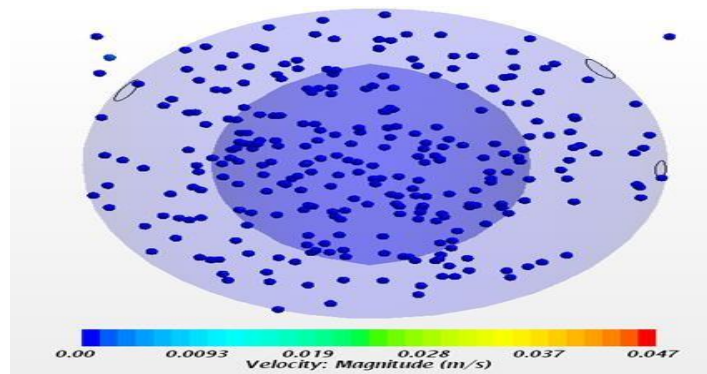


Figure 4.27 (c) 0.08 mL

Figure 4.27 Particle velocity changes at tissue-tumor region at 0.4 time

The Figure 4.27 shows the particle velocity change at time step 0.4 time with a change in dosage from 0.03mL to 0.08mL. The highest observed velocity at this time step is 0.79 m/sec for 0.03mL and least for 0.08mL as 0.047m/sec. Then the velocity decreased drastically with increase in concentration and also due to the decreased blood flow through cardiac input.

Now, to analyze the velocity within the vicinity of tumor, a line probe originating from the capillary and passing through the tumor is drawn. The following results show the velocity changes in the tumor at the central area.

4.5 Velocity Changes with respect to Cardiac Cycle in Tumor at the Central Area

The Figure 4.28 shows the velocity with which the particle is flowing in the tumor area from the capillaries penetrating through the tissue.

0.125 Time:

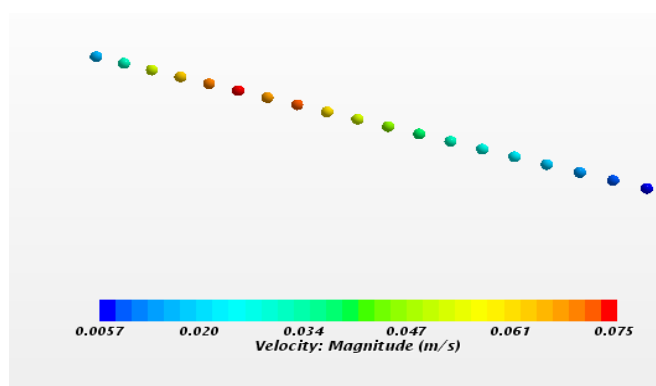


Figure 4.28 (a) 0.03mL

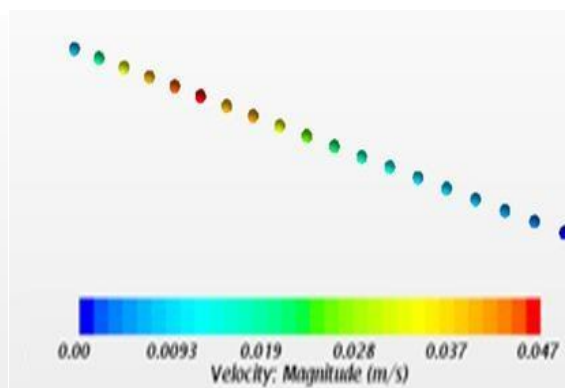


Figure 4.28 (b) 0.05mL

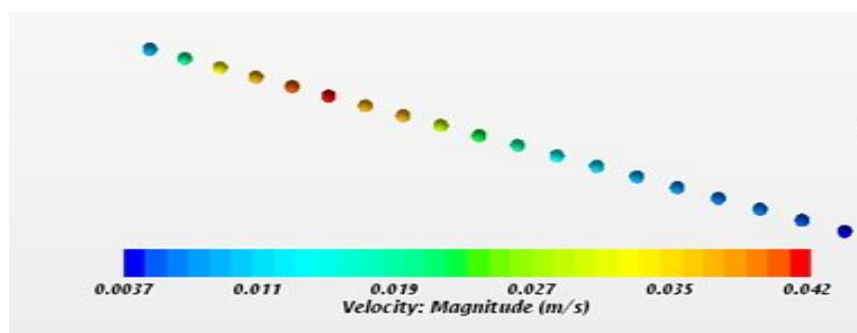


Figure 4.28 (c) 0.08 mL

Figure 4.28 Line probe of particle velocity at tissue-tumor region at 0.125 time

The Figures 4.28 (a), (b), (c) show the particle velocity change at time 0.125 sec with a change in dosage from 0.03mL to 0.08mL. The highest observed velocity at this time is 0.075m/sec for 0.03mL and least for 0.08mL as 0.042m/sec.

0.3 Time:

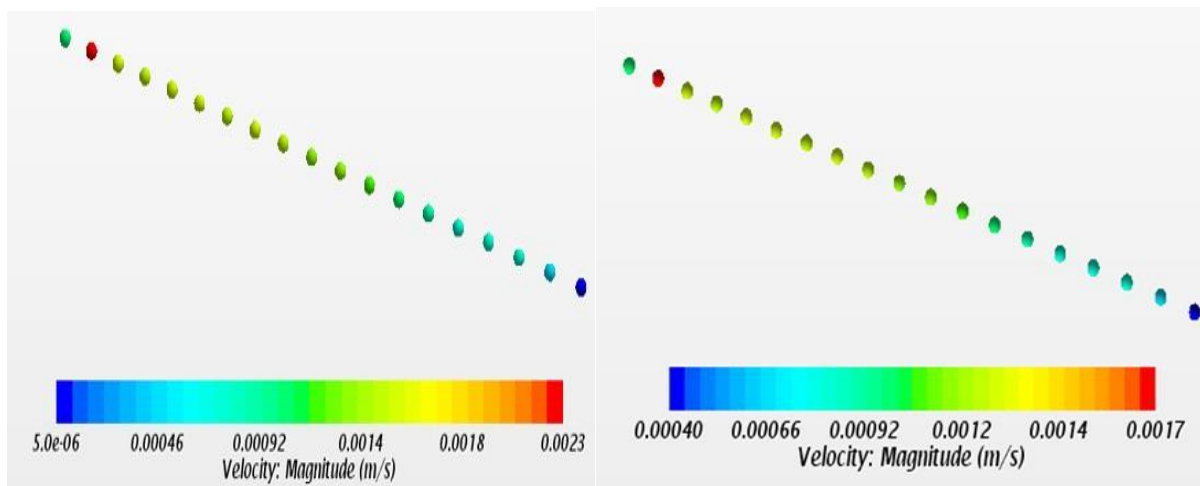


Figure 4.29 (a) 0.03mL

Figure 4.29 (b) 0.05mL

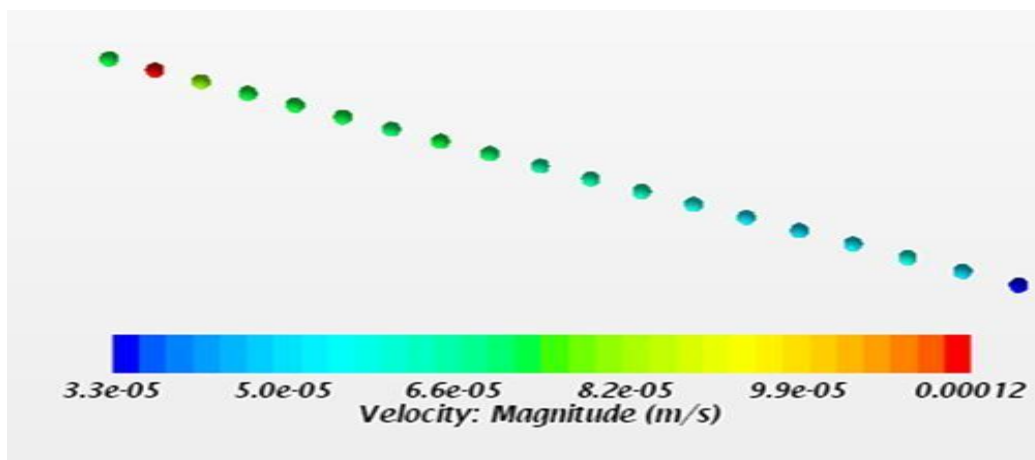


Figure 4.29 (c) 0.08 mL

Figure 4.29 Line probe of particle velocity at tissue-tumor region at 0.3 time

The Figure 4.29 shows the particle velocity change at 0.3 time with a change in dosage from 0.03mL to 0.08mL. The highest observed velocity at this time is 0.0023m/sec for 0.03mL and least for 0.08mL as 0.00012m/sec.

0.4 Time:

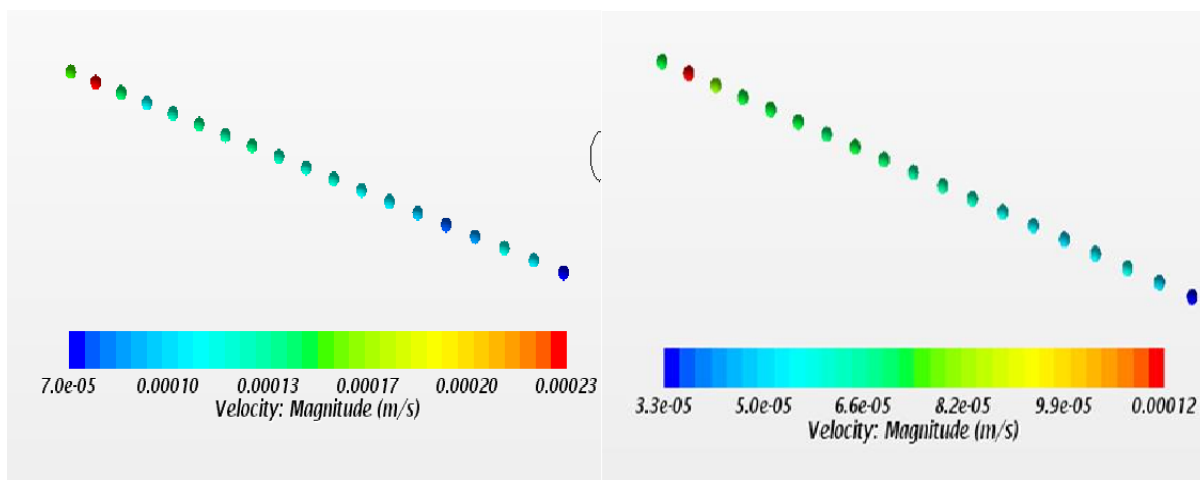


Figure 4.30 (a) 0.03mL

Figure 4.30(b) 0.05mL

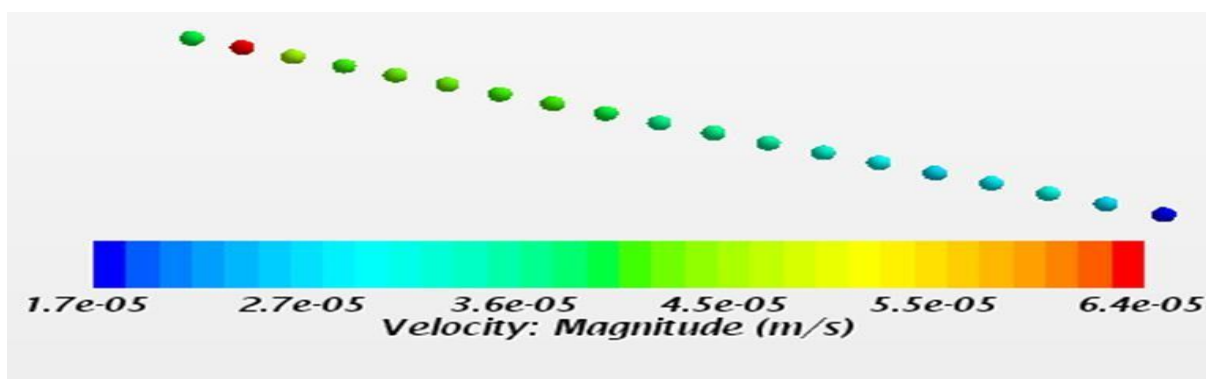


Figure 4.30 (c) 0.08 mL

Figure 4.30 Line probe of particle velocity at tissue-tumor region at 0.4 time

The Figure 4.30 shows the particle velocity change at time step 0.4 time with a change in dosage from 0.03mL to 0.08mL. The highest observed velocity at this time is 0.0023m/sec for 0.03mL and least for 0.08mL as 6.4×10^{-5} m/sec.

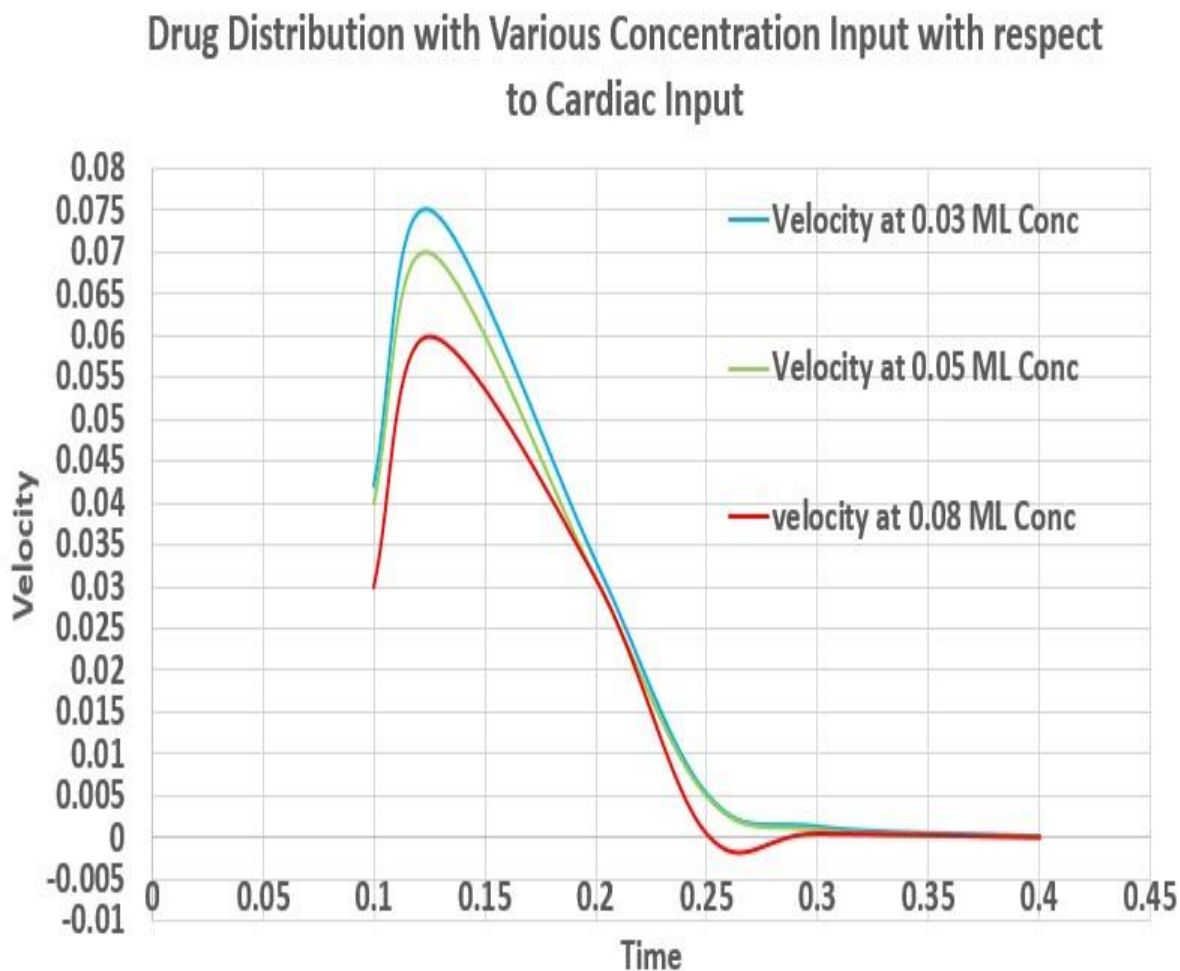


Figure 4.31 Drug distribution with various concentration input with respect to cardiac input

The plot in Figure 4.31 shows the velocity with which the particle penetrates into the tissue tumor region with different input concentrations. It is observed that with increase in concentration the particles are moving with slower velocity into the regions of tissue and tumor. However each input is following the cardiac input cycle. This plot can only emphasize the effect on velocity with increase in concentration. But in order to show the particles which are entering

into the tissue region we have to see the particle count or volume fraction.

Concentration at line probe:

Velocity alone cannot assure us to find out the effect of drug in the site of tumor. Concentration distribution analysis gives better idea. A line probe passing through the tumor is drawn to analyze the concentration of drug particles at that site. The Figure 4.23(a) and 4.23(b) show the distribution variation with respect to drug changes. It is observed in plot that with increase in dosage there is huge increment in particle settling up at the target region. But there is less difference observed with the concentration increase from 0.05mL to 0.08mL.

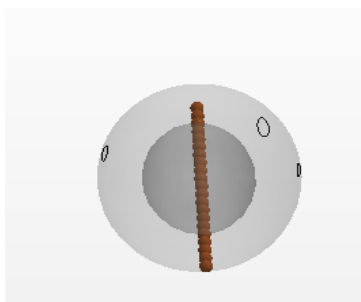


Figure 4.32 (a) Probe

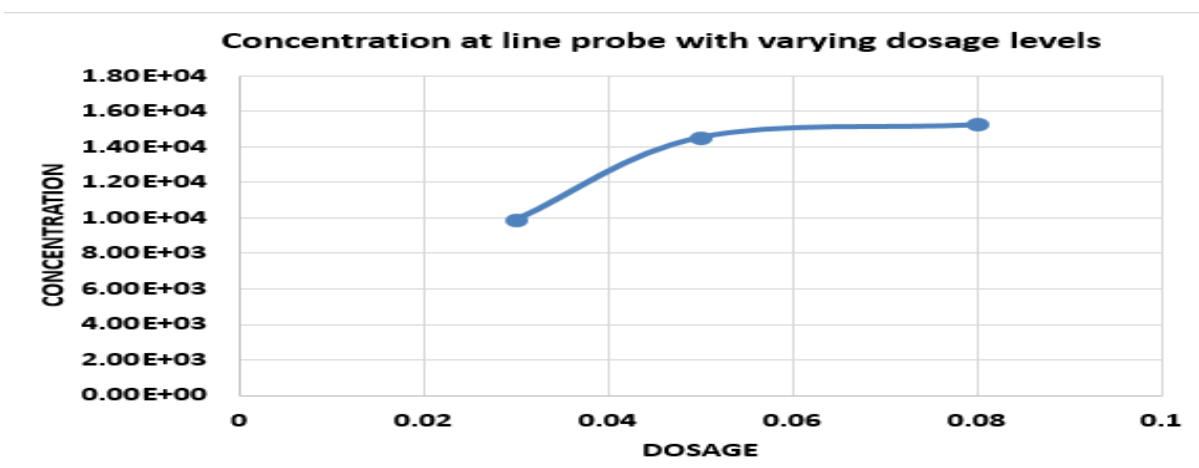


Figure 4.32 (b) Concentration at line probe with varying dosage level

4.6 Results for Drug Distribution in Reconstructed Brain

For this case two drugs which can cross the protective barriers of brain are considered. The densities of the drugs are 1460 and 1960kg/m^3 respectively. Using the human equivalent drug dosage estimation, the dosages of 0.01mL , 0.03mL and 0.05mL are considered as administering dosages for this study. The below results are obtained at time steps from 0.1 - 0.5 sec of cardiac cycle for the changed concentrations, changed particle dimensions and changed densities.

4.6.1 Dosage of 0.01 mL :

Particle Velocity at 0.1 Time with 0.01 mL Concentration:

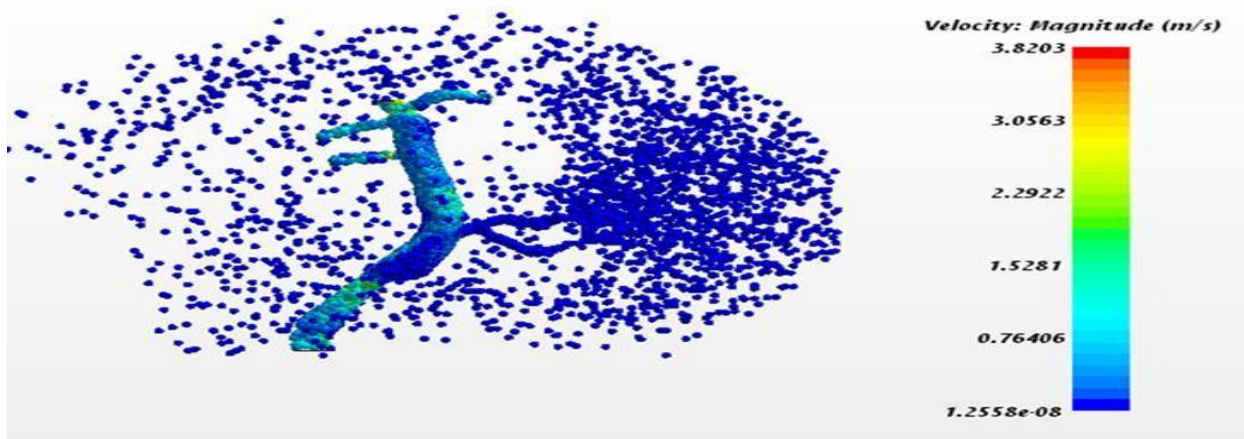
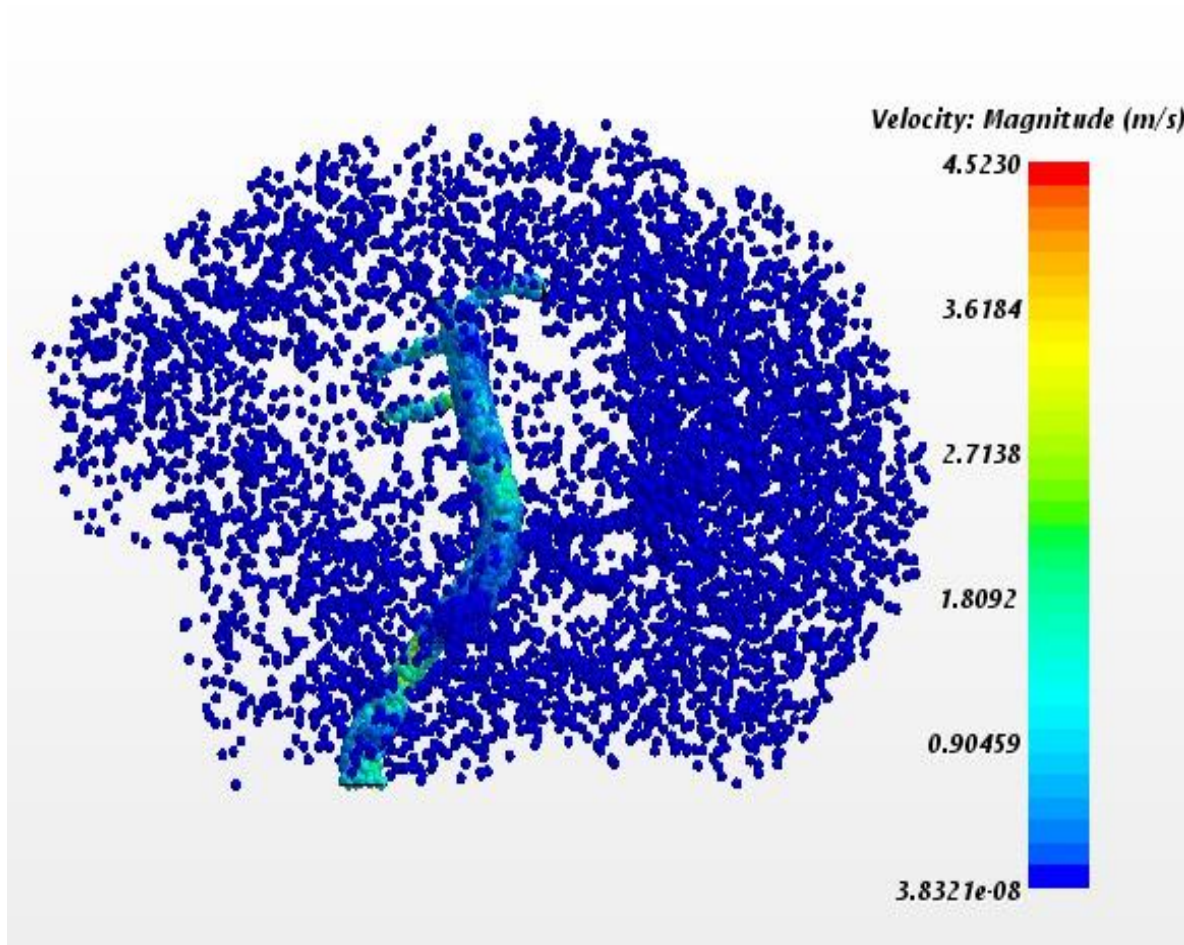


Figure 4.33(a) Particle velocity in reconstructed brain at 0.1 time with 0.01mL

The Figure 4.23(a) shows the particle velocity at 0.1 time when a dosage of 0.01mL is inserted into the blood stream. The highest velocity with which the particle flows is 3.8203m/sec . However the tissue and the tumor regions receive blood flow with lesser velocities which are numerically negative.

Particle Velocity at 0.125 Time with 0.01 mL Concentration:**Figure 4.33(b) Particle velocity in reconstructed brain at 0.125 time with 0.01mL**

The Figure 4.33(b) shows the particle velocity at 0.125 time when a dosage of 0.01mL is inserted into the blood stream. The highest velocity with which the particle flows is 4.5230m/sec. However the tissue and the tumor regions receive blood flow with lesser velocities. There is an increased particle flow due to the increased cardiac input into the tumor tissue region compared to previous and the other flows at various times shown.

Particle Velocity at 0.25 Time with 0.01 mL Concentration:

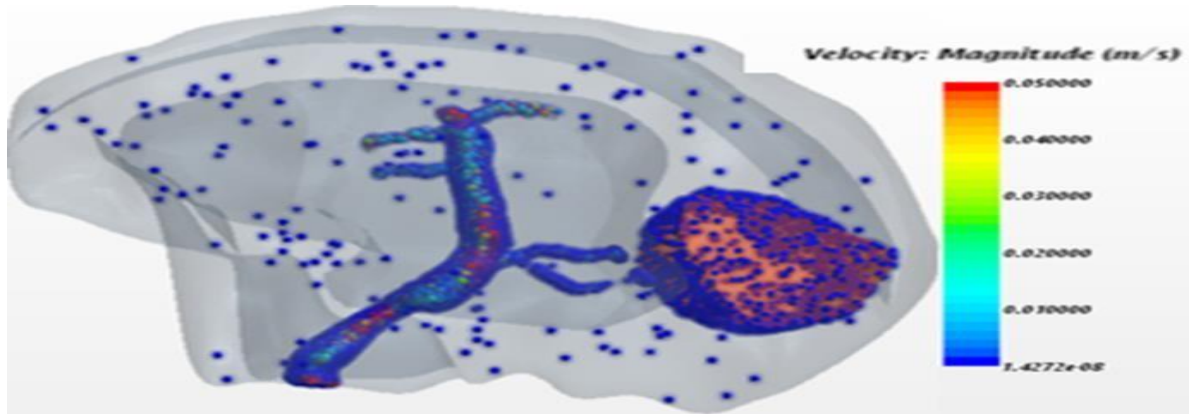


Figure 4.33(c) Particle velocity in realistic brain at 0.25 time with 0.01mL

The Figure 4.33(c) shows the scaled particle velocity at 0.25 time when a dosage of 0.01mL is inserted into the blood stream. Here the maximum particle velocity observed is 1.8m/sec.

Particle Velocity at 0.5 Time with 0.01mL Concentration:

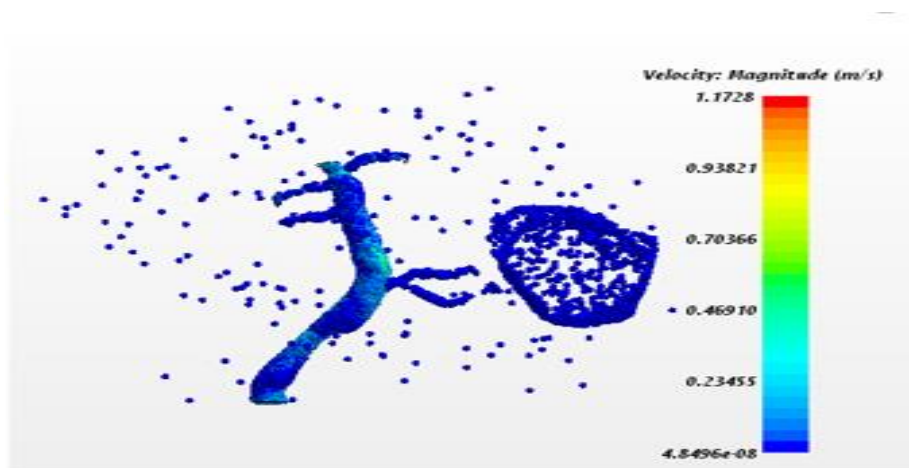


Figure 4.33 (d) Particle velocity in reconstructed brain at 0.5 time with 0.01mL

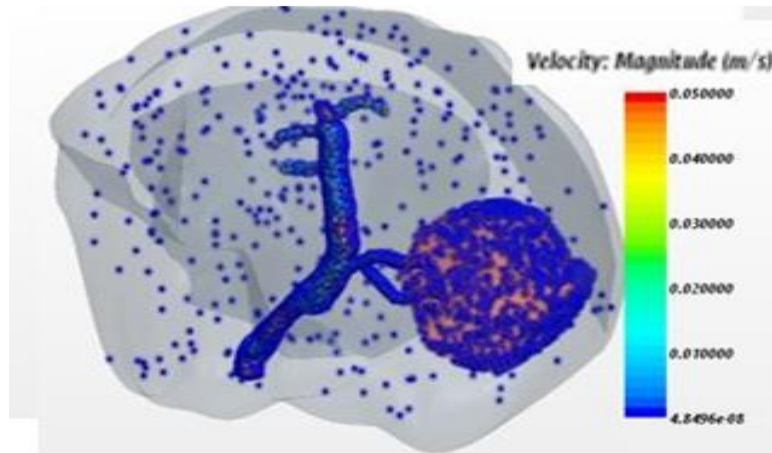


Figure 4.33 (e) Scaled particle velocity in reconstructed brain at 0.5 time with 0.01mL

The Figure 4.33(e) shows the particle velocity at 0.5 time when a dosage of 0.01mL is inserted into the blood stream. The values obtained at this time is 1.17m/sec. Here only a few particles are observed in the tissue regions and concentrated particle at the tumor region as the cycle is being finished.

4.6.2 Dosage of 0.03 mL:

Particle Velocity at 0.1 Time with 0.03 mL Concentration:

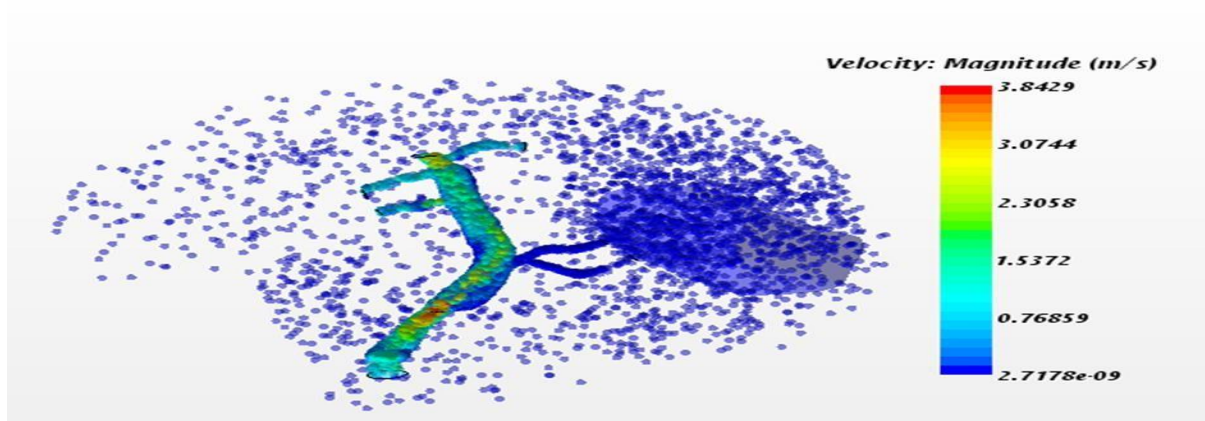


Figure 4.34 (a) Particle velocity in reconstructed brain at 0.5 time with 0.03mL

The Figure 4.34(a) shows the particle velocity at 0.1 time when the drug dosage of 0.03mL is inserted into the blood stream. The highest velocity with which the particle flows is 3.8425m/sec. However the tissue and the tumor regions receive blood flow with lower velocities compared to the 0.01mL dosage. But in both cases, the values are numerically negative.

Particle Velocity at 0.125 Time with 0.03 mL Concentration:

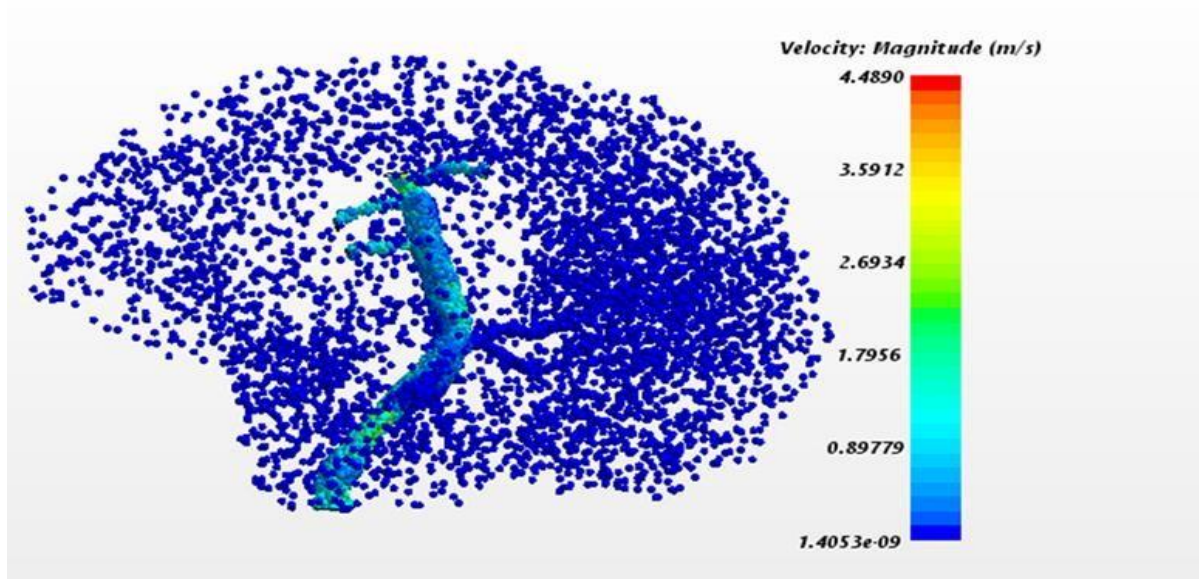


Figure 4.34(b) Particle velocity in reconstructed brain at 0.125 time with 0.03mL

The Figure 4.34(b) shows the particle velocity at 0.125 time when a dosage of 0.03mL is inserted into the blood stream. The highest velocity with which the particle flows is 4.48m/sec. This velocity is the highest peak velocity observed during the cardiac cycle at this time, reflecting the highest drug flow. Even here the tissue and the tumor regions receive blood flow with lesser velocities of 1.405E-9 m/sec.

Particle Velocity at 0.25 Time with 0.03 mL Concentration:

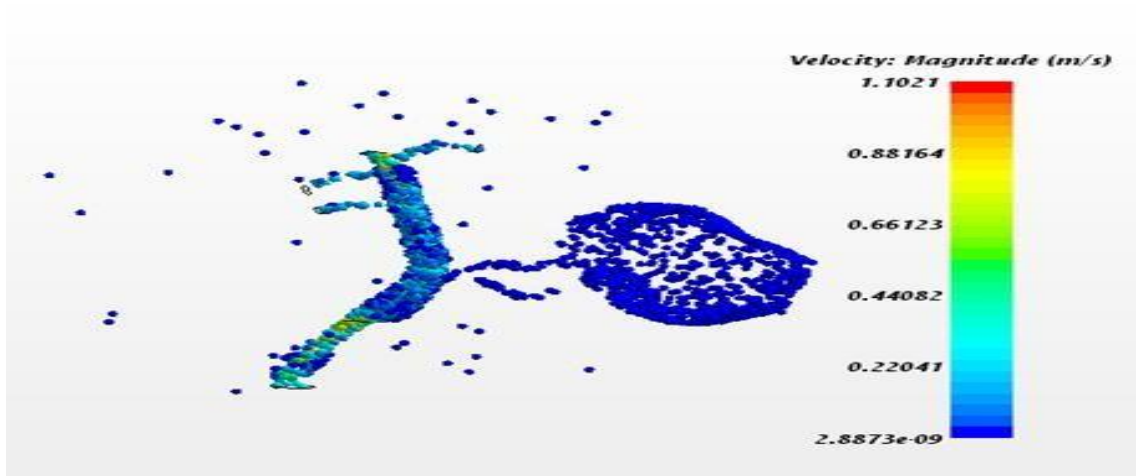


Figure 4.34(c) Particle velocity in reconstructed brain at 0.25 time with 0.03mL

The Figure 4.34(c) shows the particle velocity at 0.25 time. Here the particle flows with a maximum velocity of only 1.1021m/sec. The scaled magnitudes show the better view of changes in particle velocity. In this time the particle velocity is least and it reaches the value of 2.887E-9m/sec, which is the least velocity observed through the cycle.

Particle Velocity at 0.5 Time with 0.03mL Concentration:

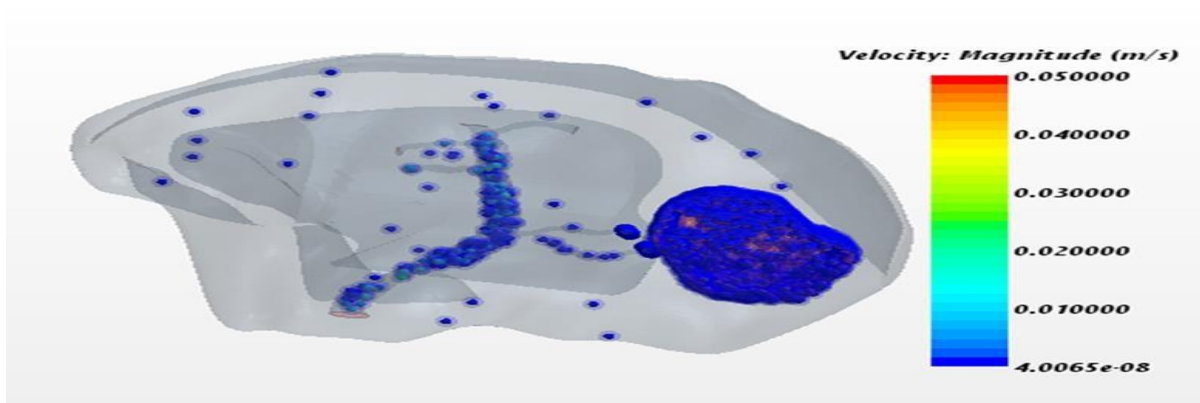


Figure 4.34(d) Scaled particle velocity in reconstructed brain at 0.5 time with 0.03 mL

The Figure 4.34(d) shows the scaled particle velocity at 0.5 time when a dosage of 0.03mL is inserted into the blood stream. The highest velocity values obtained at this time is 1.08 m/sec at the artery and $4.0065E-8$ at the target area. Here only a few particles are observed in the tissue regions and concentrated particle at the tumor region as the cycle is being finished. However the particle velocity raised with respect to rise in cardiac cycle flow.

4.6.3 Dosage of 0.05 mL:

Particle Velocity at 0.1 Time with 0.05 mL Concentration

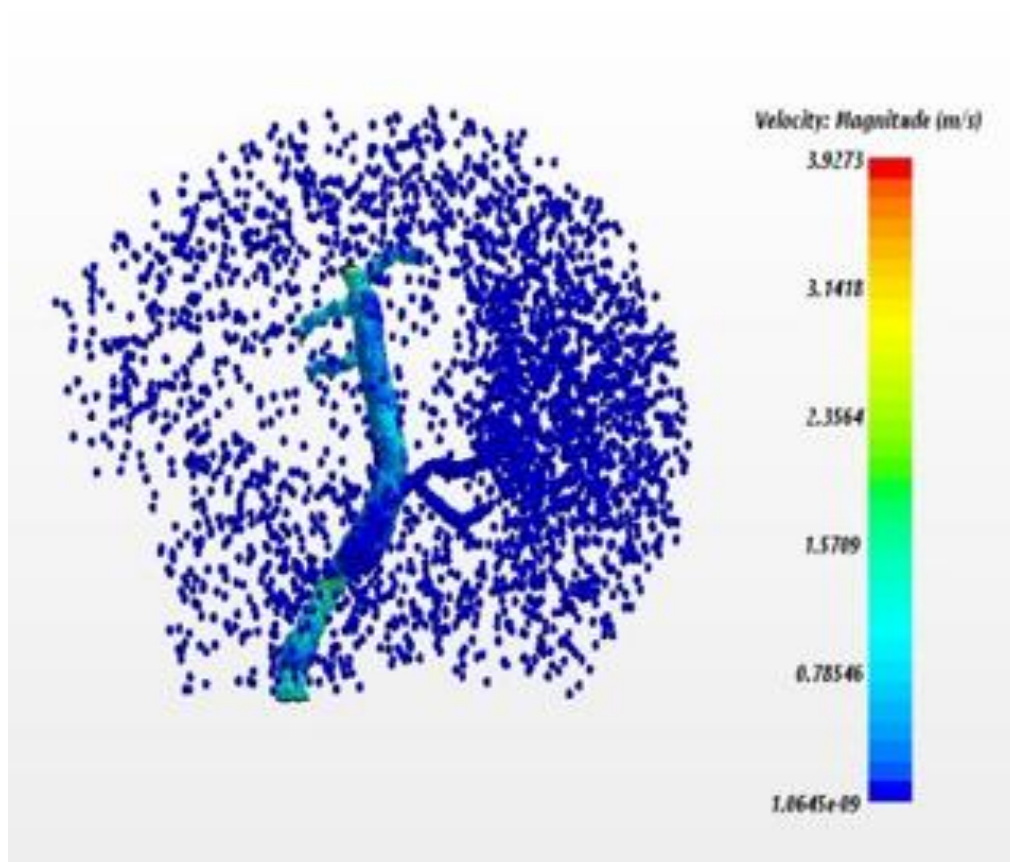


Figure 4.35(a) Particle velocity in reconstructed brain at 0.1 time with 0.05 mL

The Figure 4.35(a) shows the particle velocity at 0.1 time when the drug dosage of 0.05mL is inserted into the blood stream. The highest velocity with which the particle flows is 3.9m/sec. However the tissue and the tumor regions receives blood flow with lower velocities compared to the 0.01mL dosage, but in both cases the values are numerically negative.

Particle Velocity at 0.125 Time with 0.05 mL Concentration:

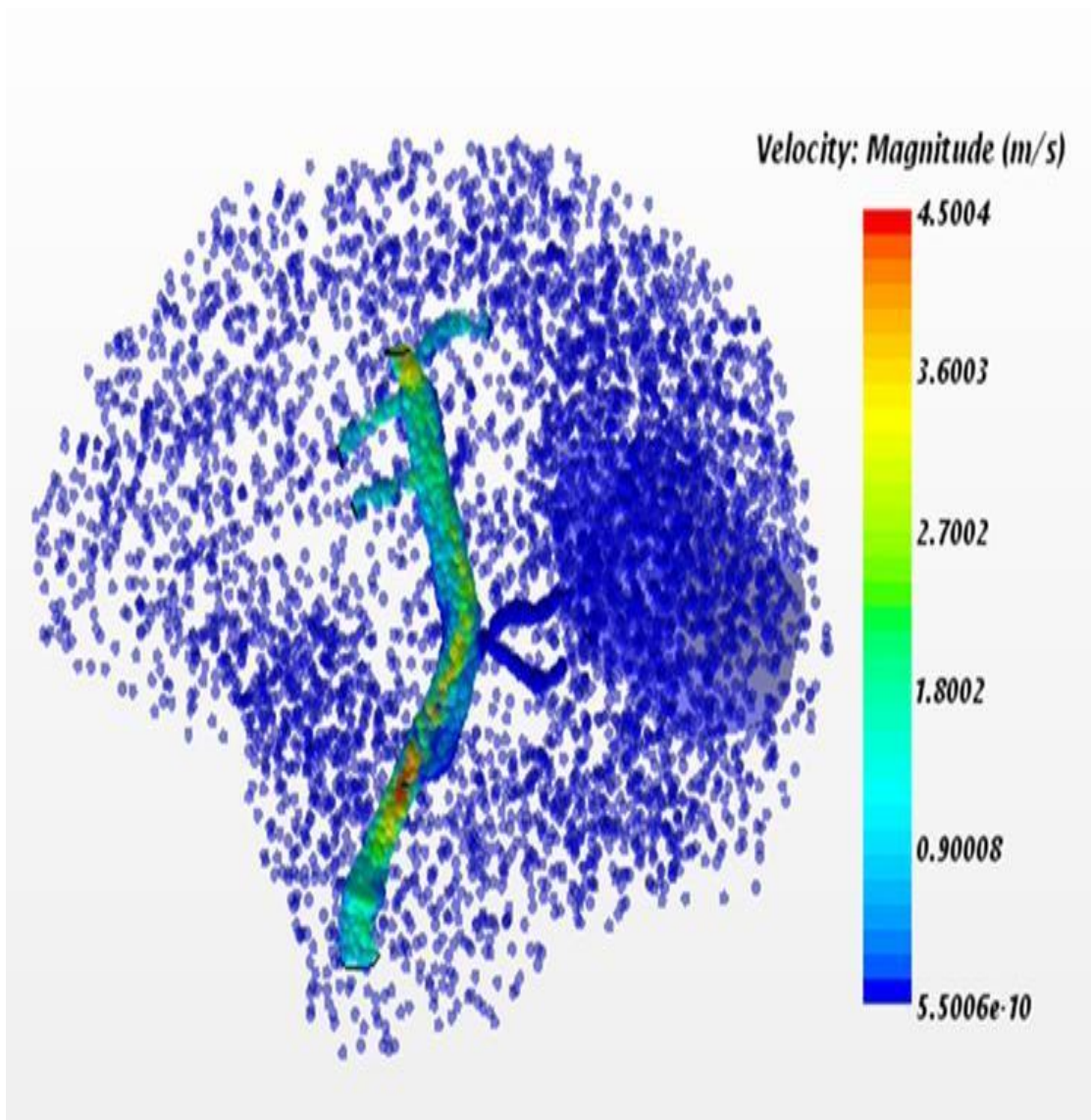


Figure 4.35(b) Particle velocity in reconstructed brain at 0.125 time with 0.05 mL

The Figure 4.35(b) shows the particle velocity at 0.125 time when a dosage of 0.05mL is inserted into the blood stream. The highest velocity with which the particle flows is 4.5004m/sec. This velocity is the highest peak velocity observed during the cardiac cycle at this time, reflecting the highest drug flow. Even here the tissue and the tumor regions receive blood flow with lesser velocities of 5.56E-10m/sec.

Particle Velocity at 0.25 Time with 0.05mL Concentration:

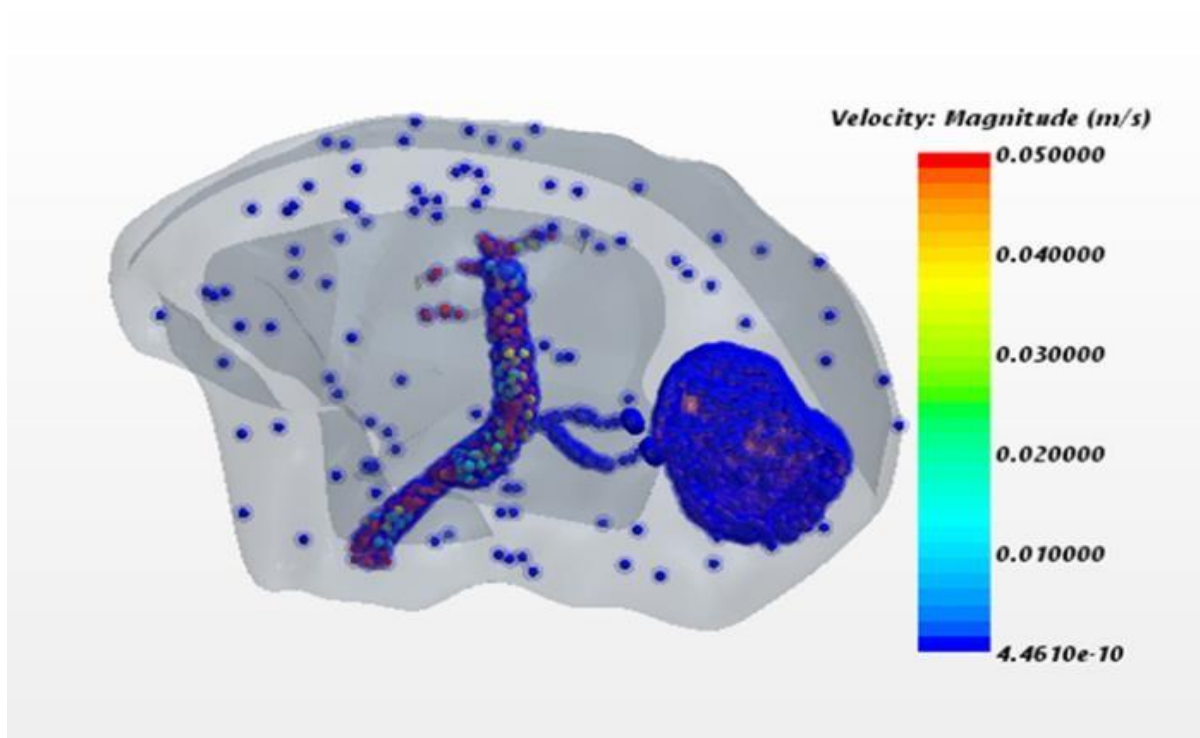


Figure 4.35(c) Scaled particle velocity in reconstructed brain at 0.25 time with 0.05 mL

The Figure 4.35(c) shows the scaled particle velocity at 0.25 time when a dosage of 0.05mL is inserted into the blood stream. The value obtained at this time step is 1.0021m/sec at the artery and 4.46E-10 at the target area, which is the least velocity observed through the cycle.

Here only a few particles are observed in the tissue regions and concentrated particle at the tumor region.

Particle Velocity at 0.5 Time with 0.05 mL Concentration:

The Figure 4.35(d) shows the particle velocity as 0.05 time. Here the particle flows with a maximum velocity of only 4.5230m/sec. The scaled magnitudes shows the better view of changes in particle velocity. In this time the particle velocity is least and it reaches the value of 1.9E-8m/sec, due to rise observed at the point of the cycle.

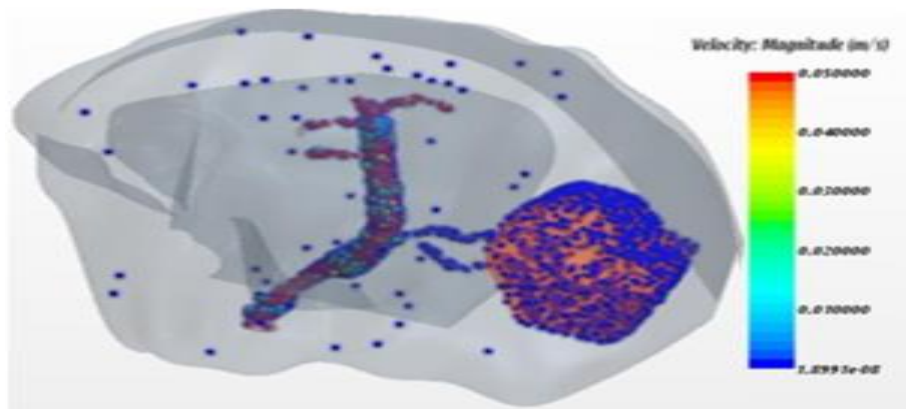


Figure 4.35(d) Scaled Particle velocity in reconstructed brain at 0.25 time with 0.05 mL

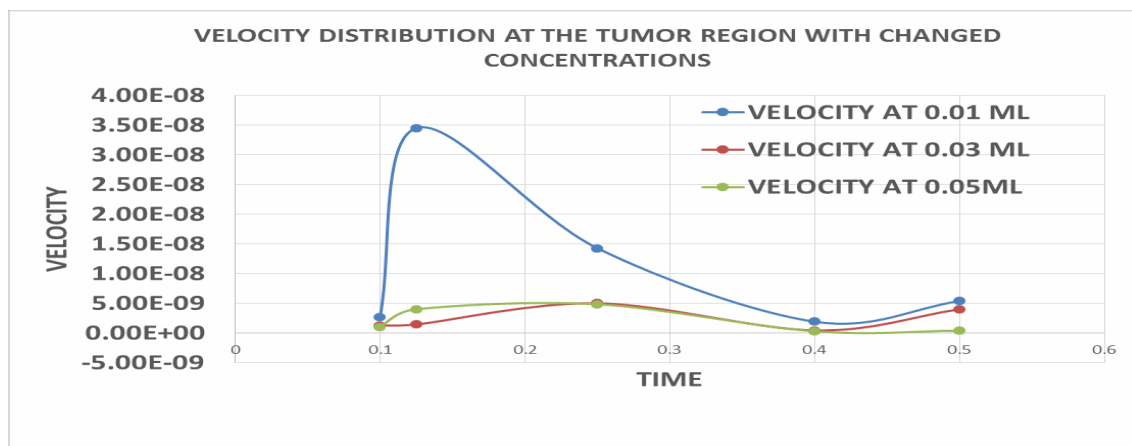


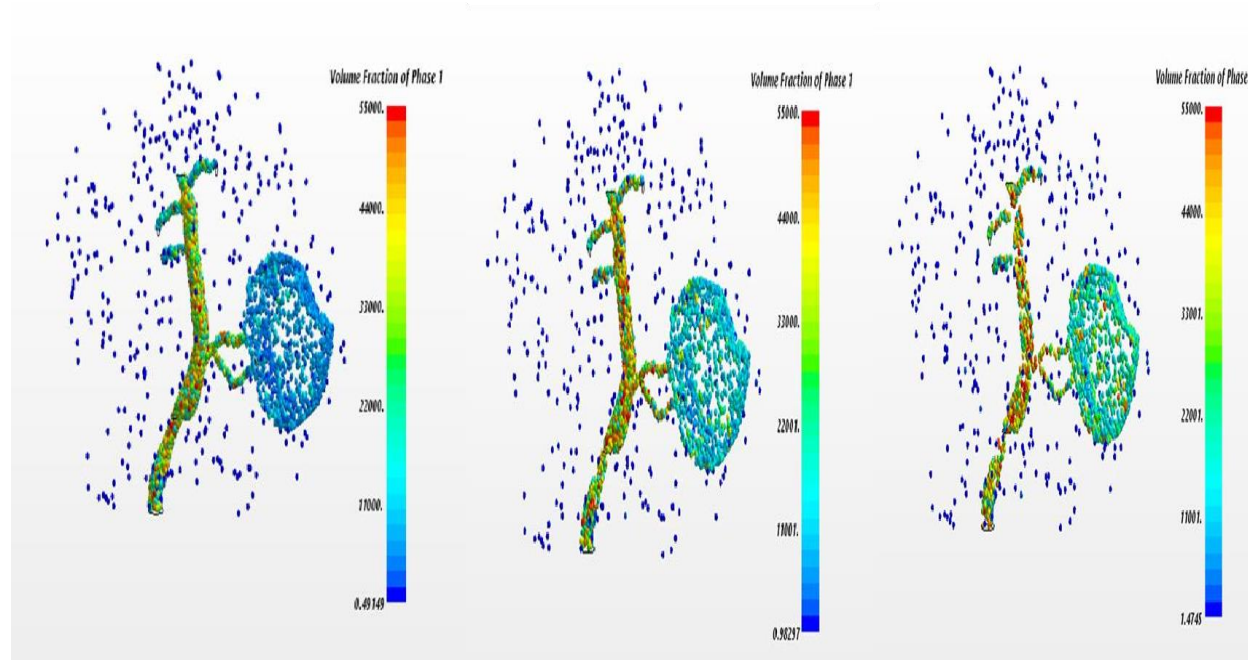
Figure 4.36 velocity distribution at the tumor region with changed concentrations

The Figure 4.36 shows the velocity penetrations of the drug with different concentrations in the realistic brain at the site of tumor. A line plot passing through the tumor from the input as artery is considered to see the results. As shown in the plot for the three different dosage inputs, the velocity of 0.01 mL is far highest when compared to the other two dosages. If the values are scaled on percentage, the 0.01mL velocities are 10% higher at the peak velocity of cardiac cycle and 5% cycle at the negative phase of cardiac cycle and then the percentage reduced to 2%. But the other two drug dosages gave almost nearer penetration velocity at every time step with less reach of drug to areas out of target. Also the results of drug flow show much delivery of drug at 0.03mL when compared to 0.05mL, where the particles also carried away to other parts in more quantity compared to 0.03mL case. With this we can say that 0.03mL could be the optimal drug dosage for this case as there is no big change observed in the penetration velocity for the two dosages. However, only velocity penetration could not definitely act as the deciding factor. Therefore concentration of particles at the site of tumor is to be analyzed.

4.7 Results for Drug Concentration Distribution in Realistic Brain and at the Site of Tumor

The concentrations at times 0.25 and 0.5 are observed to analyze the concentration at the target region. Since the two types of flows considered here are liquids, concentrations are shown as the volume fractions. Also the results are scaled and magnified such that the highest volume that can be shown in the figure is 55000, as it shows clearly the fate of concentrations of particles at that the tumor area. At this time we can observe that with the increase in dosage the concentration at the tumor site and the healthy regions is increasing. However we can see the lowest

concentrations at the site of healthy regions in each case. But if tumor targeting is considered, which is the main objective of this study, keeping in mind that healthy tissue should not be targeted more, 0.03 mL dosage does a good job in delivering the target with adequate dosage. Even though the highest dosage 0.05 mL is showing higher concentrations than the 0.03 mL, it also shows highest concentration of 1.478 at the non-tumor region, which is 50% more than the value 0.5057 shown at non-tumor sites for 0.03mL distribution. Also the difference observed in the concentration changes at the tumor site for both the concentration 0.03(b) and 0.05 (c) are very



small in numerical value, which prompts us to choose 0.03mL as the safe value that can be administered to treat the target area.

Figure 4.37 Variation in drug concentration at tumor site with different input dosages

In order to find the optimal dosage other than the concentration distribution details we also need to know the effect of particle size and particle type of the drug. For that study a line

probe is drawn at the site of tumor crossing from artery to tumor from left to right and the effects of penetration velocity changes are observed on plots by changing the parameters. The plots shown below explain the differences in penetration velocity with respect to size and particle type.

The plot in Figure 4.38 shows the velocity of drug Carmustine, which has the density 1460kg/m^3 at different time steps with change in particle diameter. Two particle diameters are analyzed for the penetration velocity and the plot shows the lowest particle size of the drug penetrates with more velocity when compared to highest diameter size. This shows that the lowest diameter 0.5 microns can get into the pores of the tumor effectively when compared to the other size 5 microns.

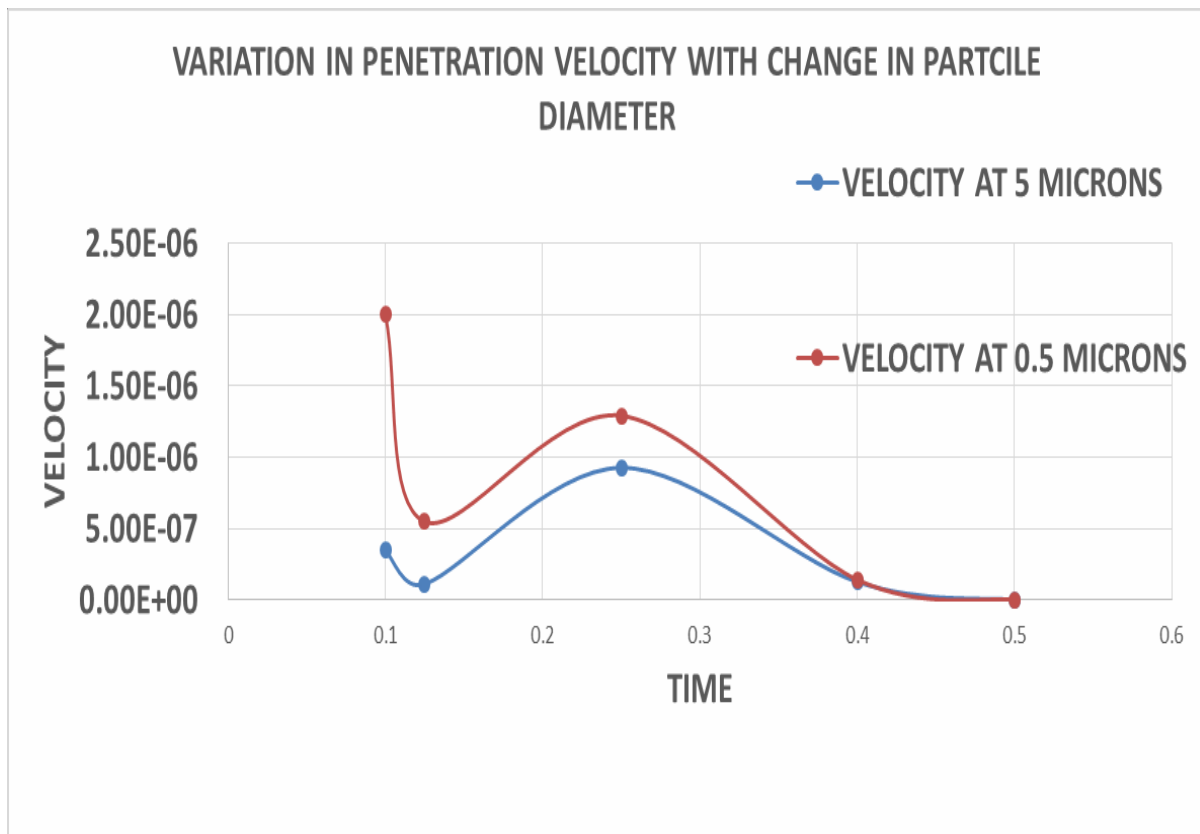


Figure 4.38 Penetration velocity with change in diameter

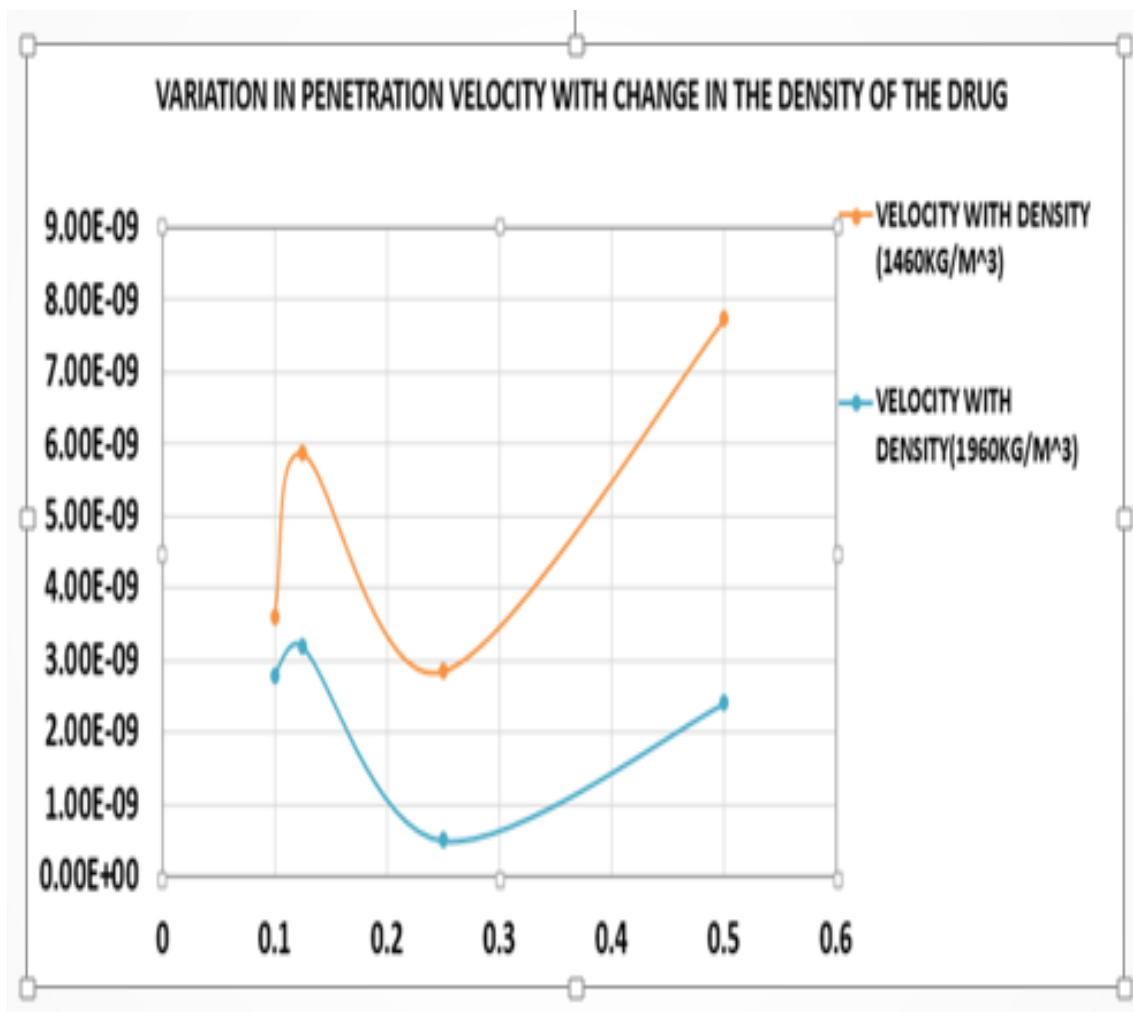


Figure 4.39 Penetration velocity with change in density

This plot in Figure 4.39 show the penetration velocity with change in particle type. Two drugs Temozolomide and Carmustine, which are commonly used as anti-cancer drugs, are used here. The plot shows the velocity penetrations with change in density considering the effects of gravity. It is seen that the lowest density drug can penetrate better into the target region when

compared to high-density drug. However in order to justify these the diameter of the particle has to be associated. The Figure 4.40 shows the variation with density of the drugs with two different diameters.

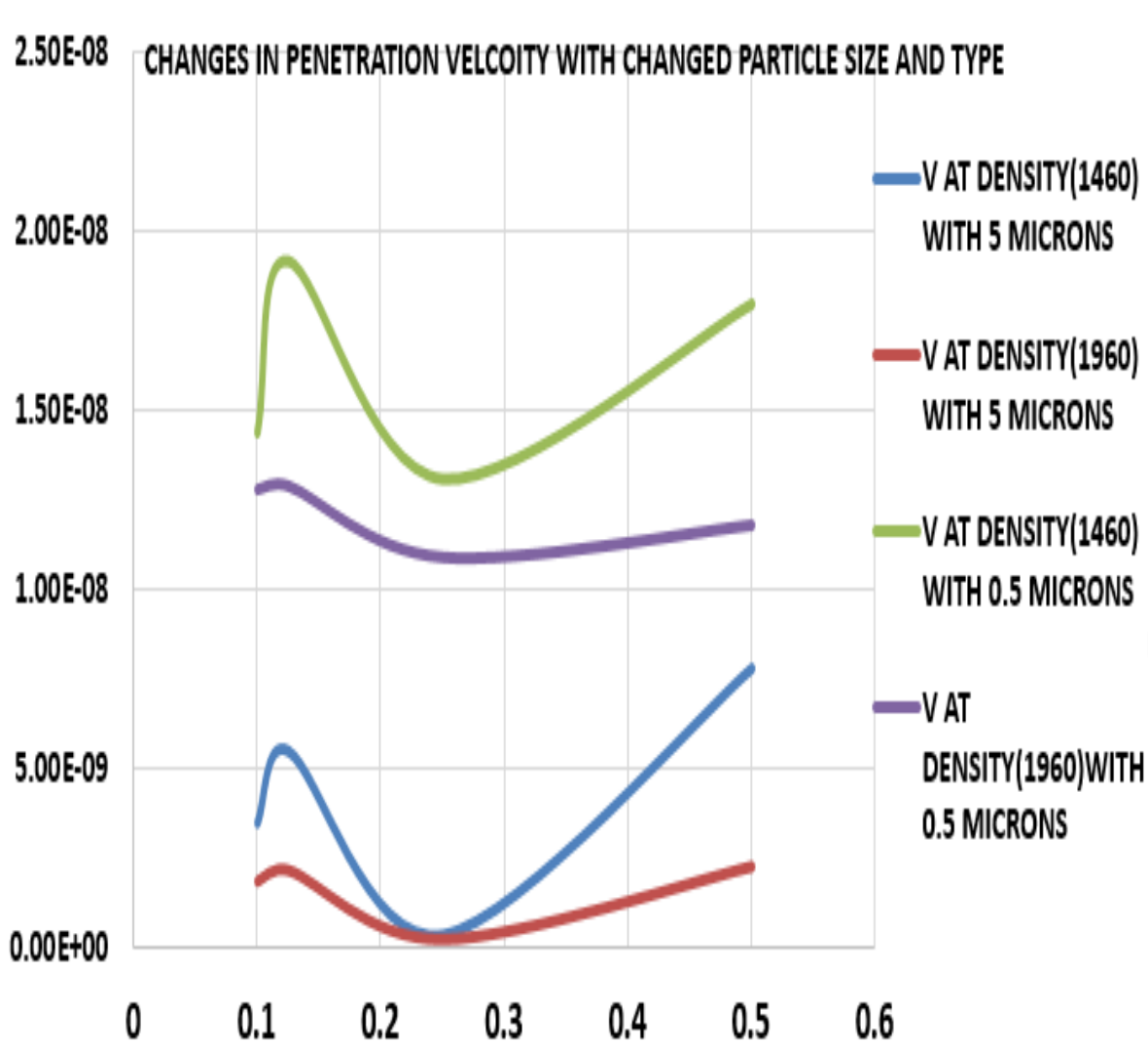


Figure 4.40 Penetration velocity with change in particle size and type

It shows that for change in diameter, two different drugs have shown increase in velocity with a decrease in diameter. However if density is taken into account, the low-density drug with lesser diameter has shown more penetrating effect than the high-density drug.

Finally the concentrations are plotted with respect to changed particle type at the site of tumor. From the plot in Figure 4.41 we can observe that the concentrations are higher for the high-density drug only at the highest peak velocity, whereas the rest of the plot shows almost equal concentration, which prompts the result that low-density drug can surround the target more when compared to high.

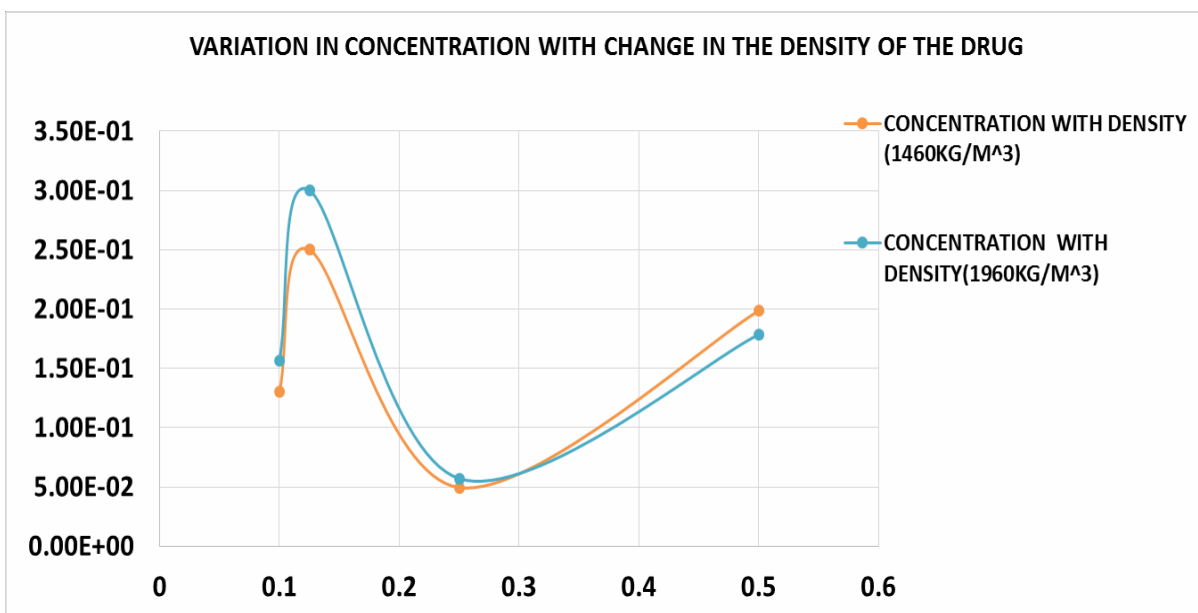


Figure 4.41 Concentration variation with change in particle size and type

5. CONCLUSION

A computational simulation model has been developed for analyzing the blood flow and drug concentration distribution in cerebral regions including the artery-capillary network. The computational analysis is done by solving governing equations of blood flow dynamics based on Navier-Stokes equations and mass species transport based on Lagrangian particle flow equations. The diffusion considered in the capillary-tissue regions is based on Brinkman's model.

Analysis of blood flow is performed using experimentally derived cardiac input as inflow and considering the blood as non-Newtonian in nature, which is closer to reality. The drug concentration distribution is also observed around the tumor which is originated in the cerebral regions, assigning it with anisotropic porosity. The drug distribution is done through intra-venal administration with the administered drug parameters varying as 0.03mL to 0.05mL in dosage, 1460kg/m³ and 1960 kg/m³ in drug density and 0.5 to 0.05 microns in particle size. The simulation analysis results show that the increase in dosage has little effect on the target after a certain amount of dosage. It also explains that the decrement in particle diameter and density as a combination could prompt us with better penetration effect of the drug to the tumor.

REFERENCES

- [1] Jhunjhunwala, P., Padole, P.M., and Thombre, S.B., 2015, “C.F.D Analysis of Pulsatile Flow and Non-Newtonian Behavior of Blood in Arteries,” *Molecular and Cellular Biomechanics*, 12(1), 37-47.
- [2] Khaled, A., and Vafai, B., 2003, “The Role of Porous Media in Modeling Flow and Heat Transfer in Biological Tissues”, *Heat and Mass Transfer*, Volume 46(26), pp.4989–5003.
- [3] Yamaguchi, T., et al., "Computational Blood Flow Analysis-New Trends and Methods," *Journal of Biomechanical Science and Engineering*, pp.29-50.
- [4] Yilmaz, F., and Gundogdu, M.Y., 2008, “A Critical Review on Blood Flow in Large Arteries; Relevance to Blood Rheology, Viscosity Models, and Physiologic Conditions,” *Korea-Australia Rheology Journal*, 20(4), 197-211.
- [5] Arifin, D.Y., Lee, K.Y.T., and Wang, C.H., 2009, “Chemotherapeutic Drug Transport to Brain Tumor,” *Journal of Controlled Release*, 137(3), 203-210.
- [6] Bello, L., and Carroll, R.S., 2001, “Low-dose Chemotherapy Combined with an Antiangiogenic Drug Reduces Human Glioma Growth in Vivo,” *Cancer Research*, 61(20), 7501-7150.
- [7] Shafiullah, M., 2013, “Computational Fluid Dynamics Analysis of Blood Flow through Stented Arteries,” master’s thesis, Northern Illinois University, DeKalb, IL.

- [8] Narmada, S., 2014, "C.F.D Analysis of Blood Flow through Stenosed Arteries," master's thesis, Northern Illinois University, DeKalb, IL.
- [9] National Heart Lung and Blood Institute, <http://www.nhlbi.nih.gov/health/health-topics/topics/hhw/anatomy.html>.
- [10] Brain Tumor Treatment Options, <http://www.cancer.net/cancer-types/brain-tumor/treatment-options>.
- [11] Djamil, F, "Brain Imaging in Arystoma," <http://emedicine.medscape.com/article/336695-overview>.
- [12]"Properties of Chemo Drug used for Brain Tumor,"2015, <http://www.cancer.org/cancer/braincnstumorsinadults/detailedguide/brain-and-spinal-cord-tumors-in-adults-treating-chemotherapy>.
- [13] Womersley, J. R., 1955, "Method for the Calculation of Velocity, Rate of Flow and Viscous Drag in Arteries when the Pressure Gradient is known," *J. Physiol.*, 127, pp. 553-563.
- [14] Resmi, S.A., and Thomas, T., 2012, "A Semi-automatic Method for Segmentation and 3D modeling of Glioma Tumors from Brain MRI," *Journal of Biomedical Science and Engineering*, 5(7), pp. 1-6.
- [15] Solid Works, 2009 <https://forum.solidworks.com/thread/26805>.
- [16] Zhang, Z., and Chen, Q., 2012, "Comparison of the Eulerian and Lagrangian Methods for Predicting Particle Transport in Enclosed Species," master's thesis, Purdue University, West Lafayette, IN.

[17] Hashimoto, J., and Ito, S., 2010, "Pulse Pressure Amplification Arterial Stiffness and Peripheral Wave Reflection Determination Pulsatile Flow Waveform of the Femoral Artery," *Hypertension*, 56, pp. 926-933.

[18] Siebert, M.W., and Fodor, P.S., 2009, "Newtonian and Non Newtonian Blood Flow over a Backward Facing Step-A Case Study," Comsol Conference Center, 1-5.